Non-normality is connection energy, and its opposite

Jeromie Beasley

21 October 2026

AI-assisted. The ideas and research direction are the author's; AI tools were used for literature search, computation, formal proof, drafting and typesetting. Every identity below is proved in the text or graded otherwise; the algebraic ones are machine-checked in Lean, and all are checked numerically by the scripts listed at the end.

Abstract

For a block transport operator $H = D + A$ on a finite graph, with Hermitian vertex blocks D_i and unitary edge blocks A_{ij}, the Frobenius self-commutator energy $\frac{1}{8}\|[H, H^*]\|_F^2$ is exactly the connection energy $\sum_E \|D_i - A_{ij} D_j A_{ij}^*\|_F^2$ of the obstruction field D, and $\frac{1}{8}\|H^2 - H^{*2}\|_F^2$ is exactly its opposite $\sum_E \|D_i + A_{ij} D_j A_{ij}^*\|_F^2$. The two are the Hermitian and skew halves of the single product DA: they share the fixed budget $2\sum_i \deg(i)\|D_i\|^2$, and their difference is the indefinite trace form $2\,\mathrm{Re}\,\mathrm{Tr}(DA)^2$, whose sign says which half wins. Both books are Born sums: on each edge they are the squared jumps $(\lambda - \mu)^2$ and squared sums $(\lambda + \mu)^2$ of the eigenvalues at the two ends, weighted by the doubly stochastic Born transition matrix of the transport. On fields of rank-k subspaces they are $2k(1 \mp p)$ with p the Born transition probability across the edge, and the finite overlap identity $k - \mathrm{Tr}(PR) = \frac{1}{2}\mathrm{Tr}((P - R)^2)$ fixes how the overlap bends. A sector sign that anticommutes with the coupling is a quarter turn, $\Gamma X = iUXU^*$; it exchanges the two halves exactly, and what it cannot exchange is twice the trace form of the coupling that stays inside a sector. The zero sets are the holonomy-fixed and sign-twisted holonomy-fixed fields, so odd loops frustrate the opposite. Balancing the two books on every edge of an odd loop is impossible for rank-one fields in two dimensions and possible in three; there the triangle becomes one complete measurement, whose Born weights sum to one, and the pentagon becomes the Klyachko–Can–Binicioğlu–Shumovsky configuration, whose weights reach $\sqrt{5}$, beyond the non-contextual bound 2. A single loop never frustrates complex subspace fields; two loops with no common invariant subspace do, and the least energies of the two Pauli bow ties are $6 - 3\sqrt{3}$ and $4 - 2\sqrt{2}$. On a twisted ring the largest total Born probability is $\frac{N}{2}(1 + \cos\frac{\delta}{N})$. The twisted Ihara zeta function has poles at $u = \pm 1$; what it carries there is its Bass pencil, whose two ends are exactly the two book operators, $K(1) = L^-$ and $K(-1) = L^+$. Each eigenvalue's share of the prime traces obeys a three-term Chebyshev recurrence. It has a geometrically minimal solution, and by Pincherle's theorem a continued fraction converging geometrically to the dominant root, exactly when the eigenvalue lies beyond the Ramanujan bound $2\sqrt{q}$, that is, exactly when its zeta zeros leave the circle; on the bound the recurrence's companion matrix is a nonzero nilpotent. On a triangle the primitive cycle carries one more number, $C_3 = 2\cos 3\phi$, that neither book sees: a scalar phase is lost to the induced transport, and a noncentral rank-two transport keeps it. The primes of arithmetic are edges. At a good prime of an elliptic curve, normalised Frobenius is a unitary edge whose books are $4p - a_p^2$

and a_p^2 on the fixed budget $4p$. They cannot see the sign of a_p, and Hasse's bound leaves the local prime traces without a minimal solution at every good prime. The local twist keeps it in $\Gamma_p = a_p/(p+1) = \tanh(\tau_p/2)$, the same reflection coefficient as a scalar edge, and a fixed global quadratic twist uses it only at primes where its character is -1. Where the trace form vanishes on a real traceless pair the operator is a nonzero nilpotent: the wall of the spinning key, of critical damping and, in an explicit encoding, of Koide's lepton relation, which there reads $\zeta^2 = 3Q - 1$. Compressed to the plane of the mass vector and the democratic ray and centered, Koide's relation is exactly the balance of the two books, $(1,1)$. It fixes a cone and leaves one number free; in Brannen's circulant form that number is the triangle's cycle coefficient C_3. Fastest asymptotic settling is the one selector found that lands on the wall. It fixes the cone, not the cubic. Both books are blind to the direction of an edge, $\mathcal{E}^{\mp}(H^{\top}) = \mathcal{E}^{\mp}(H)$, while the resolvent sees it. The author's relaxation flow spends the connection energy exactly: its stress is four times the connection energy, and the total it drains is the Henrici departure from normality of the start; in every run the opposite book fell with it. Two hidden channels have the same memory kernel exactly when their first $q_1 + q_2$ moments agree, which closes the moment-recovery question in finite dimension. A graded comparison with the Penrose inequality finds one exact point of contact: the Bunting–Masood-ul-Alam doubling of the Schwarzschild slice is the pair of books of one scalar edge, and the inversion that swaps the two sheets is the sign flip that swaps the books; every other point is structural or absent.

1 The operator and its two energies

Let $G = (V, E)$ be a finite graph and $r \geq 1$. Let

$$D = \operatorname{diag}(D_i), \qquad D_i = D_i^* \in \mathbb{C}^{r\times r}.$$

Let $A^* = -A$ be block-supported on E: $A_{ii} = 0$, $A_{ij} = 0$ for $\{i,j\} \notin E$, and A_{ij} unitary for $\{i,j\} \in E$, so $A_{ji} = -A_{ij}^*$. Set $H = D + A$. Write $\mathcal{U}_{ij}(X) := A_{ij} X A_{ij}^*$ for the induced edge transport on $\operatorname{End}(E)$; since $A_{ji} = -A_{ij}^*$ the central sign cancels and $\mathcal{U}_{ji} = \mathcal{U}_{ij}^{-1}$, so $\mathcal{U}$ is a connection on $\operatorname{End}(E)$ in the ordinary sense (`ConnectionEnergy.transport_neg`, `ConnectionEnergy.transport_inverse` [66]). Call D the obstruction field and A the transport. Then

$$\frac{1}{8}\big\|[H, H^*]\big\|_F^2 = \sum_{\{i,j\}\in E} \big\|D_i - A_{ij} D_j A_{ij}^*\big\|_F^2. \tag{1}$$

Indeed, $H^* = D - A$, hence $[H, H^*] = -2[D, A]$ and

$$[D, A]_{ij} = D_i A_{ij} - A_{ij} D_j = \big(D_i - A_{ij} D_j A_{ij}^*\big) A_{ij}.$$

Unitary invariance of the Frobenius norm and the two orientations of each edge give (1). The first step is one case of a general identity. For any Hermitian S and skew-Hermitian K,

$$\big[S + K, (S + K)^*\big] = 2[K, S], \qquad \big[H, H^{\top}\big] = -2[S, K] \quad \text{for real } H = S + K, \tag{2}$$

so a matrix is normal exactly when its Hermitian and skew halves commute [68] (bridge B2; `LightBridges.symmetric_skew_commutator` [61], `RelationalAtlas.normal_iff_commute` [69]) [DERIVED; LEAN; COMPUTED]. Here $S = D$ and $K = A$, and the block structure turns $[D, A]$ into edge terms. Thus H is normal exactly when

$$D_i = A_{ij} D_j A_{ij}^* \qquad (\{i,j\} \in E), \tag{3}$$

that is, exactly when D is parallel for the induced connection on $\mathrm{End}(E)$.

Each hypothesis does work. The blocks must be Hermitian: with $D_0 = i$, $D_1 = -i$ and $A_{01} = 1$ the operator $\left(\begin{smallmatrix} i & 1 \\ -1 & -i \end{smallmatrix}\right)$ is normal while its edge term is 4 [DERIVED; COMPUTED]. Unitarity is used only to take A_{ij} out of the norm. For any edge blocks with $A_{ji} = -A_{ij}^*$, $\|[H, H^*]\|_F^2 = 4\sum \|D_i A_{ij} - A_{ij} D_j\|_F^2$ over ordered adjacent pairs, so H is normal exactly when $D_i A_{ij} = A_{ij} D_j$ on every edge (`NonNormality.norm_sq_selfCommutator_eq` [67]); with weighted edges $A_{ij} = \sqrt{w_{ij}}\, U_{ij}$, U_{ij} unitary, (1) holds as $\sum_E w_{ij} \|D_i - U_{ij} D_j U_{ij}^*\|_F^2$ [DERIVED; LEAN; COMPUTED]. Parallel is not equal: with the swap σ_x as transport, $D_0 = \mathrm{diag}(0,1)$ and $D_1 = \mathrm{diag}(1,0)$ are parallel and H is normal [COMPUTED].

If G is connected, fix a base vertex i_0. Equation (3) transports D_{i_0} along every path by $\mathcal{U}$. Path independence holds exactly when $[D_{i_0}, W_C] = 0$ for every loop C based at i_0, where W_C is the product of the A_e along C (defined up to a central sign that the adjoint action ignores) and $\mathcal{U}_C = \mathrm{Ad}\, W_C$ is its holonomy in $\mathrm{End}(E)$. Consequently, by the classical correspondence between parallel sections of $\mathrm{End}(E)$ and endomorphisms fixed by the holonomy [3],

$$\begin{aligned} &\ker \mathcal{E}_A \;\cong\; \mathrm{Fix}_{\mathrm{Herm}(r)}\left(\mathrm{Hol}_{\mathrm{Ad}\, A}(i_0)\right) = \{X \in \mathrm{Herm}(r) :\; W_C X W_C^* = X \text{ for every loop } C\}, \\ &\mathcal{E}_A(D) := \tfrac{1}{8}\|[H, H^*]\|_F^2. \end{aligned} \tag{4}$$

Hence the Frobenius self-commutator energy of $D + A$, the standard measure of non-normality [1], is exactly the connection energy measuring the failure of its Hermitian obstruction field to be parallel under the induced transport. This is the identity of the author's one-page note [65] and of the Atlas bridge B137 [68]; its Lean companion proves (1), (3) and the holonomy direction of (4) (`ConnectionEnergy.energy_identity`, `normal_iff_parallel`, `parallel_loop_commutes` [66]). On $\mathrm{Herm}(2)$ the kernel has real dimension 4 on a tree, where every field is transported from the base; 2 on one loop whose holonomy has distinct eigenvalues, the fields diagonal in its eigenbasis; and 1 on two loops with holonomies σ_x and σ_z, the multiples of I alone [DERIVED; COMPUTED] (Figure 9a).

The opposite. The same operator measures a second failure. The commutator compares HH^* with H^*H; the other natural comparison is between H^2 and $H^{*2} = (H^2)^*$, and it vanishes exactly when H^2 is Hermitian. Since $H^2 - H^{*2} = (D + A)^2 - (D - A)^2 = 2\{D, A\}$, and the diagonal blocks of $\{D, A\}$ vanish while

$$\{D, A\}_{ij} = D_i A_{ij} + A_{ij} D_j = \left(D_i + A_{ij} D_j A_{ij}^*\right) A_{ij},$$

the same two steps give

$$\frac{1}{8}\left\|H^2 - H^{*2}\right\|_F^2 = \sum_{\{i,j\} \in E} \left\|D_i + A_{ij} D_j A_{ij}^*\right\|_F^2 =: \mathcal{E}_A^+(D). \tag{5}$$

The orientation reversal is again harmless: $\|D_j + A_{ji} D_i A_{ji}^*\| = \|D_j + A_{ij}^* D_i A_{ij}\| = \|A_{ij} D_j A_{ij}^* + D_i\|$. Write $\mathcal{E}_A^- := \mathcal{E}_A$ when both appear. Figure 2 shows the two on one edge.

The Born reading. Each book is a sum of quantum transition probabilities. Diagonalise the two blocks of an edge, $D_i = \sum_a \lambda_a P_a$ and $D_j = \sum_b \mu_b Q_b$ with rank-one spectral projectors, and put

$$W_{ab} = \mathrm{Tr}\left(P_a\, \mathcal{U}_{ij}(Q_b)\right) = \left|\langle a | A_{ij} | b \rangle\right|^2.$$

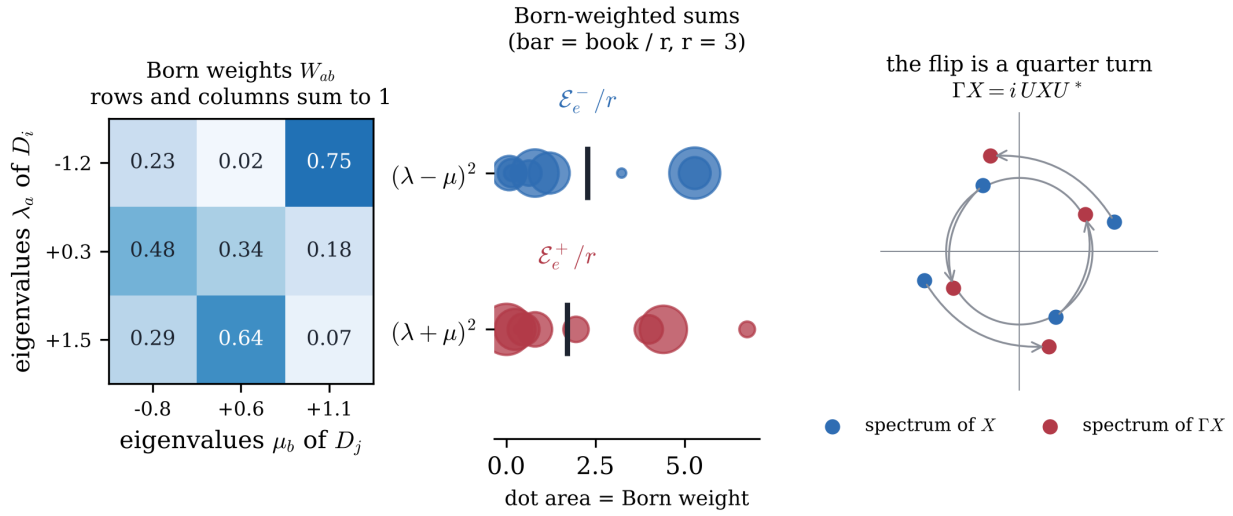


Figure 1: Left: the Born matrix W_{ab} of one edge with $r = 3$; every row and column sums to one. Middle: the two books as Born-weighted sums of $(\lambda_a - \mu_b)^2$ and $(\lambda_a + \mu_b)^2$; the bars mark each book divided by r. Right: a sector sign Γ that anticommutes with X acts as a quarter turn, $\Gamma X = iUXU^*$, rotating the spectrum by i (Section 2).

W is doubly stochastic, as the squared moduli of the entries of any unitary are (`SqrtOpEnt.entryNormSq_mem_doublyStochastic` [70]): each row and each column sums to one, and W_{ab} is the Born probability that the eigenstate $|b\rangle$ of D_j, carried along the edge, is found in the eigenstate $|a\rangle$ of D_i. Expanding the squares,

$$\mathcal{E}_e^{\mp} = \sum_{a,b} W_{ab}\,(\lambda_a \mp \mu_b)^2, \qquad \mathcal{E}_e^- - \mathcal{E}_e^+ = -4 \sum_{a,b} W_{ab}\,\lambda_a \mu_b. \tag{6}$$

The connection energy is the Born-weighted squared jump of the eigenvalue across the edge, summed over the r eigenstates at one end; the opposite is the same sum of squared sums; and their difference is minus four times the Born cross-moment of the two spectra [DERIVED]. The reading needs the transport to be unitary: for a non-unitary edge map the corresponding weights are not stochastic and (6) has no probabilistic meaning (Figure 1). If a repeated eigenvalue is kept as one spectral projector, (6) holds unchanged with $W_{ab} = \mathrm{Tr}(P_a\,\mathcal{U}_{ij}(Q_b)) \geq 0$, whose rows sum to rank P_a and columns to rank Q_b; doubly stochastic is the rank-one case. For the maximally mixed input I/r, measuring P_a and then the transported Q_b has joint probability W_{ab}/r, so each book is r times an expected squared jump or sum [DERIVED; COMPUTED]. Balance of the two books means a zero uncentered cross-moment $\sum W_{ab}\lambda_a\mu_b$. It does not mean independence, and it does not mean zero covariance unless the means vanish or are subtracted: $\lambda = (2, -1)$, $\mu = (1, 2)$ with $W = I$ balances at $10 = 10$ with covariance $-\frac{3}{4}$ [COMPUTED].

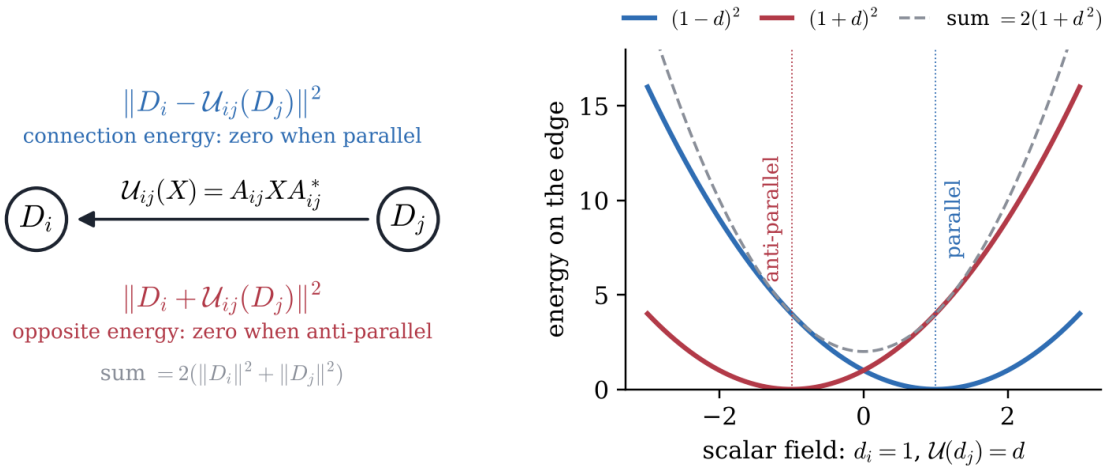


Figure 2: One edge, read twice. The transport $\mathcal{U}_{ij}$ carries D_j to the end of the edge at D_i. The connection energy measures the difference and vanishes when the field is parallel; the opposite measures the sum and vanishes when it is anti-parallel. Their sum depends only on the two norms. Right: a scalar field with $d_i = 1$ and transported value d.

2 One product, two halves

Put $X = DA$. Since $X^* = A^*D = -AD$,

$$\operatorname{Herm} X = \tfrac{1}{2}(X + X^*) = \tfrac{1}{2}[D, A], \qquad \operatorname{Skew} X = \tfrac{1}{2}(X - X^*) = \tfrac{1}{2}\{D, A\},$$

so by $[H, H^*] = -2[D, A]$ and $H^2 - H^{*2} = 2\{D, A\}$,

$$\mathcal{E}_A^- = 2\,\|\operatorname{Herm}(DA)\|_F^2, \qquad \mathcal{E}_A^+ = 2\,\|\operatorname{Skew}(DA)\|_F^2.$$

The connection energy and its opposite are the Hermitian and skew halves of the single product DA. Two identities follow at once. The halves are orthogonal, so their norms add to the norm of the whole; and $\|DA\|_F^2 = \sum_{i,j} \|D_i A_{ij}\|_F^2 = \sum_i \deg(i)\|D_i\|_F^2$ because each A_{ij} on an edge is unitary. Edge by edge this is the parallelogram law $\|a-b\|^2 + \|a+b\|^2 = 2\|a\|^2 + 2\|b\|^2$ with $a = D_i$, $b = \mathcal{U}_{ij}(D_j)$, $\|b\| = \|D_j\|$:

$$\mathcal{E}_A^- + \mathcal{E}_A^+ = 2 \sum_{\{i,j\}\in E} \left(\|D_i\|_F^2 + \|D_j\|_F^2\right) = 2 \sum_i \deg(i)\, \|D_i\|_F^2 = 2\|DA\|_F^2. \tag{7}$$

The difference of the halves is the indefinite trace form $\operatorname{Re}\operatorname{Tr} X^2 = \|\operatorname{Herm} X\|^2 - \|\operatorname{Skew} X\|^2$:

$$\mathcal{E}_A^- - \mathcal{E}_A^+ = 2\operatorname{Re}\operatorname{Tr}\left((DA)^2\right) = -4 \sum_{\{i,j\}\in E} \operatorname{Tr}\left(D_i \mathcal{U}_{ij}(D_j)\right). \tag{8}$$

The same split of a trace form, a positive Hermitian Gram minus a negative anti-Hermitian Gram with every cross term zero, is the author's Gravity Ledger Proposition 15 [13]. The budget does not depend on the transport at all. The transport decides only how the fixed amount $2\|DA\|^2$ is shared between the two halves, and the difference (8) is the signed correlation of each block with the transported block at the other end. The budget is fixed when the field and the graph are fixed and the transports vary. It is an algebraic identity of that fixed field, not a mechanical conservation law for a system that changes.

Corollary 1. *If H is normal and H^2 is Hermitian, then $D_i = 0$ at every vertex that has an edge.*

By (1) and (5) both energies vanish, so the budget (7) is zero.

Multiplying the two halves gives a third invariant, the product

$$\mathcal{E}_A^- \, \mathcal{E}_A^+ = \|DA\|_F^4 - \left(\operatorname{Re}\operatorname{Tr}(DA)^2\right)^2,$$

which vanishes exactly when one of the two is empty. Edge by edge, with $a = D_i$, $b = \mathcal{U}_{ij}(D_j)$ and $s = \|a\|^2 + \|b\|^2$,

$$\mathcal{E}_e^- \, \mathcal{E}_e^+ = s^2 - 4\langle a, b\rangle^2 = s^2\left(P_e^2 + L_e^2\right) \tag{9}$$

in the notation of (23) below, the squared radius of an edge in the duality disc (Figure 6) times s^2 [DERIVED; COMPUTED]. It is a square minus a square. That shape is useful algebra; it does not make the product a mass (Section 12).

The sector flip. The sign of the trace form $q(X) = \frac{1}{2}\operatorname{Re}\operatorname{Tr} X^2 = \frac{1}{2}(\|\operatorname{Herm} X\|^2 - \|\operatorname{Skew} X\|^2)$ says which half wins, and one operation reverses it. Let $\Gamma = \Gamma^*$, $\Gamma^2 = I$, be a sign that is $+1$ on one sector and -1 on the other, and split any X into its part A that crosses between the sectors, $\Gamma A \Gamma = -A$, and its part B that stays inside them, $\Gamma B \Gamma = B$. Then $\operatorname{Tr}(AB) = 0$ and

$$\operatorname{Herm}(\Gamma A) = \Gamma \operatorname{Skew} A, \qquad \operatorname{Skew}(\Gamma A) = \Gamma \operatorname{Herm} A, \qquad \operatorname{Tr} X^2 + \operatorname{Tr}(\Gamma X)^2 = 2 \operatorname{Tr} B^2. \tag{10}$$

For crossing coupling alone the flip exchanges the two halves exactly, keeps the budget and the self-commutator, and reverses the trace form. It is not a reflection of A itself but a quarter turn: with $U = e^{-i\pi\Gamma/4}$,

$$\Gamma A = i\, U A U^*, \tag{11}$$

a unitary change of frame followed by multiplication by i, which rotates the spectrum by a right angle and gives $(\Gamma A)^2 = -A^2$; it is not an ordinary similarity. It keeps the self-commutator itself, not only its norm: AA^* stays inside the sectors, so $\Gamma AA^*\Gamma = AA^*$ and $[\Gamma A, (\Gamma A)^*] = \Gamma AA^*\Gamma - A^*A = [A, A^*]$ as matrices [DERIVED; COMPUTED]. Since ΓA anticommutes with Γ, its spectrum is symmetric under $\lambda \mapsto -\lambda$ and its odd moments vanish, the law the author's Dirac Time paper states once for all gradings [50] (§5.3; `FOFT.odd_moment_zero_X` [72], `AtlasFormal.chiral_eigenvalue_pair` [69]) [CITED; LEAN]. With $\Gamma = 2P - 1$ for a projector P, the crossing part is the redistribution of the author's projector papers,

$$A = \tfrac{1}{2}(X - \Gamma X \Gamma) = PX(1-P) + (1-P)XP = P[P, X] - [P, X]P, \tag{12}$$

which vanishes exactly when $[X, P] = 0$ (`LightBridges.redistribute_double_commutator` [61], `UPGAlgebra.redistribution_eq_commutator_form` [74], `DiracTime.SectorReduction.redistribution_zero_iff_commute` [56]) [DERIVED; LEAN; COMPUTED]. A grading has to be found for the whole family it is applied to: on the auxiliary family $Z = h_1\sigma_z + h_2\sigma_x + sJ$ of Section 10, each two-parameter slice has a sign that anticommutes with it, and no sign anticommutes with all three of σ_z, σ_x, J [DERIVED; COMPUTED]. What the flip cannot move is the coupling inside a sector: $2\operatorname{Tr} B^2$ is exactly how far the reversal falls short. This is a signed quantity, a size only when B is Hermitian. On a bipartite graph with $\Gamma = \pm 1$ on the two sides and $X = DA$, every edge crosses, $B = 0$, and (10) is the sign flip (17) below; an edge inside one colour class is a contribution to B.

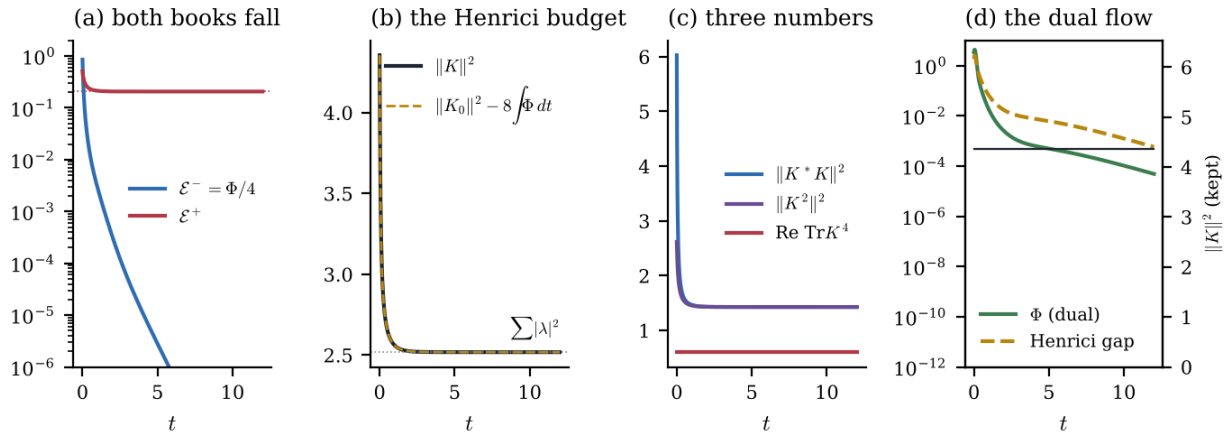


Figure 3: The relaxation flow (13) on a triangle with 2×2 blocks. (a) The connection energy drains to zero; the opposite falls too, to $2\sum(\mathrm{Re}\,\lambda\,\mathrm{Im}\,\lambda)^2$ (dotted). (b) $\|K\|^2$ falls by exactly $8\int\Phi\,dt$ and ends at $\sum|\lambda|^2$: the Henrici budget is spent. (c) The three numbers of (14): the flow keeps $\mathrm{Re}\,\mathrm{Tr}\,K^4$, and $\|K^*K\|^2$ comes down to meet $\|K^2\|^2$. (d) The dual flow keeps $\|K\|^2$ (right axis) while the stress and the Henrici gap fall.

The relaxation flow. The author's operator field theory relaxes an operator by

$$\dot{K} = -2\big[[K, K^*], K\big], \qquad \frac{d}{dt}\|K\|_F^2 = -4\,\mathrm{Tr}\,C^2 = -8\Phi, \qquad \Phi = \tfrac{1}{2}\|C\|_F^2,\ C = [K, K^*] \tag{13}$$

[71] (Theorems 8.1 and 8.2; `FOFT.henrici_rate`, `FOFT.flow_smul` [72]) [CITED; LEAN; COMPUTED]. It is a Lax flow, so it keeps the spectrum, and on the class $D + A$ its stress is four times the connection energy, $\Phi = 4\mathcal{E}^-$, by (1). Integrating, $8\int_0^T \Phi\,dt = \|K(0)\|_F^2 - \|K(T)\|_F^2$ for every T [DERIVED]. When the flow reaches a normal matrix, as it did in every run, the total is Henrici's departure from normality, $\|K(0)\|_F^2 - \sum|\lambda|^2$, which that paper calls the Henrici budget: the connection energy, spent along the relaxation, pays exactly the departure of the start [DERIVED; COMPUTED]. This is the sense in which the author reads the connection energy as a budget for transient growth. The flow does not stay in the class with unitary edges: for $K = \left(\begin{smallmatrix} d_1 & 1 \\ -1 & d_2 \end{smallmatrix}\right)$, $\dot{K} = \left(\begin{smallmatrix} -8\delta & -4\delta^2 \\ 4\delta^2 & 8\delta \end{smallmatrix}\right)$ with $\delta = d_1 - d_2$, so the edge leaves modulus one at once [DERIVED; COMPUTED]. Both books make sense for any square K, and two identities place them side by side:

$$\mathcal{E}^-(K) = \tfrac{1}{8}\|[K, K^*]\|_F^2 = \tfrac{1}{4}\big(\|K^*K\|_F^2 - \|K^2\|_F^2\big), \qquad \mathcal{E}^+(K) = \tfrac{1}{8}\|K^2 - K^{*2}\|_F^2 = \tfrac{1}{4}\big(\|K^2\|_F^2 - \mathrm{Re}\,\mathrm{Tr}\,K^4\big) \tag{14}$$

[DERIVED; COMPUTED]. The flow keeps the last of the three numbers. So it is natural to ask whether the opposite fills as the connection energy drains. It does not. Along the flow $\mathcal{E}^+$ fell in every run and ends at $2\sum(\mathrm{Re}\,\lambda\,\mathrm{Im}\,\lambda)^2$, the value (14) gives a normal matrix, fixed by the spectrum; its rate was never positive on 20000 random matrices [COMPUTED]. That the rate is never positive is not proved here. The opposite flow, the dual $\dot{K} = -2[C, K^*]$, keeps $\|K\|_F^2$ exactly ([71], Proposition 8.4; `FOFT.dual_flow_conserves`) and in the runs also ends at a normal matrix: it moves the stress into the spectrum instead of removing it [CITED; LEAN; COMPUTED] (Figure 3).

3 The zero sets, and why odd loops frustrate

By (5), H^2 is Hermitian exactly when

$$D_i = -A_{ij} D_j A_{ij}^* \qquad (\{i,j\} \in E), \tag{15}$$

that is, when D is anti-parallel. The opposite energy is the connection energy of the sign-twisted transport $X \mapsto -\mathcal{U}_{ij}(X)$, which is still invertible with $(-\mathcal{U}_{ij})^{-1} = -\mathcal{U}_{ji}$, so the argument behind (4) goes through with one change: a loop of length ℓ picks up the sign $(-1)^\ell$. For connected G, evaluation at i_0 gives

$$\ker \mathcal{E}_A^+ \;\cong\; \{X \in \mathrm{Herm}(r) :\; (-1)^{\ell(C)}\, W_C X W_C^* = X \text{ for every loop } C \text{ at } i_0\}. \tag{16}$$

An even loop asks for what the connection energy asks. An odd loop asks for $W_C X W_C^* = -X$. If the holonomy of an odd loop is trivial, this forces $X = 0$: an odd loop with no twist admits no anti-parallel field at all. The sign is a frustration in the sense of signed graphs, carried here by every odd cycle.

On a bipartite graph with sides S and T, flipping the sign of D on T changes $D_i - \mathcal{U}_{ij}(D_j)$ into $D_i + \mathcal{U}_{ij}(D_j)$ on every edge, since every edge has exactly one end in T. So

$$\mathcal{E}_A^-(\sigma D) = \mathcal{E}_A^+(D), \qquad \mathcal{E}_A^+(\sigma D) = \mathcal{E}_A^-(D), \qquad (\sigma D)_i = \begin{cases} D_i, & i \in S, \\ -D_i, & i \in T, \end{cases} \tag{17}$$

and on bipartite graphs the two energies carry the same information. The difference between them lives in the odd cycles.

The bipartite double cover makes this exact on every graph. Its vertices are the pairs $(i, \pm)$, and each edge $\{i,j\}$ lifts to $(i,+)$–$(j,-)$ and $(i,-)$–$(j,+)$, both carrying A_{ij}. The cover is bipartite. An even loop lifts to two loops; an odd loop lifts to a single loop of twice the length (Figure 5). Given fields S and T on G, put $F_{(i,\pm)} = S_i \pm T_i$ on the cover. Each pair of lifted edges contributes $\|(S_i + T_i) - \mathcal{U}(S_j - T_j)\|^2 + \|(S_i - T_i) - \mathcal{U}(S_j + T_j)\|^2$, and the cross terms cancel between the two lifts, so

$$\mathcal{E}_{\tilde{A}}^-(F) = 2\,\mathcal{E}_A^-(S) + 2\,\mathcal{E}_A^+(T). \tag{18}$$

The two energies are the even and the odd half of one connection energy on the double cover.

Balance on every edge, and the third dimension. On fields of rank-k orthogonal projectors the two books on an edge are equal exactly when the transported subspaces are orthogonal (Section 4): a mirror edge. On an odd cycle with trivial transport, a rank-one field in $\mathbb{C}^2$ cannot be a mirror on every edge. Writing $p_e = \frac{1}{2}(1 + n_i \cdot n_j)$ in Bloch vectors, the least total is

$$\min \sum_e p_e = \frac{N}{2}\Big(1 - \cos\frac{\pi}{N}\Big) > 0 \qquad (N \text{ odd}), \tag{19}$$

the ground state of the classical antiferromagnetic ring [DERIVED; COMPUTED]. In $\mathbb{R}^3$ the floor is zero: an odd cycle needs a third direction to alternate. The balanced fields that the third dimension allows are familiar objects. On the triangle the three projectors are an orthonormal basis, a single complete measurement, and for every state ψ the Born weights $\langle\psi|P_i\psi\rangle$ sum to exactly one. On the pentagon the mirror field is the configuration of Klyachko, Can, Binicioğlu and Shumovsky

[16]: with $P_i = |v_i\rangle\langle v_i|$, $v_i = (c, s\cos\frac{4\pi i}{5}, s\sin\frac{4\pi i}{5})$, $c^2 = 1/\sqrt{5}$, neighbours are orthogonal, both books equal $2|E| = 10$, and the state $\psi = (1,0,0)$ has total weight $\sqrt{5}$, above the bound 2 that any non-contextual assignment obeys and equal to the Lovász number of the pentagon [17, 18] [KNOWN; COMPUTED]. So the sentence "three is where it pins" has three exact forms: Gleason's theorem needs dimension three [14], the fixed-dimension Born theorem needs three outcomes [15], and balancing both books on every edge of an odd loop needs a third dimension, after which the Born weights obey the graph bounds of quantum contextuality (Figure 4). The balance on each edge is exactly the orthogonality that the exclusivity bound uses, so a known contextuality constraint is here a connection-energy condition [STRUCTURAL COMPARISON]. It does not make Gleason's dimension threshold, the uniqueness on equal-rank partitions and graph colouring one theorem. Nor does it select a state: an orthonormal triangle admits every normalised state, including equal mass roots, whose Koide ratio is $\frac{1}{3}$, so three dimensions do not derive three lepton generations [DERIVED]. A prescribed nontrivial transport on the edges changes the odd-cycle obstruction and has to be kept.

The scope of the Born form is narrow at both ends. Hossenfelder's argument concerns the Born rule itself [15], in five steps: (H1) unitary invariance makes the transition probability a function of the overlap $\langle\Psi|\Phi\rangle$ alone; (H2) orthogonal states give 0; (H3) consistency on a basis gives the symmetric state the weight $1/N$; (H4) combining K Fourier vectors of a block gives K/N; (H5) continuity and independence of N carry K/N to $|\langle\Psi|\Phi\rangle|^2$. The two books take the Born weight as given and touch three of the five. The Born matrix W of an edge depends only on overlaps (H1), vanishes between orthogonal eigenstates, so that a mirror edge has $p_e = 0$ (H2), and has unit row and column sums, her consistency (H3). They do not touch (H4) or (H5) [DERIVED; COMPUTED]. The author's extension replaces exactly those two steps: at rank one and for each fixed $N \geq 3$, her conclusion already follows from her conditions (1)–(3) and unitary invariance, with continuity replaced by boundedness and no use of independence of N [63] (Corollary A″) [CITED; COMPUTED]. The same extension proves $\rho(P \to R) = \mathrm{Tr}(PR)/k$ on equal-rank partitions with at least three outcomes, from unitary invariance, boundedness, consistency on partitions and certainty [15, 63] [CITED]. Binary partitions allow other rules: $f(s) = s + \epsilon \sin 2\pi s$ with $|\epsilon|$ small is consistent, bounded and certain on every two-outcome partition, and fails on three outcomes [DERIVED; COMPUTED] (Figure 7e). None of this refutes Hossenfelder's original argument. In the oblique setting, with idempotents that need not be orthogonal and dimension at least three, similarity invariance, bounded nonnegative consistency and certainty cannot all hold: the idempotent $P = (1,1,1)^\top(\frac{3}{4}, \frac{3}{4}, -\frac{1}{2})$ is, with each of the first two coordinate projectors, similar to an orthogonal pair of overlap $\frac{3}{4}$, so a similarity-invariant rule must give both outcomes weight $\frac{3}{4}$, which a resolution of the identity cannot carry [DERIVED; COMPUTED]. Tensoring with I_k carries the witness to every rank: $P \otimes I_k$ with $E_{11} \otimes I_k$ and with $E_{22} \otimes I_k$ are again pairs that a metric, $G_1 \otimes I_k$ and its coordinate swap, makes orthogonal, with normalised overlap $\frac{3}{4}$ [DERIVED; COMPUTED]. Dropping the bound and keeping continuity on generic pairs, the same note finds that in dimension three and above the similarity-invariant, consistent and certain complex rules are exactly $F(z) = az + (1-a)\bar{z}$ with $z = \mathrm{Tr}(PR)$; a real rule that also respects complex conjugation is then $\mathrm{Re}\,\mathrm{Tr}(PR)$, which is not a probability: $P = \left(\begin{smallmatrix} 1 & 3 \\ 0 & 0 \end{smallmatrix}\right)$ with $R = \left(\begin{smallmatrix} 1 & 0 \\ 1 & 0 \end{smallmatrix}\right)$ gives 4, and with $R' = \left(\begin{smallmatrix} 1 & 0 \\ -1 & 0 \end{smallmatrix}\right)$ gives -2 [63] [CITED; COMPUTED]. Dimension two is different on both counts. The bounded axioms are compatible there: the rule that gives 1 when $R = P$, 0 when $R = 1 - P$ and $\frac{1}{2}$ otherwise is similarity invariant, consistent on every resolution $\{R, 1-R\}$ and certain, though not continuous [DERIVED; COMPUTED]. And without the bound, $F(z) = z + \epsilon z(1-z)(z-\frac{1}{2})$ satisfies $F(z) + F(1-z) = 1$, $F(0) = 0$, $F(1) = 1$ and is not of the linear form [DERIVED].

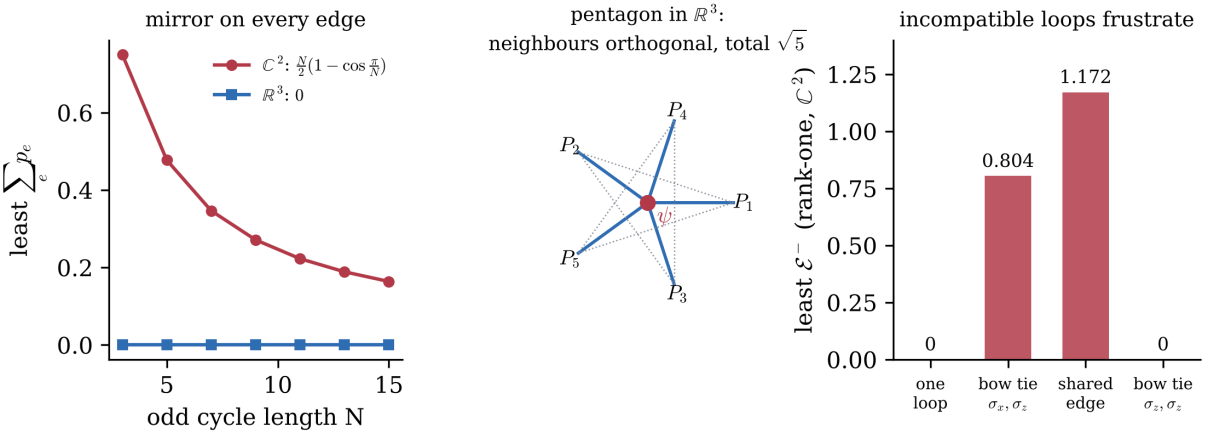


Figure 4: Odd loops. Left: the least total Born probability of a rank-one field on an odd cycle; in $\mathbb{C}^2$ it is $\frac{N}{2}(1-\cos\frac{\pi}{N})$, in $\mathbb{R}^3$ zero. Middle: the pentagon mirror field seen from ψ; neighbours are orthogonal and the weights total $\sqrt{5}$. Right: least connection energy of rank-one fields in $\mathbb{C}^2$; one loop never frustrates, two loops with σ_x and σ_z holonomy do, two compatible loops do not.

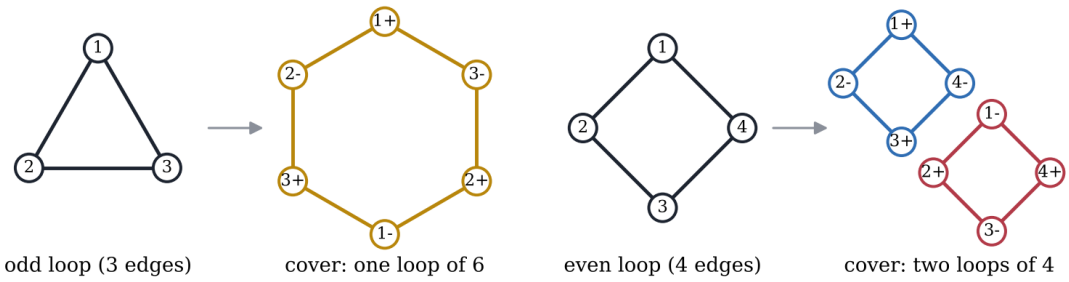


Figure 5: The double cover. Each vertex i splits into $(i,+)$ and $(i,-)$ and each edge joins opposite signs. An odd loop lifts to one loop of twice the length, which links the even and odd halves; an even loop lifts to two separate loops. Fields that are even under the sheet swap feel the connection energy, odd fields feel the opposite.

4 One edge

The scalar edge. With $r = 1$ and $D_i = d_i > 0$ the transport acts trivially on scalars, and the edge contributes $(d_i - d_j)^2$ to one energy and $(d_i + d_j)^2$ to the other. Their ratio is the square of a reflection coefficient:

$$\frac{\mathcal{E}_e^-}{\mathcal{E}_e^+} = \Gamma_e^2, \qquad \Gamma_e = \frac{d_i - d_j}{d_i + d_j} = \tanh\Big(\frac{1}{2}\ln\frac{d_i}{d_j}\Big), \qquad \mathcal{E}_e^+ - \mathcal{E}_e^- = 4d_i d_j. \tag{20}$$

This is the coefficient of a wave meeting a step between impedances d_i and d_j, and $4d_i d_j$ is the transmitted part of the flux balance $(d_i - d_j)^2 + 4d_i d_j = (d_i + d_j)^2$ (`EventHorizon.Edition10.step_matching`, `EventHorizon.Edition10.flux_balance` [59]). The tanh form is machine-checked as $\tanh(\frac{1}{2}\log\frac{s}{1-s}) = 2s - 1$ with $s = d_i/(d_i + d_j)$ (`NonNormality.tanh_half_log_odds` [67]; also `OffsetLean.Headline.asymmetry_eq_tanh_half_offset` [60] and `EventHorizon.Edition10.tanh_half_log` [59]) [DERIVED; LEAN]. A matched edge ($d_i = d_j$) has no connection energy, and the opposite carries everything.

A boost. The pair $(d_i + d_j,\ d_i - d_j)$ behaves as a Lorentz vector whose invariant is the transmitted part, $(d_i + d_j)^2 - (d_i - d_j)^2 = 4d_i d_j = \mathcal{E}_e^+ - \mathcal{E}_e^-$. The boost $d_i \mapsto e^{\varphi} d_i$, $d_j \mapsto e^{-\varphi} d_j$ keeps it, shifts the rapidity $\tau_e = \ln(d_i/d_j)$ by 2φ, and composes the reflection coefficient by the velocity law,

$$\Gamma_e \ \longmapsto\ \Gamma_e \oplus \tanh\varphi = \frac{\Gamma_e + \tanh\varphi}{1 + \Gamma_e \tanh\varphi} \tag{21}$$

(`VOTKP.Smith.tanh_add'` [62]) [DERIVED; LEAN; COMPUTED]. It is a boost of the two field values, not of spacetime (Figure 9f).

Passive fields. If every D_i is positive semidefinite, then $\mathrm{Tr}(D_i \mathcal{U}_{ij}(D_j)) \geq 0$ (a trace of a product of two positive semidefinite matrices), so on every edge

$$\mathcal{E}_e^- \leq \mathcal{E}_e^+, \qquad |\Gamma_e| \leq 1, \tag{22}$$

with equality exactly when the two blocks have orthogonal supports, a mirror edge.

The duality on every edge. For Hermitian blocks the inner product $\langle a, b\rangle = \mathrm{Tr}(ab)$ is real. With $a = D_i$, $b = \mathcal{U}_{ij}(D_j)$ and $s = \|a\|^2 + \|b\|^2$ put

$$P_e = \frac{\|a\|^2 - \|b\|^2}{s}, \qquad V_e = \frac{\mathcal{E}_e^+ - \mathcal{E}_e^-}{\mathcal{E}_e^+ + \mathcal{E}_e^-} = \frac{2\langle a, b\rangle}{s}, \qquad L_e^2 = \frac{4\big(\|a\|^2\|b\|^2 - \langle a, b\rangle^2\big)}{s^2}.$$

Then, from $s^2 = (\|a\|^2 - \|b\|^2)^2 + 4\|a\|^2\|b\|^2$,

$$P_e^2 + V_e^2 + L_e^2 = 1. \tag{23}$$

P_e says which end carries more, V_e is the normalised difference of the two energies, and $L_e^2 \geq 0$ is a Gram determinant, zero exactly when b is a real multiple of a (`NonNormality.duality_le_one` [67]). Relation (23) is the complementarity relation of Jakob and Bergou [87]: read a and b as the two branches of the state $(|0\rangle \otimes a + |1\rangle \otimes b)/\sqrt{s}$ in the Hilbert–Schmidt space; then $|P_e|$ is the predictability of the path, $|V_e|$ its visibility, and L_e the concurrence of the path with the field, and entanglement limits the duality [88] [CITED; COMPUTED]. Scalar edges have $L_e = 0$ and sit on the circle $P^2 + V^2 = 1$; matrix edges fill the disc (Figure 6).

Projector fields. If every D_i is an orthogonal projector of rank k, then $\mathcal{U}_{ij}(D_j)$ is one as well, $\|a \pm b\|^2 = 2k \pm 2\,\mathrm{Tr}(ab)$, and $\mathrm{Tr}(ab) = \sum_a \cos^2\theta_a$ over the principal angles between the two ranges:

$$\mathcal{E}_e^- = 2\sum_a \sin^2\theta_a, \qquad \mathcal{E}_e^+ = 2\sum_a \left(1+\cos^2\theta_a\right), \qquad \mathcal{E}_e^- + \mathcal{E}_e^+ = 4k. \tag{24}$$

On a field of rank-k subspaces the budget is the constant $4k$ on every edge, so the opposite is read off from the connection energy edge by edge. With $p_e = \mathrm{Tr}(ab)/k$, the Born probability that the transported subspace passes the test D_i for the maximally mixed state on it,

$$\mathcal{E}_e^{\mp} = 2k(1 \mp p_e), \qquad P_e = 0, \quad V_e = p_e, \quad L_e^2 = 1 - p_e^2, \qquad \sum_e p_e = -\frac{\mathrm{Re}\,\mathrm{Tr}(DA)^2}{2k}. \tag{25}$$

The two books are the improbability and the probability of the transition on each edge [DERIVED]. The sum over edges is a total score, not a probability: different edges are different tests. The equality $\mathcal{E}_e^- = \mathcal{E}_e^+$ means $p_e = 0$, orthogonal subspaces. The same sum $\sum_e 2k(1-p_e)$ is the coupling energy of the projector-coupled rotors in the author's Direction, Spin and Throughput [84]. For projectors of unequal rank, $\|P_s - P_t\|_F^2 = \mathrm{rk}\,P_s + \mathrm{rk}\,P_t - 2\,\mathrm{Tr}(P_sP_t)$, and in this form the author applies (1) and (24)–(26) to fields of projectors on a graph of search states in *Certified Obstructions and Exact Forcing* [85]; there, by (31), a constant field cI costs nothing on any graph [CITED; COMPUTED].

Coherent subspaces do not need equal spectra. If the transports carry each eigenprojector of D_j exactly onto the matching one of D_i, the projector fields have no connection energy while the full field keeps the jumps of its eigenvalues: with $W = I$ in (6) the book is $\sum_a(\lambda_a - \mu_a)^2$. On a three-level path with eigenvalues $(0,1,3)$, $(1,2,4)$ and $(-1,0,5)$ every projector energy is 0 and the connection energy is $3+9=12$ [DERIVED; COMPUTED] (Figure 7d). Many slightly different spectra can share one direction exactly.

How the overlap bends. For idempotents P, R of equal rank k, orthogonal or not,

$$k - \mathrm{Tr}(PR) = \tfrac{1}{2}\,\mathrm{Tr}\left((P-R)^2\right). \tag{26}$$

Along a curve $P(t) = P_0 + tV + o(t)$ of idempotents this gives $\mathrm{Re}\,\mathrm{Tr}(P_0P(t))/k = 1 - q(V)t^2/k + o(t^2)$ with $q(V) = \frac{1}{2}\,\mathrm{Re}\,\mathrm{Tr}\,V^2$. For orthogonal projectors V is Hermitian and $q(V) = g(V,V)$, the intrinsic metric, so the overlap falls below its cap at the rate of the metric. A tangent with $q < 0$ forces the overlap above one at second order (`GravityOverlap.local_cap_requires_nonnegative` [55] is the converse: a local cap forces $q \geq 0$). Such tangents are as many as the others: on the rank-k idempotent tangents in $M_n(\mathbb{C})$ the form q has neutral signature $(2k(n-k), 2k(n-k))$, the author's Gravity Ledger Theorem 6 [13] and Atlas bridge B123 [68], so the cap $\mathrm{Tr}(PR) \leq k$ is a property of self-adjointness [CITED; COMPUTED]. The sector sign exchanges the two kinds. For an orthogonal projector P_0 the reflection $\Gamma = 2P_0 - 1$ is an involution (as for any idempotent, `NonNormality.reflection_of_idempotent` [67]), and for a Hermitian tangent V the crossing part rule (10) gives

$$\Gamma V = P_0V(1-P_0) - (1-P_0)VP_0, \qquad P_0(\Gamma V) + (\Gamma V)P_0 = \Gamma V, \qquad q(\Gamma V) = -q(V), \tag{27}$$

so ΓV is again a tangent of idempotents, now oblique, and the curve $e^{tX}P_0e^{-tX}$ with $X = [\Gamma V, P_0]$ has overlap $1 + q(V)t^2/k + o(t^2)$, above the cap [DERIVED; LEAN; COMPUTED]. In two dimensions the pair is explicit: rotating E_{11} gives overlap $\cos^2 t$, and its partner $S(t)E_{11}S(t)^{-1}$, $S(t) = e^{t\sigma_x}$, whose tangent is Γ times the first with $\Gamma = \mathrm{diag}(1,-1)$, gives $\cosh^2 t$ (Figure 7a). For orthogonal

projectors the rate has a second name: the quantum Fisher information of the state P/k along the path is $F_Q = 4g(V,V)/k$, so the overlap falls as $1 - F_Q t^2/4$ [DERIVED; COMPUTED] (Figure 7b,c). $q = 0$ decides nothing at second order: $P(t) = (1-t^4)^{-1}\left(\begin{smallmatrix} 1 & t \\ -t^3 & -t^4 \end{smallmatrix}\right)$ has $q = 0$ and overlap $1/(1-t^4) > 1$. This expansion and its corollary are the author's [13] (Theorem 8 and Corollary 9); the finite identity (26) shows they need only first-order differentiability [DERIVED], and the author submitted it to Mathlib as pull request #43951 [86]. Both are machine-checked in the real-part form (`GravityOverlap.overlap_exact`, `GravityOverlap.overlap_quadratic_limit`, `GravityOverlap.negative_direction_exceeds_cap` [55]) for a family that is entrywise differentiable at $t = 0$ and idempotent with constant real trace near it. The constant trace follows from local constancy of the rank; that argument is written, not formalised, and enters the Lean statements as a hypothesis. Unequal traces break the finite identity. The formal scope is finite projector algebra: no gravitational field equation follows from the trace form alone [CITED; LEAN; COMPUTED].

A positive metric at each point is not by itself a rule for comparing two points. Suppose $P(t)^*\eta(t) = \eta(t)P(t)$ and $P_0^*\eta_0 = \eta_0 P_0$, and a transport $T(t)$ with $T(0) = I$ and $T^*\eta_0 T = \eta(t)$ is specified. Then $Q = TPT^{-1}$ is η_0-self-adjoint, the finite identity becomes the nonnegative square

$$k - \operatorname{Tr}(P_0 Q) = \tfrac{1}{2}\left\|\eta_0^{1/2}(P_0 - Q)\,\eta_0^{-1/2}\right\|_F^2 \geq 0, \tag{28}$$

and its tangent is $\dot{P}(0) + [\dot{T}(0), P_0]$ [DERIVED; COMPUTED]. The number depends on the declared transport. The raw overlap of E_{11} with $S(t)E_{11}S(t)^{-1}$ is $\cosh^2 t > 1$; transported by $T = S(t)^{-1}$ it is 1, and by $T = R_\theta S(t)^{-1}$, R_θ a rotation, it is $\cos^2\theta$ [COMPUTED]. Time-dependent coordinates likewise carry the term $\dot{S}S^{-1}$ in $G' = SGS^{-1} + \dot{S}S^{-1}$. A moving unitary frame does the same. If $i\hbar\dot{\psi} = H\psi$ and $\psi = R\chi$ with R unitary, then

$$i\hbar\,\dot{\chi} = \left(R^*HR - i\hbar R^*\dot{R}\right)\chi \tag{29}$$

[50] (§9.3, item T4; `DiracTime.MovingFrame.moving_frame_identity` [56]) [CITED; LEAN; COMPUTED]: matching the instantaneous spectrum of R^*HR is not enough, and the frame connection $-i\hbar R^*\dot{R}$ has to be kept. Leaving out the transport or the derivative of the metric can make growth appear where there is none.

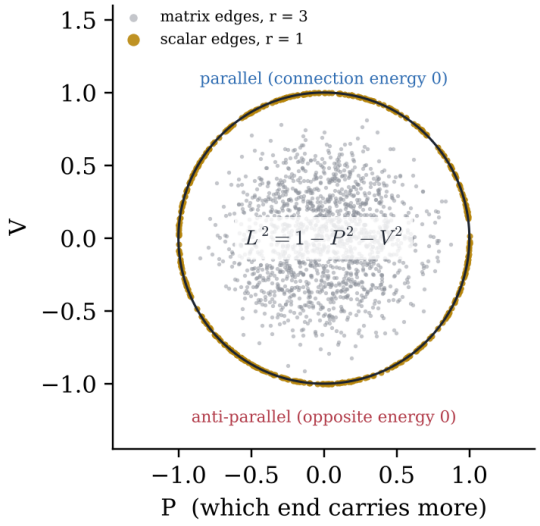


Figure 6: The duality (23). Each point is one edge. Scalar edges lie on the circle; matrix edges fill the disc, and the depth $L^2 = 1 - P^2 - V^2$ is the Gram determinant of the two blocks. The top of the circle is a parallel edge, the bottom an anti-parallel one.

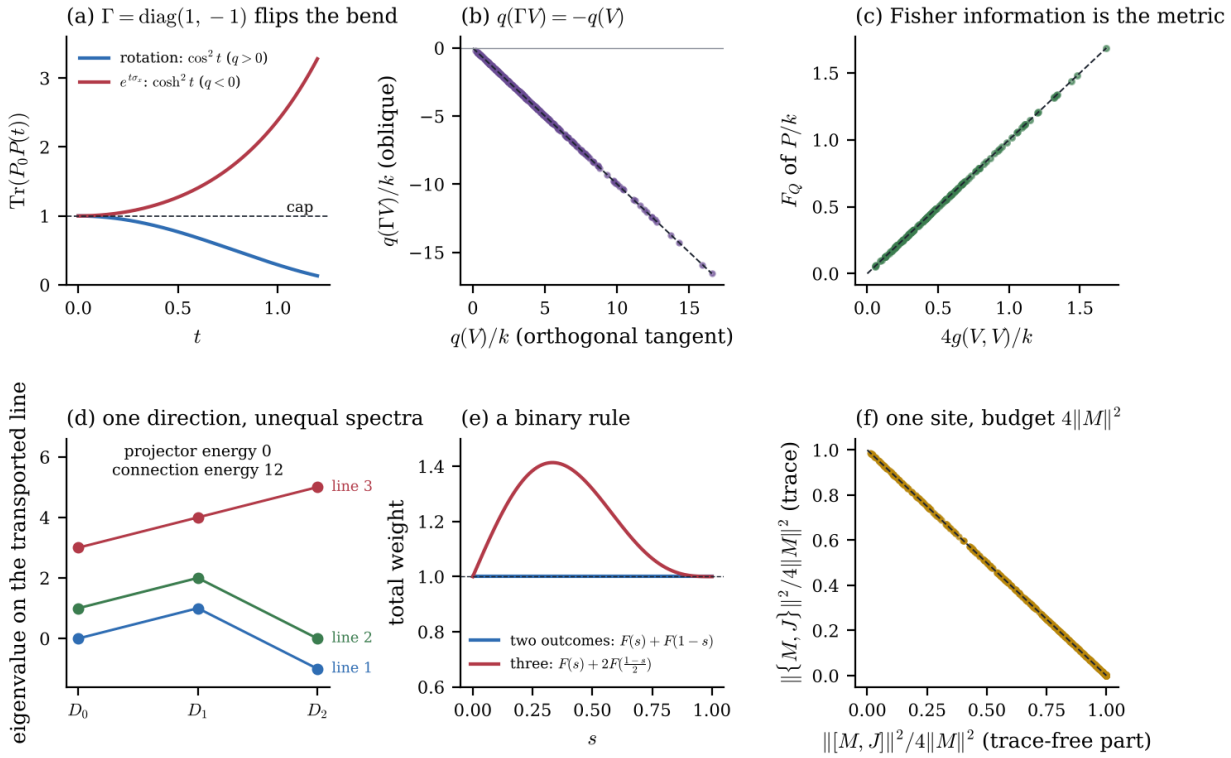


Figure 7: Overlaps and one edge. (a) The two exact curves through E_{11}: a rotation bends the overlap down as $\cos^2 t$, its partner under $\Gamma = \mathrm{diag}(1, -1)$ bends it up as $\cosh^2 t$, above the cap. (b) For random orthogonal-projector tangents, $q(\Gamma V) = -q(V)$. (c) The quantum Fisher information of P/k equals $4g(V, V)/k$. (d) Eigenlines transported exactly along a path, with unequal eigenvalues: the projector fields cost nothing, the field costs 12. (e) The binary rule $F(s) = s + \sin(2\pi s)/2\pi$ is consistent on two outcomes and fails on three. (f) One site with transport J: the two books of a symmetric M share the budget $4\|M\|^2$.

5 The constant

The opposite book was introduced to understand the offset and direction. A constant is invisible to the connection energy and is recorded by the opposite; a direction is a signed difference that both books erase and that Section 11 keeps. This section is the first half of that answer.

Split each block into its trace and trace-free parts, $D_i = c_i I + T_i$ with $\operatorname{Tr} T_i = 0$. Transport preserves the identity and the trace, and $\langle I, T\rangle = \operatorname{Tr} T = 0$, so both energies split with no cross term:

$$\mathcal{E}_A^{\mp}(D) = r \sum_{\{i,j\}\in E} (c_i \mp c_j)^2 + \sum_{\{i,j\}\in E} \big\| T_i \mp \mathcal{U}_{ij}(T_j) \big\|_F^2. \tag{30}$$

A uniform constant $c_i = c$ is invisible to the connection energy and adds $4rc^2$ per edge to the opposite. At the level of the operator, for real c,

$$\big[H + cI, (H + cI)^*\big] = [H, H^*], \qquad (H + cI)^2 - (H + cI)^{*2} = H^2 - H^{*2} + 4cA. \tag{31}$$

The self-commutator cannot see a constant; the opposite records it, multiplied by the transport. In the author's four-sector form $H_N(\varepsilon, \Lambda) = \Lambda I + A + D_0 + \varepsilon E$ [71], the baseline preload ΛI is this constant.

One site. The smallest case has one site and the transport $J = \left(\begin{smallmatrix} 0 & 1 \\ -1 & 0 \end{smallmatrix}\right)$. For a real symmetric 2×2 matrix M,

$$MJ + JM = (\operatorname{Tr} M)\, J, \qquad [M, J] = [M_0, J], \qquad \|[M, J]\|_F^2 + \|\{M, J\}\|_F^2 = 4\|M\|_F^2, \tag{32}$$

with M_0 the trace-free part: the opposite sees only the trace, the connection energy only the trace-free part, on the budget $4\|M\|_F^2$ (`SpectralStability.Coupling.anticomm_eq_trace`, `SpectralStability.Coupling.anticomm_traceless` [79]) [DERIVED; LEAN; COMPUTED] (Figure 7f).

Centered projectors. The same split moves the balance point of a projector field. Let P, Q be orthogonal projectors of rank k in $\mathbb{C}^r$, U unitary, $\rho = \operatorname{Tr}(PUQU^*)/k$, and center both, $D = P - \frac{k}{r} I$, $E = Q - \frac{k}{r} I$. Then

$$\big\|D - UEU^*\big\|_F^2 = 2k(1 - \rho), \qquad \big\|D + UEU^*\big\|_F^2 = 2k(1 + \rho) - \frac{4k^2}{r} \tag{33}$$

[DERIVED; COMPUTED]. The centered books balance at $\rho = k/r$, while the uncentered books (25) balance at $\rho = 0$. The connection energy is the same in both; only the opposite moves. So the scalar background must be declared before two balance conditions are compared. Section 10 uses (33) with $r = 2$, $k = 1$, where the books are $\big(2(1 - \rho), 2\rho\big)$ and balance at $\rho = \frac{1}{2}$.

A common clock. The author's Dirac Time paper calls a frame a common clock when the frame generator of (29) has the form $\dot{\tau} H_0 + aI$, with $\dot{\tau}$ and a real and H_0 fixed. Then the frame state advances by H_0 at rate $\dot{\tau}$ up to a scalar phase; every gap of the generator is $\dot{\tau}$ times the matching gap of H_0; and if H_0 is not scalar, the rate and the shift are unique [50] (Corollaries P4.1–P4.3; Atlas bridge B160 [68]; `DiracTime.MovingFrame.common_clock`, `DiracTime.CommonClock.co`

mmon_gap_scaling, DiracTime.CommonClock.rate_shift_unique [56]) [CITED; LEAN]. In the two books the two numbers do different things. With $H_0 = D + A$ and $G = \dot{\tau} H_0 + aI$,

$$[G, G^*] = \dot{\tau}^2 [H_0, H_0^*], \qquad G^2 - G^{*2} = \dot{\tau}^2 (H_0^2 - H_0^{*2}) + 4\dot{\tau} a\, A \tag{34}$$

[DERIVED; COMPUTED]. The shift a is the constant of (31): invisible to the connection energy, recorded by the opposite and multiplied by the transport. The rate is a common scale. Rescaling keeps every eigenvector (DiracTime.CommonClock.rescale_same_eigenvectors), so the Born matrices W_{ab} of (6) do not change, both books of a field $D \mapsto sD$ are multiplied by s^2, and every ratio of books, Γ_e, p_e and V_e among them, is unchanged [DERIVED; COMPUTED]. At the level of the operator, $\|[cX, (cX)^*]\|^2 = c^4 \|[X, X^*]\|^2$ and the normalised stress does not see c (MatterAtAScale.stress_scales, MatterAtAScale.departure_span_free [80]). No ratio of the books can fix a clock rate. The rate is read only against a declared non-scalar reference generator; with $H_0 = I$ the rates 1 and 0 give the same generator. The same blindness is why a horizon need not be a projector wall: the model local symbol $N(r)(k\sigma_x + m\sigma_z)$, $N = 1 - 2M/r$, has band projectors independent of the lapse N for $r > 2M$, and only the coordinate gap closes [33] [CITED].

6 The scalar shore

With $r = 1$ and edge weights $w_{ij} = |A_{ij}|^2$ (the identities above hold for scalar edges of any modulus once the weight is kept), the two energies are quadratic forms in $d = (d_i)$:

$$\tfrac{1}{8}\|[H, H^*]\|_F^2 = d^\top L_w d = \sum_E w_{ij}(d_i - d_j)^2, \qquad \tfrac{1}{8}\|H^2 - H^{*2}\|_F^2 = d^\top Q_w d = \sum_E w_{ij}(d_i + d_j)^2, \tag{35}$$

with L_w the weighted Laplacian and Q_w the weighted signless Laplacian. The first gives the Fiedler bound $\|[H, H^*]\|_F^2 \geq 8\lambda_2(L_w)\|d\|^2$ only after $d \perp \mathbf{1}$, because constants cost nothing. The second needs no projection: $\|H^2 - H^{*2}\|_F^2 \geq 8\lambda_{\min}(Q_w)\|d\|^2$ for every d, and $\lambda_{\min}(Q_w) = 0$ exactly when G has a bipartite component, the number of zero eigenvalues being the number of bipartite components (an isolated vertex counts as one). So the opposite has a spectral gap precisely on graphs where every component contains an odd cycle.

The same incidence structure decides what the books of the single edges fix. Added, the two books of an edge give its budget, $\frac{1}{2}(\mathcal{E}_e^- + \mathcal{E}_e^+) = \|D_i\|_F^2 + \|D_j\|_F^2$ by (7), which is the unsigned incidence matrix applied to the vertex norms. On a connected graph that matrix has full rank exactly when the graph has an odd cycle. So on a graph with an odd loop the edge books return every vertex norm, while on a bipartite graph one direction, $+t$ on one side and $-t$ on the other, is invisible [DERIVED; COMPUTED] (Figure 9b). Odd loops make the distribution of the budget visible.

The Fiedler bound has a matrix form. Since $\mathcal{E}_A^-(D) = \langle D, L_U D\rangle$ for the connection Laplacian L_U on $\mathrm{Herm}(r)^n$, any field satisfies

$$\operatorname{dist}\left(D, \ker L_U\right)^2 \leq \frac{\mathcal{E}_A^-(D)}{\lambda_+(L_U)}, \tag{36}$$

with λ_+ the least positive eigenvalue, and equality on its eigenvector: a small connection energy holds the field close to a parallel one [DERIVED; COMPUTED] (Figure 9c).

7 A twisted ring

Take a ring of N vertices, $r = 2$, fields in one plane, $D_k = \cos\vartheta_k\,\sigma_z + \sin\vartheta_k\,\sigma_x$, and each edge turning that plane by $\varphi = d/N$, so the ring carries total twist d. Each edge contributes $4(1-\cos x_k)$ to the connection energy and $4(1+\cos x_k) = 4(1-\cos(x_k+\pi))$ to the opposite, where $x_k = \vartheta_k - \vartheta_{k+1} - \varphi$ and $\sum_k x_k \equiv -d \pmod{2\pi}$. The opposite is the same ring with the twist moved by $N\pi$. The lowest reachable energies over in-plane fields are

$$\min\mathcal{E}^- = \min_{w\in\mathbb{Z}} 4N\Big(1-\cos\frac{d-2\pi w}{N}\Big), \qquad \min\mathcal{E}^+ = \min_{w\in\mathbb{Z}} 4N\Big(1-\cos\frac{d+N\pi-2\pi w}{N}\Big), \tag{37}$$

attained by sharing the twist equally among the edges [DERIVED]. For even N the shift $N\pi$ is a whole number of turns and the two floors coincide. For odd N it is a half turn, and the floors interleave: whatever twist frustrates one energy, the other is nearly free. The worst case of the lower of the two over all twists drops from $4N(1-\cos(\pi/N))$ to $4N(1-\cos(\pi/2N))$, about a quarter (Figure 8). At $d = \pi$ two windings tie, and the floor of $\mathcal{E}^-$ has a corner there, with slope $4\sin(\pi/N)$ from the left and $-4\sin(\pi/N)$ from the right; at $d = 0$ it is smooth [DERIVED; COMPUTED] (Figure 9e).

In Born terms the ring reads more simply. The rank-one projectors $P_k = \frac{1}{2}(I + D_k)$ have $p_k = \frac{1}{2}(1+\cos x_k)$, and with δ the total twist folded into $[-\pi,\pi]$,

$$\max\sum_k p_k = \frac{N}{2}\Big(1+\cos\frac{\delta}{N}\Big). \tag{38}$$

Writing $z_k = e^{i\vartheta_k}$, the total is $\frac{N}{2} + \frac{1}{2}\operatorname{Re}\sum_k \bar z_k e^{-i\varphi} z_{k+1}$, a Rayleigh quotient of the Hermitian part of the twisted cyclic shift over vectors of norm $\sqrt{N}$. That part has eigenvalues $\cos\frac{2\pi j - d}{N}$, and its top eigenvector is a Fourier mode with unit-modulus entries, so the bound is attained inside the ring's own field family. This proves the equal share of (37) [DERIVED; COMPUTED].

The frustration of this ring comes from keeping the field in one real plane. A complex rank-one projector escapes it: $\frac{1}{2}(I+\sigma_y)$ is fixed by every rotation in the z–x plane, so every edge reaches $p = 1$. More generally a single loop never frustrates complex subspace fields: its unitary holonomy has invariant subspaces of every rank, and transporting one around the graph makes the connection energy vanish. Genuine frustration needs several loops whose holonomies share no invariant subspace. For rank-one fields in $\mathbb{C}^2$ on two triangles joined at a vertex, with tree edges trivial and closing holonomies σ_x and σ_z, the least connection energy is

$$\min\mathcal{E}^- = 6 - 3\sqrt{3} \approx 0.804, \tag{39}$$

and for two triangles sharing an edge with the same holonomies it is $4 - 2\sqrt{2} \approx 1.172$ [DERIVED; COMPUTED]. With both closing holonomies σ_z, which share an invariant line, the least energy is zero (Figure 4).

Two different obstructions must be kept apart here. A loop admits a positive metric in which its holonomy is unitary exactly when the holonomy is diagonalisable with spectrum on the unit circle; for a Jordan block W, $W^*\eta W = \eta$ forces $\eta_{11} = 0$. The second obstruction is the absence of a common invariant subspace. The bow ties pass the first test, since σ_x and σ_z are unitary, and fail the second: every rank-one $P = \frac{1}{2}(I + n\cdot\sigma)$ has $\|[P,\sigma_x]\|_F^2 + \|[P,\sigma_z]\|_F^2 = 2(1+n_y^2) \geq 2$ [DERIVED; COMPUTED]. The frustration of (39) is of the second kind (Figure 4, right); the non-unitary transports of Section 8 meet the first.

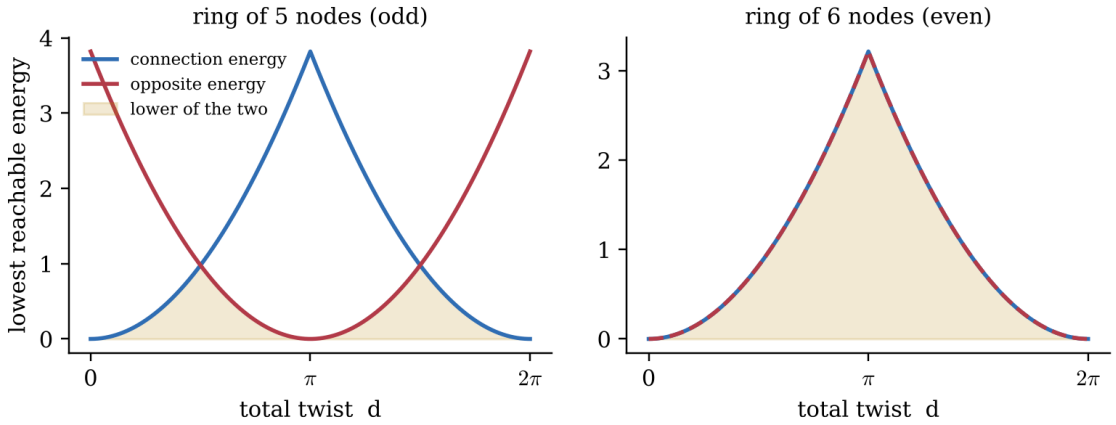


Figure 8: The lowest reachable energy on a twisted ring, against the total twist. On an odd ring (left) the two energies take turns, and the lower of the two (shaded) never rises far. On an even ring (right) they coincide.

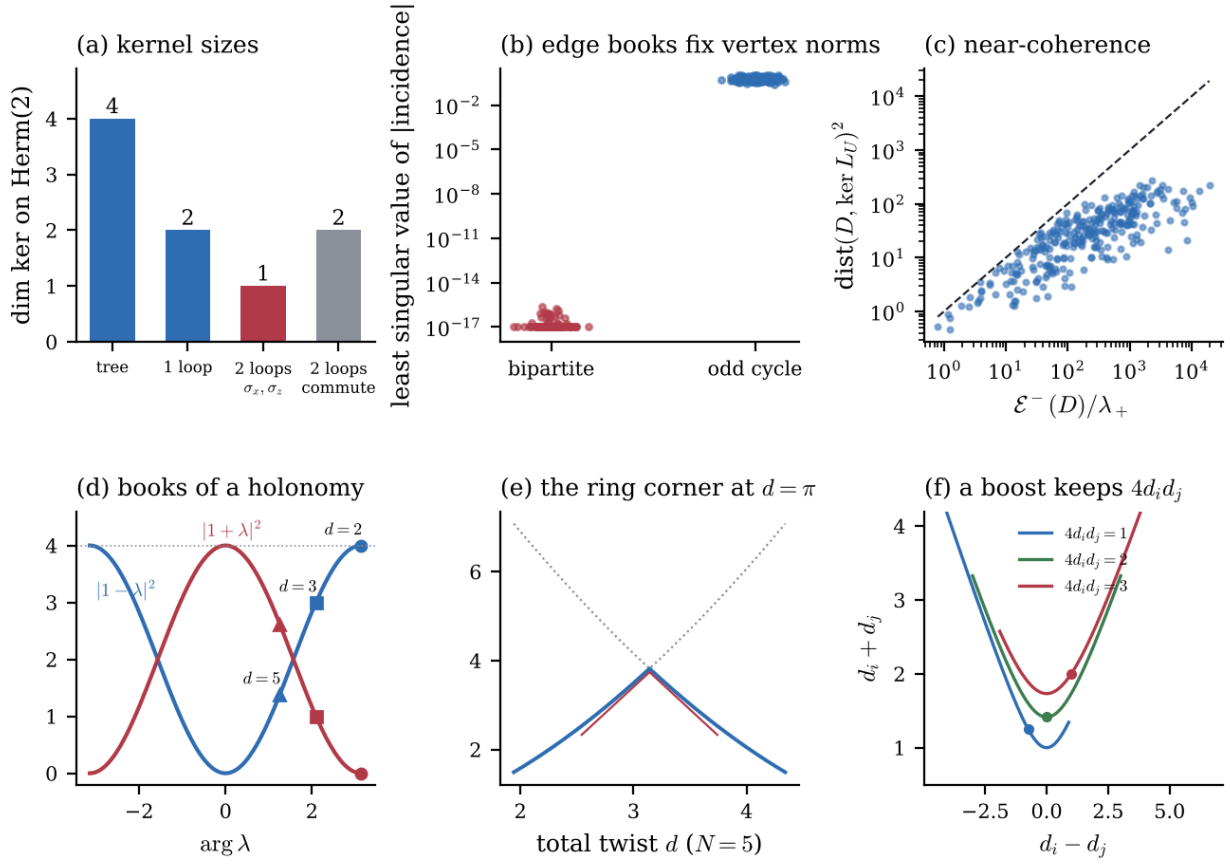


Figure 9: Graph relations. (a) The kernel of the connection energy on Herm(2): 4 on a tree, 2 on one loop, 1 on two loops with holonomies σ_x, σ_z, and 2 again when the two holonomies commute. (b) The least singular value of the unsigned incidence matrix of random connected graphs: zero exactly on bipartite graphs, so on graphs with an odd cycle the edge books return the vertex norms. (c) The matrix Fiedler bound (36): every random field lies below the diagonal. (d) The two books of a unit holonomy eigenvalue on the budget 4, with the clock relators for $d = 2, 3, 5$; at $d = 2$ the guard closes. (e) The ring floor of $\mathcal{E}^-$ for $N = 5$: two windings tie at $d = \pi$, with one-sided slopes $\pm 4 \sin(\pi/N)$. (f) Boosts move a scalar edge along the hyperbola of fixed $4d_id_j$.

8 Graph primes between the two books

The two energies can be read off one generating function. Let ρ assign to each oriented edge $i \to j$ an invertible $d \times d$ matrix ρ_{ij} with $\rho_{ji} = \rho_{ij}^{-1}$. Two choices matter here. The gain transport $\rho_{ij} = A_{ij}$ acts on vectors, with $d = r$. The induced transport $\rho_{ij} = \mathcal{U}_{ij} = \mathrm{Ad}\, A_{ij}$ acts on $\mathrm{Herm}(r)$, with $d = r^2$; it is orthogonal for $\langle X, Y\rangle = \mathrm{Tr}(XY)$, and the central sign of $A_{ji} = -A_{ij}^*$ drops out. Let B_ρ be the non-backtracking arc matrix: its block from arc e to arc f is $\rho(f)$ when the head of e is the tail of f and f is not the reverse of e. A prime P is a class of primitive closed non-backtracking walks without tail, of length $\ell(P)$ and holonomy $\rho(P)$; the two orientations of a cycle are different primes. The twisted zeta function is

$$\zeta_\rho(u) = \prod_P \det\left(I - \rho(P)\, u^{\ell(P)}\right)^{-1} = \det\left(I - uB_\rho\right)^{-1}, \qquad \log \zeta_\rho(u) = \sum_{n\geq 1} \tfrac{u^n}{n} \,\mathrm{Tr}\, B_\rho^n, \tag{40}$$

the product and the series converging for $|u|\,\|B_\rho\| < 1$ [19, 20, 21, 22, 23, 24, 25] [KNOWN]. These graph primes are closed walks. They are not the prime integers; those enter in Section 9. Bass's determinant formula carries over to the twisted case [21, 23, 26]. With n vertices, m edges, Deg the degree matrix and A_ρ the block matrix with ρ_{ij} on each oriented edge,

$$\begin{aligned} \det\left(I - uB_\rho\right) &= (1-u^2)^{(m-n)d}\, P_\rho(u), \qquad P_\rho(u) = \det K_\rho(u), \\ K_\rho(u) &= I - uA_\rho + u^2(\mathrm{Deg} - I) \otimes I_d \end{aligned} \tag{41}$$

[KNOWN; COMPUTED]. Call K_ρ the Bass pencil. A proof in finite matrices, by Sylvester's determinant identity, is in the appendix; it needs only $\rho_{ji}\rho_{ij} = I$. The check finds agreement to 4.5×10^{-15} on random graphs with gain and induced transports, and to 1.4×10^{-15} with non-unitary ρ, as long as $\rho_{ji} = \rho_{ij}^{-1}$. When the reverse arc carries $\overline{\rho_{ij}}$ with $|\rho_{ij}| \neq 1$ instead, the formula fails on every graph tried. The backtracking term needs $\rho_{ji}\rho_{ij} = I$ [COMPUTED]. So a failure seen with non-unitary weights is a failure of inverse reversal or of the degree correction, not of non-unitarity as such.

The two ends. The factor $(1-u^2)^{(m-n)d}$ puts poles of ζ_ρ at $u = +1$ and $u = -1$ whenever $m > n$. So the zeta itself is not the energy at either end. What carries the two values is the pencil. At $u = \pm 1$ it is a matrix, not only a determinant:

$$K_\rho(+1) = \mathrm{Deg} \otimes I - A_\rho =: L^-, \qquad K_\rho(-1) = \mathrm{Deg} \otimes I + A_\rho =: L^+, \tag{42}$$

and $P_\rho(\pm 1) = \det L^\mp$ [DERIVED; COMPUTED]. The check finds $\det(I - B_\rho) = 0$ on every graph tried with $m > n$, while $\det(I - uB_\rho)/(1-u^2)^{(m-n)d}$ tends to $\det K_\rho(1)$ [COMPUTED]. For the induced transport the two ends are the two books. On fields $D = (D_i)$ with $D_i \in \mathrm{Herm}(r)$, expanding each edge,

$$\langle D, L^- D\rangle = \sum_E \left\|D_i - \mathcal{U}_{ij}(D_j)\right\|_F^2 = \mathcal{E}_A^-(D), \qquad \langle D, L^+ D\rangle = \sum_E \left\|D_i + \mathcal{U}_{ij}(D_j)\right\|_F^2 = \mathcal{E}_A^+(D) \tag{43}$$

[DERIVED; COMPUTED]. The check compares these with $\frac{1}{8}\|[H, H^*]\|^2$ and $\frac{1}{8}\|H^2 - H^{*2}\|^2$ computed from the full $H = D + A$, to 1.1×10^{-15}. So the $u = +1$ end of the Bass pencil is the connection-energy operator, and the $u = -1$ end is its opposite (Figure 11). Both operators are positive semidefinite. An end is singular exactly when its book has a nonzero field of zero energy, which is (4) at $u = +1$ and (16) at $u = -1$ [DERIVED]. For the induced transport the constant field $D_i = I$

is always parallel, so $P_{\mathrm{Ad}}(+1) = 0$ on every graph. This is the constant of Section 5, invisible to the connection energy, now seen as a zero of the pencil's $u = +1$ end [DERIVED; COMPUTED]. The $u = -1$ end vanished on every bipartite graph tried, where σI is anti-parallel, and on none of the non-bipartite ones [COMPUTED].

The sign is the parity of the prime. Since $B_{-\rho} = -B_\rho$,

$$\zeta_\rho(-u) = \zeta_{-\rho}(u), \qquad \det\big(I - \rho(P)(-u)^{\ell(P)}\big) = \det\big(I - (-1)^{\ell(P)}\rho(P)\,u^{\ell(P)}\big). \tag{44}$$

Replacing u by $-u$ multiplies the holonomy of every prime by $(-1)^{\ell(P)}$ [DERIVED; COMPUTED]. The check confirms $\operatorname{Tr} B_{-\rho}^k = (-1)^k \operatorname{Tr} B_\rho^k$ for $k \le 8$, exactly. So the $u = -1$ end of K_ρ is the $u = +1$ end of the sign-twisted transport $-\rho$. That is the transport whose connection energy is the opposite (Section 3). On a bipartite graph every prime is even, so $\zeta_\rho(-u) = \zeta_\rho(u)$ and the two ends agree, as the swap (17) says. On the bipartite double cover, with each lifted edge carrying the same ρ,

$$\zeta_{\tilde\rho}(u) = \zeta_\rho(u)\,\zeta_\rho(-u) \tag{45}$$

[DERIVED; COMPUTED]. This is the zeta form of (18): the cover holds both ends at once. The factorisation is the standard splitting of a cover's zeta into the L-functions of the deck group [23]. The check confirms it to 1.0×10^{-15}. It is a statement about graphs. A quadratic character on arithmetic primes also attaches signs to primes, but those signs vary with the prime (Section 9). Finally, the induced transport preserves the splitting $\mathrm{Herm}(r) = \mathbb{R}I \oplus \{\operatorname{Tr} X = 0\}$, so ζ_{Ad} always contains the plain zeta of G as a factor [DERIVED; COMPUTED].

The books of a holonomy. For the gain transport the two books of a loop are those of its holonomy spectrum. If $Wv = \lambda v$ with $\|v\| = 1$ and $|\lambda| = 1$, then

$$\begin{aligned} \|v - Wv\|^2 &= |1-\lambda|^2, & \|v + Wv\|^2 &= |1+\lambda|^2, \\ |1-\lambda|^2 + |1+\lambda|^2 &= 4, & |1+\lambda|^2 - |1-\lambda|^2 &= 4\operatorname{Re}\lambda \end{aligned} \tag{46}$$

(`NonNormality.normSq_one_sub_add_normSq_one_add`, `NonNormality.normSq_one_add_sub_normSq_one_sub` [67]; in matrix form `LightBridges.graph_parallelogram` [61]) [DERIVED; LEAN; COMPUTED]. The author's projector-geometry paper names the two for a relator $R = UVU^*V^*$: the defect $\delta = \text{mean}\,|\lambda - 1|^2$ and the guard $g^2 = \min|\lambda + 1|^2$ over the spectrum of R, with $\delta + g^2 \le 4$ [73] (`UPGTorusAnchor.unit_defect_add_guard` [74]; Atlas bridge B128 [68]). For the clock and shift in dimension d the relator is the scalar $e^{2\pi i/d}$, with defect $4\sin^2(\pi/d)$ and guard $4\cos^2(\pi/d)$. At $d = 2$ the relator is $-I$ and the guard closes (`UPGTorusAnchor.clock_refused_at_two`): the opposite book of the holonomy is empty, the gain-side twin of an anti-parallel field (15) [CITED; LEAN; COMPUTED] (Figure 9d).

The mirror and the circle. On a $(q+1)$-regular graph, $\mathrm{Deg} = (q+1)I$ and the pencil itself has a mirror. For $u \neq 0$,

$$K_\rho\big(1/(qu)\big) = (qu^2)^{-1} K_\rho(u) \tag{47}$$

[DERIVED; COMPUTED], as a matrix identity, to 2.2×10^{-15} on cubic graphs with unitary and with non-unitary twists. Taking determinants, with $P_\rho(u) = \prod_\lambda (1 - \lambda u + qu^2)$ over the $N = nd$ eigenvalues λ of A_ρ,

$$P_\rho(u) = (qu^2)^N\, P_\rho\big(1/(qu)\big) \tag{48}$$

[DERIVED; COMPUTED]. The check confirms this to 2.6×10^{-14} on 1000 random regular graphs with unitary twists. The mirror uses only $\rho_{ji} = \rho_{ij}^{-1}$, not unitarity: it holds to 1.4×10^{-15} with non-unitary twists. On non-regular graphs no value of q gives a mirror; the best error over $q \in [0.5, 4]$ stays above 0.33 for the determinant and above 1.7 for the pencil [COMPUTED]. Unitarity supplies something else: a Hermitian A_ρ, real λ, and a positive connection form. The roots of $1 - \lambda u + qu^2$ have product $1/q$. When λ is real, both roots lie on the circle $|u| = 1/\sqrt{q}$ exactly when $|\lambda| \le 2\sqrt{q}$; otherwise they are a real pair, one inside and one outside. So

$$\#\{\text{zeros of } P_\rho \text{ off } |u| = 1/\sqrt{q}\} = 2\,\#\{\lambda \in \operatorname{spec} A_\rho : \ |\lambda| > 2\sqrt{q}\} \tag{49}$$

[DERIVED; COMPUTED]. This held in 1000 of 1000 trials. With non-unitary twists, λ becomes complex and the zeros leave the circle (all of them did in the trials) while staying in mirror pairs [COMPUTED]. For the untwisted graph, (49) is the classical statement that G is Ramanujan exactly when its zeta satisfies the graph Riemann hypothesis [19, 20, 22, 25, 29] [KNOWN]. The control, the plain Petersen graph, has 18 zeros on $|u| = 2^{-1/2}$ and two at $u = \frac{1}{2}$ and 1. Counting zeros or poles in this way needs the prefactor and the trivial modes to be removed or counted explicitly, as here. For a twisted graph the same reading holds with spec A_ρ in place of the adjacency spectrum. For signings this is the condition studied by Bilu and Linial and by Marcus, Spielman and Srivastava [12, 30] [KNOWN]. The coalescence $\lambda^2 = 4q$, where the two roots meet on the real axis, is a boundary of this transfer polynomial. It is a different condition from the balance of the Frobenius books of Section 9; below it is the balance of the two halves of a companion matrix.

A minimal solution off the circle. Each eigenvalue also leaves a sequence in the prime counts. Put $u = z/\sqrt{q}$, so that $1 - \lambda u + qu^2 = 1 - cz + z^2$ with $c = \lambda/\sqrt{q}$. Taking logarithms in (41),

$$\operatorname{Tr} B_\rho^\ell = \sum_{\lambda \in \operatorname{spec} A_\rho} q^{\ell/2}\, t_\ell\big(\lambda/\sqrt{q}\big) + (m-n)d\big(1 + (-1)^\ell\big), \qquad t_\ell = c\,t_{\ell-1} - t_{\ell-2}, \quad t_0 = 2,\ t_1 = c, \tag{50}$$

so $t_\ell(c) = 2T_\ell(c/2)$ is the normalised share of one eigenvalue in the length-ℓ prime traces [DERIVED; COMPUTED]. The check confirms (50) for $\ell \le 8$ on twisted cubic graphs with $d = 2$, to 1.1×10^{-13}. Read it as a three-term recurrence. Its solutions are spanned by z_1^ℓ and z_2^ℓ, the roots of $z^2 - cz + 1$, with $z_1 z_2 = 1$. If $|c| > 2$ the roots are real, $|\lambda_s| < 1 < |\lambda_d|$, and $Z_\ell = \lambda_s^\ell$ is a minimal solution: $Z_\ell / D_\ell \to 0$ for every independent D. Pincherle's theorem [53, 54] then says that the continued fraction

$$c - \cfrac{1}{c - \cfrac{1}{c - \cdots}}, \qquad \frac{P_n}{Q_n} = \frac{U_n(c/2)}{U_{n-1}(c/2)} \ \longrightarrow\ c - \frac{Z_1}{Z_0} = \lambda_d, \tag{51}$$

converges, with error of order $(\lambda_s/\lambda_d)^n$ [KNOWN; COMPUTED]. If $|c| < 2$, write $c = 2\cos\theta$. Every solution is $A\cos\ell\theta + B\sin\ell\theta$, no ratio of two independent solutions tends to zero, and there is no minimal solution. The convergents $\sin((n+1)\theta)/\sin n\theta$ never settle, and when θ/π is rational some denominators $Q_n = \sin n\theta/\sin\theta$ vanish [DERIVED; COMPUTED]. At $|c| = 2$ the roots meet; $Z_\ell = (\pm 1)^\ell$ is minimal against $D_\ell = \ell(\pm 1)^\ell$, but only polynomially, and the convergents approach ± 1 with error $1/n$ [DERIVED; COMPUTED]. By (49), then, a zero of P_ρ lies off the circle $|u| = 1/\sqrt{q}$ exactly when the recurrence of its eigenvalue has a geometrically minimal solution, and the twisted graph Riemann hypothesis says that no eigenvalue has one, apart from trivial modes counted separately [DERIVED; COMPUTED]. The check runs the continued fraction for every eigenvalue of 200 cubic graphs (Figure 10), plain and with random $U(1)$ twists: it converges for exactly the

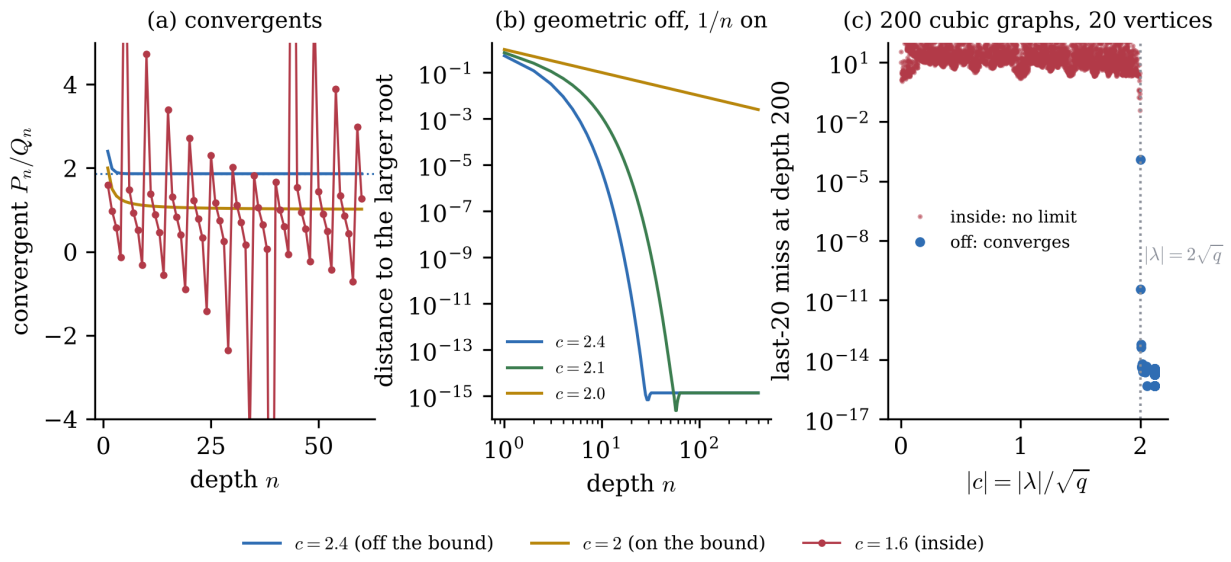


Figure 10: The prime-trace recurrence of one eigenvalue, read as the continued fraction (51). (a) Off the bound the convergents settle on the larger root (dotted); on the bound they creep to 1; inside they never settle. (b) Off the bound the error falls geometrically, faster the further c sits from 2; on the bound it falls like $1/n$. (c) Every eigenvalue of 200 cubic graphs on 20 vertices, half of them with random $U(1)$ twists, $q = 2$: the continued fraction converges exactly for the eigenvalues with $|\lambda| > 2\sqrt{q}$, and misses by order one for all the others.

$|\lambda| > 2\sqrt{q}$ ones, in 2400 of 2400 cases. The convergence direction of Pincherle's theorem is machine-checked for real coefficients in the author's library [57] (`RamanujanChallenge.pincherle`); with constant coefficients its hypotheses are met by the explicit solutions λ_s^n and λ_d^n, which is `RamanujanChallenge.pincherle_of_ratio` with exact ratios [CITED; LEAN]. The same library shows why minimality must ask the dominant solution to be eventually nonzero: `RamanujanChallenge.technion_pincherle_fails` gives period-two coefficients for which $Z_n = 2^{-n}$ solves the recurrence, the denominators Q_n vanish at every even n, the odd convergents tend to 8, and the convergents have no limit [CITED; LEAN; COMPUTED]. Inside the bound with θ/π rational the denominators vanish in the same periodic way.

The companion and the wall. The author's companion-matrix diagnostic [58] follows a recurrence through its companion matrix M, the stress $\Phi = \frac{1}{2}\|[M, M^\top]\|_F^2$ and the norm of the Riesz projector onto the dominant eigenline. For (50), $M = \left(\begin{smallmatrix} c & -1 \\ 1 & 0 \end{smallmatrix}\right)$, and its traceless part $T = M - \frac{c}{2}I$ is a real traceless 2×2 matrix:

$$T^2 = \left(\frac{c^2}{4} - 1\right) I, \qquad \|\operatorname{Herm} T\|_F^2 = \frac{c^2}{2}, \qquad \|\operatorname{Skew} T\|_F^2 = 2, \qquad \Phi = 4c^2 \tag{52}$$

[DERIVED; COMPUTED]. So $q(T) = \frac{1}{2}(\|\operatorname{Herm} T\|^2 - \|\operatorname{Skew} T\|^2) = c^2/4 - 1$, the trace form of Section 10. The Hermitian half wins exactly off the bound, where the recurrence has a growing and a decaying solution. The skew half wins inside it, where the solutions turn. At the coalescence $\lambda^2 = 4q$ the halves balance and T is a nonzero nilpotent, the wall of Section 10 [DERIVED; COMPUTED]. The single-step stress $\Phi = 4c^2$ has no mark at $|c| = 2$, and at $c = 0$, inside the bound, M is normal.

The accumulated stress of the same diagnostic does mark it. For $|c| > 2$ the normalised powers $M^N/\|M^N\|_F$ tend to $B = uv^\top$, with u and v the unit right and left dominant eigenvectors, and

$$\Phi_\infty = \tfrac{1}{2}\big\|[B, B^\top]\big\|_F^2 = 1 - (u \cdot v)^2 = \frac{4}{c^2}, \tag{53}$$

which rises to 1 exactly at $|c| = 2$, where $u = (1, \pm 1)/\sqrt{2}$ and $v = (1, \mp 1)/\sqrt{2}$ become orthogonal [DERIVED; COMPUTED]. So the bound is seen by the sign of the trace form and by the accumulated stress, not by the stress of one step (Figure 18e). The Riesz projector sees it too. For $|c| > 2$ the projector P_d onto the λ_d eigenline has

$$\|P_d\|_F\,(\lambda_d - \lambda_s) = \|M - \lambda_s I\|_F \;\longrightarrow\; \|M - \lambda I\|_F = 2 \qquad (|c| \to 2), \tag{54}$$

so a single eigenline diverges like the inverse gap, while the pair projector, here the identity, and $\det M = 1$ do not move [DERIVED; COMPUTED]. This is the law the author's black-hole paper finds at its Jordan points (Section 10).

The triangle and the cubic record. The books are quadratic. A primitive cycle carries a number that is not. Let F be the unitary three-point Fourier matrix and $x = (x_1, x_2, x_3)$ real. Then $\Phi = F\,\mathrm{diag}(x)F^*$ is the Hermitian circulant

$$\Phi = \begin{pmatrix} d & z & \bar{z} \\ \bar{z} & d & z \\ z & \bar{z} & d \end{pmatrix}, \qquad d = \frac{x_1 + x_2 + x_3}{3}, \quad z = te^{i\phi},\ t \geq 0, \tag{55}$$

after an orientation convention, with eigenvalues $d + 2t\cos(\phi + 2\pi j/3)$, $j = 0, 1, 2$ [37]. Direct trace and determinant calculations give

$$\begin{aligned} \mathrm{Tr}\,\Phi^2 &= 3d^2 + 6t^2, & e_2 &= \textstyle\sum_{i<j} x_i x_j = 3(d^2 - t^2), \\ e_3 &= x_1x_2x_3 = d^3 - 3dt^2 + 2t^3\cos 3\phi, & \mathrm{Tr}\,\Phi^3 &= 3d^3 + 18dt^2 + 6t^3\cos 3\phi \end{aligned} \tag{56}$$

[DERIVED; COMPUTED]. The quadratic data fix d and t. The angle enters only through $\cos 3\phi$, at third order.

Theorem 2 (Primitive-cycle completion)**.** *Put the $U(1)$ connection $e^{i\phi}$ on each oriented edge of a triangle, in one sense of rotation, and $e^{-i\phi}$ on each reverse edge. Its two primitive cycles have holonomies $e^{\pm 3i\phi}$, and*

$$\zeta_\phi(u)^{-1} = (1 - e^{3i\phi}u^3)(1 - e^{-3i\phi}u^3) = 1 - C_3u^3 + u^6, \qquad C_3 = 2\cos 3\phi. \tag{57}$$

The data (d, t, C_3) recover the unordered spectrum of Φ:

$$e_3 = d^3 - 3dt^2 + t^3C_3, \qquad \det(vI - \Phi) = (v - d)^3 - 3t^2(v - d) - t^3C_3. \tag{58}$$

[DERIVED; COMPUTED]. The coefficient of u^3 in $\log\zeta_\phi$ is C_3, and there are no terms of order one or two. The quadratic information fixes d and t; the first primitive cycle supplies the cubic invariant. This is the precise sense in which a graph prime completes a two-book record. It does not say that any prime generates masses. The check confirms (57) to 4.5×10^{-15} and the recovery of the spectrum from (d, t, C_3) to 1.7×10^{-12} (Figure 16d).

Which transports keep the cycle. The representation has to be declared. A scalar phase has trivial adjoint action, $\mathrm{Ad}(e^{i\phi} I) = 1$, so the induced transport of a scalar connection cannot carry the phase of (57) at all [DERIVED; COMPUTED]. A noncentral one can.

Proposition 3 (A noncentral rank-two realisation)**.** *Let $U = \mathrm{diag}(e^{i\phi}, 1)$ on every forward edge of the triangle, U^* on every reverse edge. On $\mathrm{End}(\mathbb{C}^2)$ the holonomy $\mathrm{Ad}(U^3)$ has eigenvalues $1, 1, e^{3i\phi}, e^{-3i\phi}$, so*

$$\mathrm{Tr}\,\mathrm{Ad}(U^3) = 2 + C_3, \qquad \zeta_{\mathrm{Ad}\,U}(u)^{-1} = (1-u^3)^4\,(1 - C_3 u^3 + u^6)^2. \tag{59}$$

The field $D_i = \sigma_z$ at all three vertices has books $(\mathcal{E}^-, \mathcal{E}^+) = (0, 24)$ for every ϕ.

[DERIVED; COMPUTED]. So one graph with one field and the same two books can carry different cycle coefficients, and with them different reconstructed spectra. The full connection, or a holonomy probe, supplies what that field's energies do not. Adding such a reference channel changes the representation. It cannot recover a sign that was discarded before the channel was supplied; Section 9 meets exactly that case.

Climb or swap. Twist one edge by a complex parameter, $\rho_{ij} \mapsto w\rho_{ij}$ and $\rho_{ji} \mapsto w^{-1}\rho_{ji}$, and follow the non-trivial eigenvalues of B_ρ around a loop in w. Around a single exceptional point they always swap in pairs. Where symmetry does not prevent it, the swaps chain together: on K_4 with random gains, the swaps around the exceptional points reach all eight moving eigenvalues, and a loop around two of them carries one eigenvalue through a cycle of four. With trivial gains the same graph splits into separate orbits [COMPUTED]. Across nine families of graphs and twists, generic gains always gave one orbit, swaps were typical and climbs a minority (about 10 to 50% of the loops around two exceptional points), and the Petersen graph with trivial gains only swapped [COMPUTED; EXPLORATORY]. The local mechanism is the normal form $\left(\begin{smallmatrix} 0 & 1 \\ \delta & 0 \end{smallmatrix}\right)$: its square-root branch swaps after one loop and returns after two, while the product of the pair stays branch-free (`Suns.exchange_one_loop`, `Suns.restore_two_loops` [83]). The name and the idea, that how loops permute a family of exceptional points labels the family, are the author's Atlas bridge B178 [68]. These are statements about this family. No universal monodromy law, and no arithmetic statement, is drawn from them.

A frustration signal in the prime counts. Prime counts can also be sorted, in the spirit of murmurations [44]. For a signing s of a $(q+1)$-regular graph, the Bass formula gives the length-ℓ prime traces from the spectrum of the signed adjacency A_s; normalise them as $a_\ell = \langle t_\ell(\lambda/\sqrt{q})\rangle_\lambda$ with $t_0 = 2$, $t_1 = c$, $t_\ell = c\,t_{\ell-1} - t_{\ell-2}$. Flipping every sign obeys $a_\ell(-s) = (-1)^\ell a_\ell(s)$ exactly, the parity of the primes again [DERIVED; COMPUTED]. Sort random signed graphs into two classes and compare the class averages, $\Delta_\ell = \langle a_\ell\rangle_+ - \langle a_\ell\rangle_-$. Sorted by the sign of $\det A_s$, nothing separates: permutation $p = 0.25$ to 0.91 in six families of cubic and quartic graphs. Sorted by the parity of the frustration index, cubic graphs split: $\Delta_\ell > 0$ for $\ell = 3, \ldots, 9$, with z up to 8.9 at $n = 16$ and 7.0 at $n = 20$ (permutation $p = 0.005$), while the class profiles stay correlated at $+0.91$ to $+0.97$, so the effect is a shift, not a mirror. Quartic graphs show none ($p = 0.41$) [COMPUTED; EXPLORATORY]. The mechanism is open.

What is classical and what is new. The twisted zeta, the Bass formula and its matrix-weighted forms, the cover factorisation and the graph Riemann hypothesis are classical [19, 20, 21, 22, 23, 24, 25, 26]. That the twisted zeta's $u = 1$ value is the determinant of a twisted Laplacian is known for

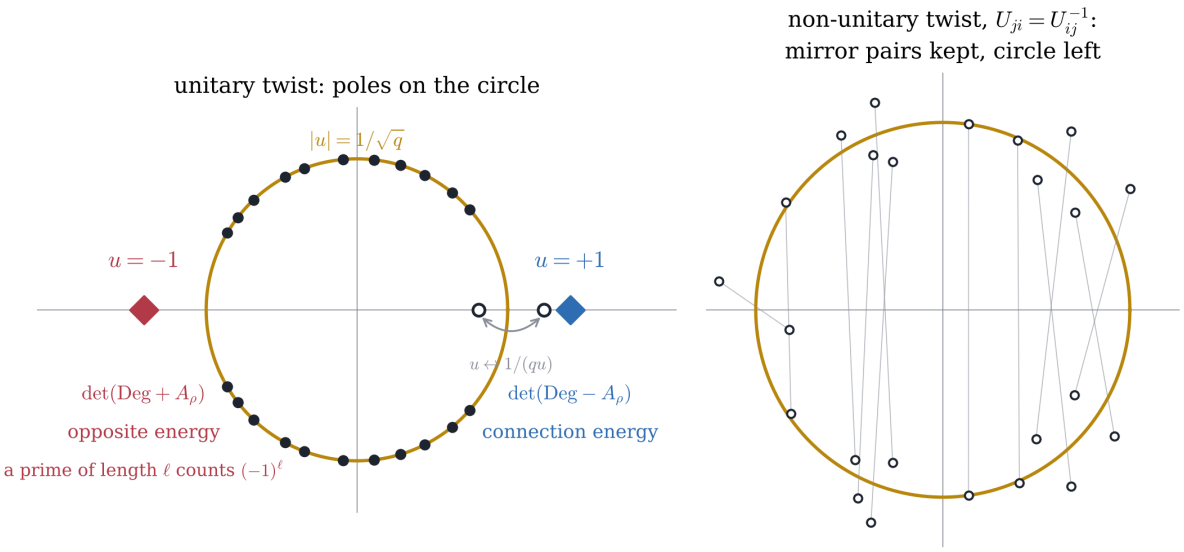


Figure 11: One zeta, two ends. Left: zeros of P_ρ for a cubic graph ($q = 2$) with random unitary gains. All lie on $|u| = 1/\sqrt{q}$ except one real pair, swapped by the mirror $u \leftrightarrow 1/(qu)$, which comes from the single eigenvalue of A_ρ beyond $2\sqrt{q}$. At the two ends $u = \pm 1$ the Bass pencil is the connection-energy operator and its opposite; the zeta itself has poles there. At $u = -1$ each prime counts with the sign $(-1)^\ell$. Right: the same graph with non-unitary twists, $\rho_{ji} = \rho_{ij}^{-1}$. The zeros leave the circle but stay in mirror pairs (thin lines).

characters [27], and determinants of connection Laplacians have forest expansions [28] [KNOWN]. Pincherle's theorem and the theory of minimal solutions are classical [53, 54]. The balance of signed and gain graphs is [9, 10], and the circulant parametrisation of the lepton roots is Brannen's [37]. What is observed here is narrower. With the transport induced on $\mathrm{End}(E)$, the two ends of one Bass pencil have as quadratic forms exactly the connection energy $\frac{1}{8}\|[H, H^*]\|^2$ and its opposite $\frac{1}{8}\|H^2 - H^{*2}\|^2$ of $H = D + A$. The sign separating the ends is the parity of the primes. An eigenvalue's zeros leave the circle exactly when its prime-trace recurrence has a geometrically minimal solution, and the coalescence on the bound is the wall of the recurrence's companion. And the first primitive cycle of a triangle carries the cubic record that both books leave free.

9 Arithmetic primes as connection edges

Graph primes are closed walks. The primes of arithmetic enter the two books another way: each good prime of an elliptic curve is one edge. Let $E/\mathbb{Q}$ be an elliptic curve and p a prime of good reduction. Write

$$N_{E,p} = \#E(\mathbb{F}_p), \qquad a_p = p + 1 - N_{E,p}, \qquad L_p(E,s)^{-1} = 1 - a_p p^{-s} + p^{1-2s}. \tag{60}$$

Hasse's theorem gives $|a_p| \le 2\sqrt{p}$ [40]. Equality cannot occur: $a_p^2 = 4p$ would make the power of p in a square odd. So

$$a_p = 2\sqrt{p}\cos\theta_p, \qquad 0 < \theta_p < \pi, \qquad U_p = \mathrm{diag}\left(e^{i\theta_p}, e^{-i\theta_p}\right). \tag{61}$$

U_p is a unitary representative of the normalised Frobenius conjugacy class. It is not a choice of physical inner product on the Tate module, and it is not a time evolution.

Theorem 4 (The Frobenius edge). *On a single edge with transport U_p and the field $D_p = \sqrt{p/2}\,\sigma_x$ at both ends,*

$$\mathcal{E}_p^- = 4p - a_p^2, \qquad \mathcal{E}_p^+ = a_p^2, \qquad \mathcal{E}_p^- + \mathcal{E}_p^+ = 4p. \tag{62}$$

Equivalently, with $P_x = \frac{1}{2}(I + \sigma_x)$,

$$\rho_p = \mathrm{Tr}\left(P_x U_p P_x U_p^*\right) = \cos^2\theta_p = \frac{a_p^2}{4p}, \tag{63}$$

and the books are $2p$ times the centered rank-one books $\big(2(1-\rho_p), 2\rho_p\big)$ of (33).

[DERIVED; COMPUTED]. The check counts points on the curve 37a1, $y^2 + y = x^3 - x$, at every good prime up to 1000, by brute force and by the character sum (66) below; the two counts agree exactly, and (62)–(63) hold to 1.8×10^{-12} (Figure 12). In Born terms, ρ_p is the probability that the $+1$ eigenstate of σ_x, carried once by Frobenius, is found again. The same overlap parameter governs Koide's centered plane in Section 10. That shared parameter identifies two normalised books. It does not identify the operators, the particles or the dynamics behind them [STRUCTURAL COMPARISON].

Corollary 5 (Arithmetic restrictions). *At an odd prime the Frobenius books are never balanced: $a_p^2 = 2p$ has no integer solution. The prime $p = 2$ can balance, with $a_2 = \pm 2$. At no prime is the Hasse endpoint $a_p^2 = 4p$ reached. A positive three-root Koide preimage of ρ_p, with*

$$Q_p = \frac{1}{3\rho_p} = \frac{4p}{3a_p^2}, \tag{64}$$

exists exactly when $\rho_p > \frac{1}{3}$; the case $a_p = 0$ has none.

[DERIVED; COMPUTED]. The power of p in $2p$ or $4p$ is one, and in a square it is even. Positive roots have $\frac{1}{3} \le Q < 1$, so $\frac{1}{3} < \rho \le 1$, and every value in between is reached continuously. The check finds no odd prime below 20000 with $a^2 = 2p$ for any integer a in the Hasse range, and builds the positive preimage at all 162 primes of 37a1 below 1000 with $\rho_p > \frac{1}{3}$ [COMPUTED].

The local factor is a Ramanujan factor. With $u = p^{-s}$ the local factor is $1 - a_p u + p u^2$. This is the factor $1 - \lambda u + q u^2$ of a $(q+1)$-regular graph in (48), with $q = p$ and $\lambda = a_p$. Hasse's bound is then exactly the circle condition $|\lambda| \le 2\sqrt{q}$ of (49): both roots lie on $|u| = p^{-1/2}$ at every good prime, and since $a_p^2 = 4p$ is impossible no prime sits at the coalescence. This parallel is the origin of the graph Riemann hypothesis [19, 25] [KNOWN; COMPUTED]. The check confirms the roots on the circle at every good prime of 37a1 below 1000, to 1.8×10^{-15}. The coalescence $a_p^2 = 4p$ of the factor and the balance $a_p^2 = 2p$ of the books are two different conditions. In the language of (50), $c_p = a_p/\sqrt{p} = 2\cos\theta_p$ lies strictly inside $(-2, 2)$ at every good prime. So the recurrence of the local prime traces has no minimal solution, the continued fraction (51) of the local factor does not converge, and the companion (52) has $q = -\sin^2\theta_p < 0$: the skew half wins at every good prime [DERIVED; COMPUTED]. The check finds $\max|c_p| = 1.976$ over the odd good primes of 37a1 below 1000, and no convergence at any of the 166.

The sign the books erase.

Theorem 6 (Adjoint sign-blindness). *The central-sign replacement $U \mapsto -U$ induces the same endomorphism transport, $\mathrm{Ad}(-U) = \mathrm{Ad}(U)$. So no function of bare adjoint data distinguishes the two lifts without an additional lift or reference record. In particular the adjoint classes of the Frobenius classes with traces a_p and $-a_p$ agree, and the books (62) cannot recover the sign of a_p.*

[DERIVED; COMPUTED]. Changing the sign of both Frobenius eigenvalues replaces U_p by $-U_p$, and the books depend on a_p^2 only. Ordering the eigenlines separately at a_p and $-a_p$ can replace U_p by $-U_p^*$ rather than $-U_p$; a direction-dependent comparison under that extra convention is not a recovery of the central sign from the same adjoint data. The representation and its reference must stay part of the specification. The fundamental trace $\mathrm{Tr}\, U_p = a_p/\sqrt{p}$ is an odd record; ρ_p is even. So the squared two-book statistic cannot carry any signal defined by the sign of the Frobenius trace. In particular it cannot recover signed murmuration averages from their squared versions. Murmurations themselves are established arithmetic observations [44, 45]; this theorem neither rediscovers them nor supplies a rank classifier.

For a curve without complex multiplication the Sato–Tate density is $\frac{2}{\pi}\sin^2\theta\, d\theta$ [41]. Its share of primes where the opposite book wins, $a_p^2 > 2p$, is

$$\frac{4}{\pi}\int_0^{\pi/4} \sin^2\theta\, d\theta = \frac{1}{2} - \frac{1}{\pi} \approx 0.1817 \tag{65}$$

[KNOWN; COMPUTED]. This is a distributional fact under the Sato–Tate theorem, not a law that selects rank. A curve with complex multiplication has a different distribution, and equal second moments do not make two distributions equal. Table 1 counts three curves directly. Equations and reference ranks are those of the LMFDB [42]; the rank is a label, not something the count estimates. The figures are descriptive finite samples.

curve	$[a_1, a_2, a_3, a_4, a_6]$	Δ	rank	good p	mean ρ_p	share $\mathcal{E}_p^+ > \mathcal{E}_p^-$	$\#\{a_p = 0\}$
32a2	$[0,0,0,-1,0]$	64	0	668	0.243848	0.242515	339
37a1	$[0,0,1,-1,0]$	37	1	668	0.240120	0.164671	8
389a1	$[0,1,1,-2,0]$	389	2	668	0.250633	0.178144	4

Table 1: Direct point counts at every good prime $p \le 5000$, by (66) for odd p and by enumeration at $p = 2$. 32a2 has complex multiplication; half its primes have $a_p = 0$. The two others sit near the non-CM share 0.1817 of (65). [COMPUTED]

Local complements and the signed record. For odd p and a long Weierstrass model, completing the square gives the exact count

$$N_{E,p} = p + 1 + \sum_{x \bmod p} \chi_p\big((a_1x + a_3)^2 + 4(x^3 + a_2x^2 + a_4x + a_6)\big), \tag{66}$$

with χ_p the Legendre symbol [KNOWN; COMPUTED]. A local nonsquare twist negates the character sum. Its two complementary counts are

$$N_p^- = p + 1 - a_p, \qquad N_p^+ = p + 1 + a_p, \qquad N_p^- + N_p^+ = 2(p+1). \tag{67}$$

Define their signed edge coordinate and rapidity:

$$\Gamma_p = \frac{N_p^+ - N_p^-}{N_p^+ + N_p^-} = \frac{a_p}{p+1}, \qquad \tau_p = \log \frac{N_p^+}{N_p^-} = 2 \operatorname{artanh} \Gamma_p. \tag{68}$$

[DERIVED; COMPUTED]. This is the scalar edge (20) with ends $d_i = N_p^+$ and $d_j = N_p^-$: its reflection coefficient is $\Gamma_p = \tanh(\frac{1}{2} \ln N_p^+ / N_p^-)$, the same Cayley and logarithm form, and its own books are $(N_p^+ - N_p^-)^2 = 4a_p^2$ and $(N_p^+ + N_p^-)^2 = 4(p+1)^2$. Hasse keeps both counts positive and $|\Gamma_p| < 1$. The step from the two counts to $\tau_p = 2 \operatorname{artanh} \Gamma_p$ is the offset algebra of the author's offset paper: if $N^{\mp} = d(1 \mp \gamma)$ then $\log N^+ - \log N^- = \log(1+\gamma) - \log(1-\gamma)$, machine-checked as `OperatorFirst.Offset.offset_of_assumed_connection_factors` [60], here with $d = p+1$ and $\gamma = \Gamma_p$ [CITED; LEAN]. Unlike the squared books, Γ_p changes sign under the local twist. The check counts the twisted curve directly at every odd good prime of 37a1 below 1000; (67) holds exactly and (68) to 2.2×10^{-16} [COMPUTED].

Proposition 7 (The global-twist correction)**.** *Fix a global quadratic twist $E^{(d)}$. At an odd prime of good reduction for both curves with $p \nmid d$,*

$$a_p\big(E^{(d)}\big) = \chi_d(p)\, a_p(E), \qquad \log \frac{N_{E^{(d)},p}}{N_{E,p}} = \big(1 - \chi_d(p)\big) \operatorname{artanh} \frac{a_p(E)}{p+1}. \tag{69}$$

So the two counts are complementary only when $\chi_d(p) = -1$, or when $a_p = 0$. When $\chi_d(p) = +1$ they coincide.

[DERIVED; COMPUTED]. The check counts both curves for 37a1 and its twists by $d = 5, -1, -3$ at every good prime below 1000; (69) holds to 2.2×10^{-16}. A fixed global twist does not complement at every prime. For $E : y^2 = x^3 - x$ and $E^{(2)} : y^2 = x^3 - 4x$, at $p = 17$ both have 16 points, whose sum is $32 \neq 36$; at $p = 13$ they have 8 and 20, whose sum is $28 = 2(p+1)$ [COMPUTED]. A prime-dependent local nonsquare twist is not one global elliptic curve and has no single global rank to compare.

The partial product is a conditional statement. For fixed curves the finite sum

$$T_{E,d}(x) = \sum_{\substack{p \le x \\ p \text{ good for both}}} \log \frac{N_{E^{(d)},p}}{N_{E,p}} \tag{70}$$

is exact and computable; by (69) it equals $\sum (1 - \chi_d(p)) \operatorname{artanh}(a_p/(p+1))$ computed from E alone (to 8.9×10^{-16} for 37a1, $d = 5$, $x = 1000$) [DERIVED; COMPUTED]. If each curve satisfies the strong form of the original partial-product asymptotic

$$\prod_{\substack{p \le x \\ p \text{ good}}} \frac{N_{E,p}}{p} \sim C_E (\log x)^{r_E}, \tag{71}$$

then, by subtracting logarithms,

$$T_{E,d}(x) = \big(r_{E^{(d)}} - r_E\big) \log\log x + \log \frac{C_{E^{(d)}}}{C_E} + o(1), \tag{72}$$

up to a finite-prime change of the constant [CONDITIONAL]. This rests on (71); it is not a consequence, proved here, of the usual rank-equals-order form of the Birch–Swinnerton-Dyer conjecture, and Euler products at the edge of convergence need further analytic control [43]. A finite-range test of (72) was registered before it was run. Forty curves of conductor below 2000 from Cremona's tables, each with its quadratic twists by $d = -3, -4, 5$, give 120 pairs; the ranks are PARI's analytic ranks, the sum runs over good primes up to about 2×10^5, and the slope of $-T_{E,d}$ against $\log\log x$ is fitted on $x \in [10^4, 2 \times 10^5]$; by (72) it should approach $r_E - r_{E^{(d)}}$. The registered kill was a sign agreement below 0.75 or a correlation below 0.7 between the slope and $r_E - r_{E^{(d)}}$. The mean slopes are ordered by the rank difference, -1.76, -0.93, $+0.22$, $+0.95$ for $r_E - r_{E^{(d)}} = -2, -1, 0, +1$ (with 3, 27, 61, 29 pairs), and the sign agrees on 0.80 of the 59 pairs whose ranks differ; but the correlation is 0.468, below the registered 0.7, so the test fails as registered [COMPUTED]. On this range the mean law holds and the pair-by-pair reading does not; this is neither evidence that (72) is false nor a rank predictor. On the three curves of Table 1 the weighted switch sum $x^{-1}\sum_{p\le x}(-a_p)\log p$ at $x = 3000$ is -1.12, 0.14 and 1.50, ordered by rank [COMPUTED; DESCRIPTIVE]; three curves fix no law.

The books also meet the murmurations directly. One curve from each of the 10293 isogeny classes of conductor $7500 \le N < 10000$ in Cremona's tables (5099 of even rank, 5194 of odd), with primes below 10^4 binned by p/N, gives two profiles. The signed record $a_p/\sqrt{p}$ reproduces the murmurations [44]: the even and odd profiles are mirror images, correlation -0.985, apart by more than three standard errors in 24 of 25 bins, against $+0.732$ for shuffled parities. The book balance $\cos 2\theta_p = a_p^2/(2p) - 1$, the even record, sits at $-\frac{1}{2}$ for both parities, as Sato–Tate gives; the two profiles are apart by more than three standard errors in 2 of 25 bins, with median separation 0.59 standard errors, and the largest gap, 0.013 in the first bin $p/N < 0.04$, is a shift, not a mirror [COMPUTED]. This is the empirical companion of Theorem 6: the squared books cannot carry the signed statistic that separates the parities. A registered prediction that the rank-two profile would side with rank zero failed: its correlations with the rank-zero and rank-one profiles are -0.048 and -0.151 [COMPUTED] (Figure 13). The checks of the identities in this section make no rank prediction.

What the arithmetic and triangle factors share. Writing $z = \sqrt{p}\,p^{-s}$ normalises the local factor to

$$1 - 2\cos\theta_p\, z + z^2. \tag{73}$$

It agrees with the triangle factor (57) on setting $z = u^3$ and $\cos\theta_p = \cos 3\phi$. This is a parameterised equality of two local quadratics. The triangle parameter comes from a connection; the arithmetic one comes from counting points. No mechanism forcing them equal is supplied [STRUCTURAL COMPARISON]. There is a further obstruction to reading it as a positive Koide construction. Positive Koide roots need $\cos 3\phi > 1/\sqrt{2}$ (Proposition 8), that is $a_p > \sqrt{2p}$. Under Sato–Tate that is a share $\frac{1}{4} - \frac{1}{2\pi} \approx 0.091$ of primes; for 37a1 below 5000 it is 0.079 [KNOWN; COMPUTED]. A local sign choice can replace a_p by $|a_p|$, but that still needs $a_p^2 > 2p$ and does not define one global twist. An algebraic match of factors is therefore not a universal positive mass correspondence.

These results are finite identities and statements about what each record can recover. They do not prove the Birch–Swinnerton-Dyer conjecture or any Riemann hypothesis, they make no rank prediction, and they give no prime origin of lepton masses.

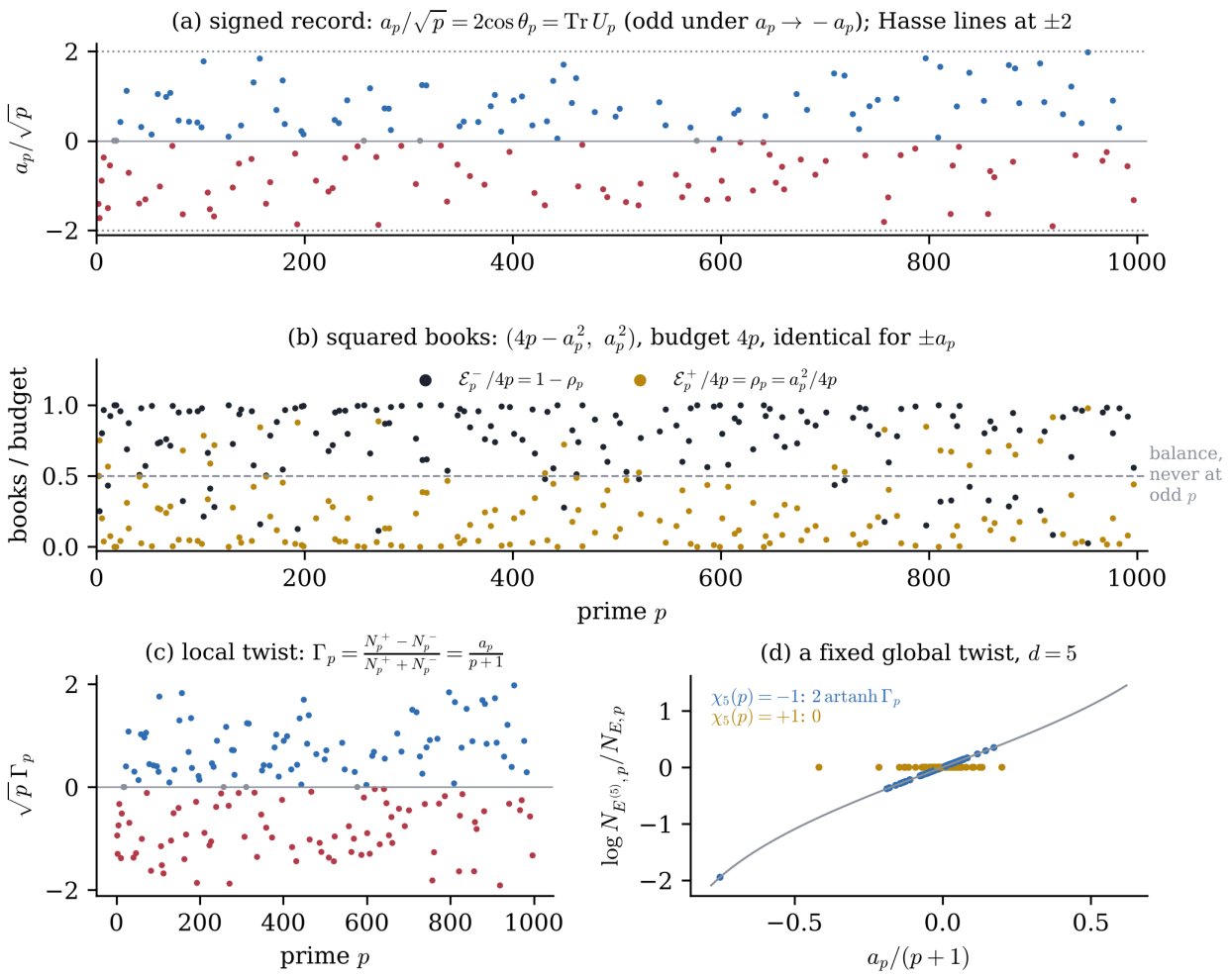


Figure 12: The Frobenius edge on 37a1, from direct point counts at every good prime $p \leq 1000$. (a) The signed record $a_p/\sqrt{p} = \mathrm{Tr}\, U_p$; blue positive, red negative. (b) The two books divided by the budget $4p$; they are the same for a_p and $-a_p$, and at odd p they never balance. (c) The local twist record $\Gamma_p = a_p/(p+1)$, scaled by $\sqrt{p}$; it keeps the sign. (d) A fixed global twist by $d = 5$: primes with $\chi_5(p) = +1$ give zero, those with $\chi_5(p) = -1$ lie on $2\,\mathrm{artanh}\,\Gamma_p$.

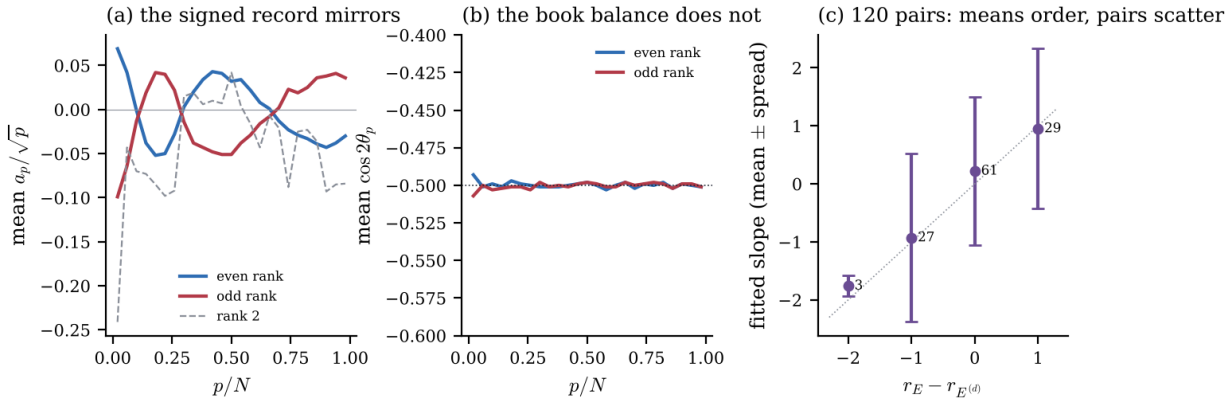


Figure 13: The two arithmetic runs. (a) One curve from each of 10293 isogeny classes, $7500 \le N < 10000$: the signed record $a_p/\sqrt{p}$ averaged in bins of p/N mirrors between even and odd rank; rank two (dashed) follows neither. (b) The book balance $\cos 2\theta_p$ in the same bins sits at $-\frac{1}{2}$ for both parities. (c) 120 curve–twist pairs: the fitted slope against the rank difference, mean and spread with the number of pairs; the means are ordered, the pairs scatter, and the correlation 0.468 is below the registered 0.7.

10 The wall

The difference of the two halves, $\operatorname{Re}\operatorname{Tr} X^2 = \|\operatorname{Herm} X\|^2 - \|\operatorname{Skew} X\|^2$ of (8), has a sharp meaning on the smallest blocks. Every real traceless 2×2 matrix T satisfies $T^2 = -\det(T)\, I$ (Cayley–Hamilton), so

$$T^2 = q(T)\, I, \qquad q(T) = \tfrac{1}{2} \operatorname{Tr} T^2 = \tfrac{1}{2}\big(\|\operatorname{Herm} T\|_F^2 - \|\operatorname{Skew} T\|_F^2\big) \tag{74}$$

[DERIVED]. For the real 2×2 wall link of the author's Price of a Direction the same split decides real against complex eigenvalues (`PriceOfDirection.wall_charpoly`, `wall_real_iff`, `wall_complex_iff` [81]). When $q > 0$ the eigenvalues are a real pair $\pm\sqrt{q}$: one mode grows and one decays. When $q < 0$ they are an imaginary pair and the motion turns. When $q = 0$ and $T \neq 0$, T is a nonzero nilpotent, a Jordan block with a single eigenvector. Call that the wall. The same wall turns up in five places below, one of them only in a declared chart, and in a sixth in Section 8.

The spinning key. A rigid body with principal moments $I_1 < I_2 < I_3$ spins at rate Ω about the middle axis. Euler's equations, linearised in the two other components, give

$$M = \begin{pmatrix} 0 & a \\ b & 0 \end{pmatrix}, \qquad a = \frac{(I_2 - I_3)\Omega}{I_1}, \quad b = \frac{(I_1 - I_2)\Omega}{I_3}.$$

With $h = \frac{1}{2}(a + b)$ and $r = \frac{1}{2}(a - b)$, the symmetric part of M is $h\sigma_x$ and the skew part is rJ, where $J = \left(\begin{smallmatrix} 0 & 1 \\ -1 & 0 \end{smallmatrix}\right)$. Then

$$M^2 = (h^2 - r^2)\, I, \qquad q(M) = h^2 - r^2, \qquad \big\|[M, M^\top]\big\|_F^2 = 32\, h^2 r^2 \tag{75}$$

[DERIVED; COMPUTED]. The sign of q decides growth against oscillation, and the product hr is the non-normality. When the middle axis tumbles its rate is

$$\sqrt{ab} = |\Omega| \sqrt{\frac{(I_3 - I_2)(I_2 - I_1)}{I_1 I_3}}, \tag{76}$$

linear in $|\Omega|$: the angular momentum sets how fast the flip climbs [DERIVED; COMPUTED] (Figure 18a). They are different numbers. The key with $I = (3, 5, 6)$ and $\Omega = 1$ has $a = b = -\frac{1}{3}$, so $r = 0$: M is symmetric, hence normal, and its eigenvalues $\pm\frac{1}{3}$ are real. It tumbles [COMPUTED]. Instability does not need non-normality; the tumbling of the middle axis is classical [31]. The wall $h^2 = r^2$ is $ab = 0$ with $M \neq 0$, a nonzero nilpotent between growth and turning (Figure 15a). A generic flip does not sit on it. For every body with distinct moments both a and b are negative, so $ab > 0$; the wall needs two equal moments [DERIVED; COMPUTED]. During a flip the marked axis loses its sign and moves, while the angular momentum stays fixed in inertial space. No absolute orientation follows from the flip. The marked axis is an unsigned line, an even record; the angular momentum is signed, an odd one, and it is the first of the records of Section 11. The sector sign of Section 2 turns growth into turning at fixed non-normality: for $I = (2, 3, 4)$ and $\Omega = 1$, M has eigenvalues ± 0.3536 and $q = \frac{1}{8}$, $\sigma_z M$ has $\pm 0.3536\, i$ and $q = -\frac{1}{8}$, and both have $\|[\cdot, \cdot^\top]\|_F^2 = \frac{9}{128}$ [DERIVED; COMPUTED] (Figure 15a).

The normal envelope. For a normal generator G, $\|e^{tG}\|_2 = e^{t \max \mathrm{Re}\,\sigma(G)}$ for $t \geq 0$ [DERIVED; COMPUTED]. Zero non-normality rules out gain beyond this envelope; it does not rule out growth from a positive eigenvalue, as the key shows. In the author's words the connection energy is a budget for transient growth; the relaxation flow (13) makes that exact, and two facts bound the reading. The instantaneous gain does not see the transport: for $\dot{y} = Hy$ with $H = D + A$, $\mathrm{Herm}\, H = D$, so $\frac{d}{dt}\|e^{tH}x\|^2$ at $t = 0$ is $2\langle x, Dx\rangle$ and the numerical abscissa is $\lambda_{\max}(D)$ (`NonNormality.add_conjTranspose_of_skew` [67]) [DERIVED; LEAN; COMPUTED]. Transient gain beyond the envelope builds up over time and is read from the pseudospectra [89]. And the self-commutator does not measure gain: $[L - dI, (L - dI)^*] = [L, L^*]$ while $\|e^{t(L-dI)}\| = e^{-dt}\|e^{tL}\|$, so $L_1 = \left(\begin{smallmatrix} -1 & 4 \\ 0 & -1 \end{smallmatrix}\right)$ and $L_1 - \frac{1}{2}I$ have the same self-commutator and peak gains 1.5698 and 1.1433 [DERIVED; COMPUTED]. The same connection energy accompanies any release rate (Figure 18b). Conversely the non-normal $\left(\begin{smallmatrix} -2 & 1 \\ 0 & -2 \end{smallmatrix}\right)$ contracts, because its Hermitian part is negative definite, while $\left(\begin{smallmatrix} -1 & 10 \\ 0 & -2 \end{smallmatrix}\right)$ has a stable spectrum and still grows by a factor 2.6 before it decays [COMPUTED]. For $\dot{y} = Gy$ the loss of norm is governed by $\mathrm{Herm}\, G$; $\mathrm{Skew}\, G$ alone rotates without changing the norm. The convention $i\dot{y} = H_{\mathrm{eff}}y$ adds a factor $-i$ and exchanges which half does which: the Hermitian part of $-iH$ is $-iA$, and there the transport sets the gain [DERIVED; COMPUTED]. Normality also depends on the declared inner product; the four-body transport below is the example.

The damped oscillator. Write $\ddot{x} + 2\zeta\omega\dot{x} + \omega^2 x = 0$ in energy coordinates $y = (\omega x, \dot{x})$. The generator and its traceless part are

$$G = \omega \begin{pmatrix} 0 & 1 \\ -1 & -2\zeta \end{pmatrix}, \qquad T = G + \zeta\omega I, \qquad T^2 = \omega^2(\zeta^2 - 1)\, I, \tag{77}$$

with $\|\,\mathrm{Herm}\, T\|_F^2 = 2\omega^2\zeta^2$ and $\|\,\mathrm{Skew}\, T\|_F^2 = 2\omega^2$ [DERIVED; COMPUTED]. So $q(T) = \omega^2(\zeta^2 - 1)$, and critical damping $\zeta = 1$ is the wall. There $e^{tG} = e^{-\omega t}(I + tT)$. The asymptotic decay rate, minus the largest real part of the spectrum, is

$$\alpha(\zeta) = \begin{cases} \omega\zeta, & \zeta \leq 1, \\ \omega\left(\zeta - \sqrt{\zeta^2 - 1}\right), & \zeta \geq 1, \end{cases} \tag{78}$$

and it has a single maximum, $\alpha = \omega$, at $\zeta = 1$. At $\zeta = 1.01$ it has already fallen to $0.8682\,\omega$ [DERIVED; COMPUTED]. This is a statement about the exponent, not about the clock. At the wall no constant C gives $\|e^{tG}\| \leq Ce^{-\omega t}$ for all t, because of the factor $I + tT$. At a finite tolerance the order can reverse, and two finite criteria must be kept apart. For the displacement, with $\omega = 1$, $x(0) = 1$ and $\dot{x}(0) = 0$, the response enters and stays inside a 2% band at $t = 3.756$ for $\zeta = 0.8$ and only at $t = 5.834$ for $\zeta = 1$ [COMPUTED]. For the operator norm, at $t_* = \pi/0.6$,

$$\begin{aligned} e^{t_* G_{0.8}} &= -e^{-0.8 t_*} I, & \|e^{t_* G_{0.8}}\|_2 &= 0.0151646, \\ e^{t_* G_1} &= e^{-t_*}(I + t_* T), & \|e^{t_* G_1}\|_2 &= e^{-t_*}\left(\sqrt{1 + t_*^2} + t_*\right) = 0.0562309 \end{aligned} \tag{79}$$

[DERIVED; COMPUTED]. Both semigroups are contractions, since $\mathrm{Herm}\, G \leq 0$, so from t_* on the underdamped one stays below a 2% norm threshold for every initial state, and the critical one does not. In its Schur form the critical generator is $\left(\begin{smallmatrix} -\omega & \pm 2\omega \\ 0 & -\omega \end{smallmatrix}\right)$, the Jordan block $J = \left(\begin{smallmatrix} -b & \mu \\ 0 & -b \end{smallmatrix}\right)$ with $\kappa = |\mu|/b = 2$. For that family $\|e^{tJ}\|_2 = e^{-bt}\left(\sqrt{4 + \mu^2 t^2} + |\mu| t\right)/2$, and some $t > 0$ has $\|e^{tJ}\|_2 > 1$ exactly when $|\mu| > 2b$ (`FilamentFracture.growth_iff`, `FilamentFracture.gain_eq` [77]; Atlas bridge B122 [68]) [CITED; LEAN; COMPUTED]. Critical damping sits exactly on the

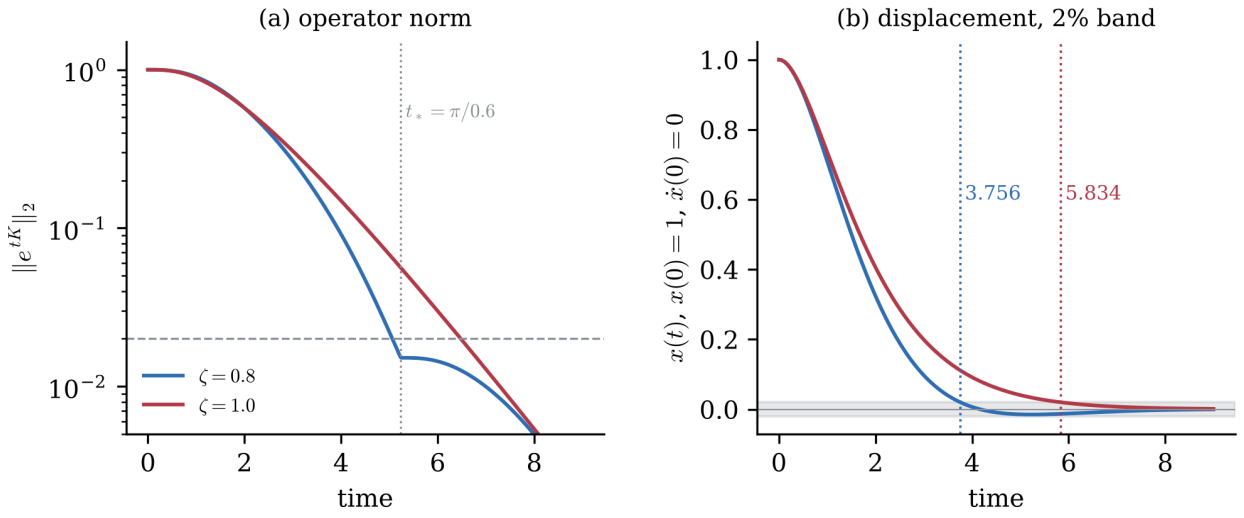


Figure 14: The exponent and the clock. (a) Operator norm of the propagator for $\zeta = 0.8$ and $\zeta = 1$ at unit frequency. At $t_* = \pi/0.6$ the underdamped propagator is $-e^{-0.8t_*}I$ and lies under the 2% line (dashed) for good; the critical one, with its prefactor $I + tT$, is still above it. (b) The displacement from rest: the underdamped response enters the 2% band first, at 3.756 against 5.834.

threshold of transient growth: it never grows, which is Herm $G \leq 0$, and a larger coupling at the same decay rate would; the norm in (79) is that formula at $b = 1$, $|\mu| = 2$ (Figure 18c). Critical damping is fastest among responses that do not oscillate [KNOWN]. Among all responses it is fastest only in the asymptotic exponent, and that exponent is the selector used below (Figures 15b and 14).

Many degrees of freedom. Take $\ddot{x} + C\dot{x} + Kx = 0$ with K a random positive definite matrix, $C = \mathrm{diag}(c)$, $c \geq 0$, and $n = 2$ or 3. Choose c to minimise the spectral abscissa of the generator $\left(\begin{smallmatrix} 0 & I \\ -K & -C \end{smallmatrix}\right)$, that is, for the fastest asymptotic settling. In 40 random systems the optimum carried a coalesced, defective pair every time. The median fraction of modes sharing the common decay rate was 1: at the optimum the modes settle together [COMPUTED]. That optimisation of the spectral abscissa drives eigenvalues together into defective clusters is known [32]. The opposite runs behave as they should. Maximising the abscissa, for the slowest settling, gave no fold in 40 of 40 systems [COMPUTED]. Reversing time, $G \mapsto -G$, leaves q unchanged, since q is quadratic [DERIVED]. A family of Hermitian generators never folds, because Hermitian matrices are diagonalisable; the check finds eigenvector condition number 1 at every optimum [DERIVED; COMPUTED]. An exceptional point alone is not evidence that a physical system has optimised anything.

What does not carry over is the global balance. Inside each coalesced pair the shifted 2×2 block is nilpotent, so its own q is 0 [DERIVED]. But the q of the full traceless generator was nonzero at all 40 optima, at least 1% of its natural scale $\frac{1}{2}\sum_k |\lambda_k - \bar{\lambda}|^2$ [COMPUTED]. Conversely, $q = 0$ does not make a wall in higher rank. The matrix $X = \left(\begin{smallmatrix} 0 & I_2 \\ \mathrm{diag}(1,-1) & 0 \end{smallmatrix}\right)$ has $\mathrm{Tr}\, X^2 = 0$, yet $X^2 = \mathrm{diag}(1,-1,1,-1)$, X is normal, and its eigenvalues $\pm 1, \pm i$ are simple [DERIVED; COMPUTED]. Nor does it make one for complex 2×2 blocks: $X = e^{i\pi/4}\sigma_z$ has $\mathrm{Re}\,\mathrm{Tr}\, X^2 = 0$ and $X^2 = iI \neq 0$ [DERIVED; COMPUTED]. And balanced books are not a wall either. On one edge with identity transport and the centered fields

$D_0 = P - \frac{1}{2}I_2$, $D_1 = R - \frac{1}{2}I_2$ of two lines in the plane,

$$X = DA = \begin{pmatrix} 0 & D_0 \\ -D_1 & 0 \end{pmatrix}, \qquad XX^* = X^*X = \tfrac{1}{4}I_4, \tag{80}$$

normal and invertible at every overlap, including $\rho = \frac{1}{2}$ where the two books are equal [DERIVED; COMPUTED]. Equal halves mean a wall only for real traceless 2×2 blocks, where (74) holds.

The orbit. The radial wobble of a circular orbit is generated by $\left(\begin{smallmatrix} 0 & 1 \\ -\kappa^2 & 0 \end{smallmatrix}\right)$, whose square is $-\kappa^2 I$. At the innermost stable circular orbit the epicyclic rate κ vanishes and the generator is a nonzero nilpotent between oscillation and growth [33] [STRUCTURAL COMPARISON]; that the effective potential has $V' = V'' = 0$ exactly at $r = 6M$ with $L^2 = 12M^2$ is `RussellOrbits.isco_from_potential` [96]. This is the same matrix family, with no damping, so it has no settling to optimise. A horizon need not be such a wall, and a static spacetime with zero twist does not by that fact give a normal operator.

The four-body transport. The author's black-hole paper studies the transport block of four-body shape space on the simplex $w_1 + w_2 + w_3 = 1$, $w_i \geq 0$, with scalings t_1, t_2, t_3 [33]:

$$A = \begin{pmatrix} (t_1 + t_2) - (t_1 - t_2)(w_1 - w_2) & \big((t_1 - t_2) - (t_1 + t_2 - 2t_3)(w_1 - w_2)\big)/\sqrt{3} \\ \sqrt{3}\,(t_1 - t_2)\,w_3 & 2t_3 + w_3(t_1 + t_2 - 2t_3) \end{pmatrix}.$$

It is the map $H \mapsto TH + HT - 2\,\mathrm{Tr}(TH)\,W$, with $T = \mathrm{diag}(t)$ and $W = \mathrm{diag}(w)$, on diagonal traceless tangents in the basis $E_1 = \mathrm{diag}(1, -1, 0)$, $E_2 = \mathrm{diag}(1, 1, -2)/\sqrt{3}$. It is self-adjoint, $g_W A = A^\top g_W$, for $g_W(H, K) = \sum_i H_{ii}K_{ii}/(4w_i)$, which is the Bures metric of W read as a density matrix [64] (Theorem 1; Atlas bridge B171 [68]; for the N-body transport `SquareCase.Transport.weighted_symmetric` [82]) [CITED; LEAN; COMPUTED]. In that metric it is normal at every interior point, and every eigenprojector has metric norm 1. For any real 2×2 block with traceless part T, the discriminant is $(A_{11} - A_{22})^2 + 4A_{12}A_{21} = 4q(T)$ [DERIVED; COMPUTED]. The black-hole library proves that this discriminant is a quadratic form in $(t_1 + t_2 - 2t_3,\ t_1 - t_2)$ with determinant exactly $16w_1w_2w_3$, hence nonnegative on the whole simplex (`EventHorizon.disc_form`, `EventHorizon.disc_det`, `EventHorizon.spectrum_real`) [59] [CITED; LEAN]. In the language of (74): on the regular stratum the Hermitian half of T never loses.

In the Euclidean (Gram) chart the block is normal exactly when the trace-free parts of t and w are parallel. Indeed

$$\begin{aligned} \sqrt{3}\,(A_{12} - A_{21}) &= (t_1 - t_2)(w_1 + w_2 - 2w_3) - (t_1 + t_2 - 2t_3)(w_1 - w_2), \\ \big\|[A, A^\top]\big\|_F^2 &= 2(A_{12} - A_{21})^2\big((A_{12} + A_{21})^2 + (A_{11} - A_{22})^2\big), \end{aligned} \tag{81}$$

the first a cross product of the two trace-free parts; the second factor vanishes only on a rotation branch, which the nonnegative discriminant excludes unless the block is scalar [DERIVED; COMPUTED]. Isotropic scalings and the isotropic configuration are the two simplest parallel cases (`EventHorizon.normal_if_T_isotropic`, `EventHorizon.normal_if_W_isotropic`); $t_i = \alpha w_i + \beta$ is normal with both anisotropic.

At the coplanar wall $w_3 = 0$ the back-coupling A_{21} vanishes, and under the joint condition $t_1 + t_2 - 2t_3 = (t_1 - t_2)(w_1 - w_2)$ the diagonal entries meet at $\lambda_* = 2t_3$ with $(A - \lambda_* I)^2 = 0$; if

also $A_{12} \neq 0$ the Gram-chart block is a nonzero nilpotent (`EventHorizon.wall_triangular`, `EventHorizon.wall_jordan`) [CITED; LEAN; COMPUTED]. That nilpotent belongs to the chart. The metric coefficient $g_W(E_2, E_2)$ grows like $1/(3w_3)$ while A_{21} vanishes like w_3, so $g_W A = A^\top g_W$ holds up to the wall with a singular metric. In the lifted chart $q^2 = w_3$, where the metric is regular, the block $J^{-1}AJ$ with $J = \mathrm{diag}(1, -\sqrt{3}\,q)$ tends to the scalar $2t_3 I$, linearly in q; along the approach the Euclidean norm of an eigenprojector grows like $1/q$ while its Bures norm stays 1 [64] (Theorems 4, 6 and 8; Atlas bridges B171 and B172) [CITED; COMPUTED]. The wall is at finite distance. Along $W(x) = \mathrm{diag}\left(a(1-x^2), (1-a)(1-x^2), x^2\right)$ the Bures length from x_0 to the wall is $\arcsin x_0$: the metric coefficient diverges like $1/\varepsilon$, but $\int d\varepsilon/(2\sqrt{\varepsilon})$ is finite, where a coefficient $1/\varepsilon^2$ would give a length growing like $\log(1/\varepsilon)$ [CITED; DERIVED; COMPUTED] (Figure 17). Off the joint condition the wall block has two distinct real eigenvalues.

What survives at such a point is contour data. For $\left(\begin{smallmatrix} \lambda & c \\ 0 & \lambda+g \end{smallmatrix}\right)$ the eigenprojector onto the λ line is $\left(\begin{smallmatrix} 1 & -c/g \\ 0 & 0 \end{smallmatrix}\right)$, so

$$\|P_\lambda\|_F\, g = \sqrt{g^2 + c^2} \;\longrightarrow\; |c| \quad (g \to 0), \qquad \log\det \begin{pmatrix} \lambda & c \\ 0 & \lambda \end{pmatrix} = 2\log\lambda \quad (\lambda > 0), \tag{82}$$

the second with no reference to eigenvectors (`EventHorizon.projector_norm_gap`, `EventHorizon.snapped_law`, `EventHorizon.ledger_at_jordan`; the projector itself is computed by hand there) [33, 59] [CITED; LEAN; COMPUTED]. In a chart where the block is a Jordan block, a single eigenline diverges with the inverse gap, and its divergence constant is the Jordan coupling; the pair projector and the trace-log ledger stay finite. The companion of the prime-trace recurrence obeys the same law at $\lambda^2 = 4q$ (54).

The charged leptons. Let $x = (\sqrt{m_e}, \sqrt{m_\mu}, \sqrt{m_\tau})$ and

$$s = \frac{x_1 + x_2 + x_3}{\sqrt{3}}, \qquad h_1 = \frac{x_1 - x_2}{\sqrt{2}}, \qquad h_2 = \frac{x_1 + x_2 - 2x_3}{\sqrt{6}}, \qquad h^2 = h_1^2 + h_2^2.$$

Then $|x|^2 = s^2 + h^2$ and $(\sum_k x_k)^2 = 3s^2$, so Koide's ratio [34, 35] is

$$Q = \frac{m_e + m_\mu + m_\tau}{(\sqrt{m_e} + \sqrt{m_\mu} + \sqrt{m_\tau})^2} = \frac{s^2 + h^2}{3s^2}, \qquad \frac{h^2}{s^2} = 3Q - 1 \tag{83}$$

[DERIVED; COMPUTED]. In the Compton wavelengths $\lambda_k \propto 1/m_k$ the same ratio reads $Q = \sum_k \lambda_k^{-1} / \left(\sum_k \lambda_k^{-1/2}\right)^2$; this is the form in which the author received the relation, from Caleigh Fisher (@Kali_fissure), who wrote the generations as stress expressions, and it is Q itself [DERIVED; COMPUTED]. Koide's relation is the null cone $h^2 = s^2$ of a declared quadratic form in the roots. Put the three numbers into one real traceless matrix,

$$Z = h_1\sigma_z + h_2\sigma_x + sJ, \qquad Z^2 = (h^2 - s^2)\, I, \qquad \left\|[Z, Z^\top]\right\|_F^2 = 32\, s^2 h^2 \le 2\|Z\|_F^4, \tag{84}$$

since σ_z, σ_x and J anticommute in pairs and $J^2 = -I$ [DERIVED; COMPUTED]. The inequality is the arithmetic–geometric mean on this family, and Koide saturates it; that restates the cone rather than explaining it. So the following are equivalent: Koide's value $Q = \frac{2}{3}$; $h = s$; $Z^2 = 0$ with $Z \neq 0$; the vector x at 45° to $(1,1,1)$ [36]; and the weight of the democratic ray,

$$p = \frac{(x \cdot (1,1,1))^2}{3\,|x|^2} = \frac{1}{3Q},$$

equal to $\frac{1}{2}$ [DERIVED; COMPUTED]. The weight reading assumes the three amplitudes share one positive phase. Relative phases change it while the masses and Q stay fixed. Over relative phases the weight fills exactly the interval

$$\frac{\max(0,\, 2\max_k x_k - S)^2}{3M} \;\le\; p \;\le\; \frac{S^2}{3M} = \frac{1}{3Q}, \qquad S = \sum_k x_k, \tag{85}$$

both ends attained, $[0.171868,\, 0.500002]$ for the measured masses, and mixing the coherent state with its dephased version in proportion λ gives $\frac{1}{3} + \lambda\left(\frac{1}{3Q} - \frac{1}{3}\right)$ [DERIVED; COMPUTED] (Figure 18d). Full dephasing gives $\mathrm{Tr}(\mathrm{diag}(m)R)/M = \frac{1}{3}$ exactly for every mass triple, with R the democratic projector and $M = \sum m_k$, and independent random phases give $\frac{1}{3}$ on average [DERIVED; COMPUTED]. So the encoding does not by itself establish a coherent preparation of lepton generations. The empirical relation concerns pole masses; it must not be transferred to running masses, where radiative corrections are physical input [39].

Three declared fields. Koide is a balance of the two books, on the right field. Let $\psi = x/|x|$, $e = (1,1,1)/\sqrt{3}$, $P = \psi\psi^\top$ and $R = ee^\top$, with overlap $\rho_K = \mathrm{Tr}(PR) = p = 1/(3Q)$. For unequal positive roots, $W = \mathrm{span}\{\psi, e\}$ is a plane. Compress P and R to W and center them by $\frac{1}{2}I_W$. By (33) with $r = 2$, $k = 1$, on one edge with identity transport,

$$\left(\mathcal{E}_W^-, \mathcal{E}_W^+\right) = \left(2(1-\rho_K),\, 2\rho_K\right), \tag{86}$$

which at Koide is exactly $(1,1)$ [DERIVED; COMPUTED]. The uncentered projectors in $\mathbb{C}^3$ give $(1,3)$ at Koide, and centering in all of $\mathbb{C}^3$ gives $(1, \frac{5}{3})$. These are three formulas for three declared fields, not three predictions for one operator (Figure 16a). For the measured masses $\rho_K = 0.5000016525$, and the centered plane books are $(0.999997, 1.000003)$ [COMPUTED].

The circulant and the free cubic. Brannen's form $\sqrt{m_k} = \mu\left(1 + \sqrt{2}\cos(\delta + 2\pi k/3)\right)$ [37] is the spectrum of the circulant Φ of (55) with $t = d/\sqrt{2}$: by (56), $Q = \left(1 + 2(t/d)^2\right)/3$, and $Q = \frac{2}{3}$ exactly when $t = d/\sqrt{2}$. The diagonal and off-diagonal Frobenius norms of Φ are $3d^2 = s^2$ and $6t^2 = h^2$, so Koide's equality is a split of the Hermitian matrix Φ into diagonal and off-diagonal parts, not its Hermitian and skew split. At Koide $e_2 = S^2/6$ with $S = \sum_k x_k$, and the roots solve

$$v^3 - Sv^2 + \frac{S^2}{6}\,v - e_3 = 0 \tag{87}$$

[DERIVED; COMPUTED]. The quadratic balance fixes a cone, not a point on it. Fixing the scale leaves exactly the unordered cubic invariant $e_3 = \sqrt{m_e m_\mu m_\tau}$, and by Theorem 2 that is the primitive-cycle coefficient $C_3 = 2\cos 3\phi$ of the triangle (Figure 16b,c).

Proposition 8 (Positive phase domain)**.** *For $d > 0$ and $t = d/\sqrt{2}$, all three roots of (55) are strictly positive exactly when $\cos 3\phi > 1/\sqrt{2}$.*

[DERIVED; COMPUTED]. For the measured masses the reduced hopping phase is $|\phi| = 0.22222476$, taken in $[-\pi/3, \pi/3]$ [COMPUTED]. Its closeness to the phenomenological value $2/9$ is an observation, not a prediction; nothing here enforces that number.

The leptons as a damped oscillator. Shift Z by the least multiple of I that makes it passive. The symmetric part of $K = Z - hI$ is $h_1\sigma_z + h_2\sigma_x - hI$, whose top eigenvalue is exactly 0. A rotation in the plane commutes with J and turns $h_1\sigma_z + h_2\sigma_x$ into $h\sigma_z$, so

$$K \sim s\begin{pmatrix} 0 & 1 \\ -1 & -2h/s \end{pmatrix}, \qquad \omega = s, \quad \zeta = \frac{h}{s}, \quad \zeta^2 = 3Q - 1 \tag{88}$$

[DERIVED; COMPUTED]. The minimally passive lepton generator is exactly the damped oscillator (77), and Koide's relation is critical damping. At fixed s, the asymptotic rate (78) is largest exactly at $h = s$. The same holds on any resource $ah^2 + bs^2 = R^2$ with $a, b > 0$; fixed total mass is $a = b = 1$ [DERIVED; COMPUTED]. A fixed extra scalar loss shifts the whole rate curve and keeps its maximiser. If instead the total scalar loss is fixed independently of h, the rate is flat on the whole undercritical side and has no unique maximiser, and with no bound at all fastest relaxation is not a meaningful optimisation [DERIVED; COMPUTED]. Positive masses give $Q < 1$, so $\zeta < \sqrt{2}$, and the critical point is inside the range. The entries of Z have the units of square-root masses. Reading K as an inverse-time generator needs a positive conversion factor, and choosing it predicts no absolute mass scale.

This is a conditional reformulation, not a derivation. The generator Z, the minimal shift, the fixed resource, the asymptotic objective, and a law that moves h toward the fastest rate are all assumptions here [CONDITIONAL]. An optimisation over damping is not an evolution law that adjusts it, and ordinary relaxation at fixed h does not optimise h. Even granted, they fix one ratio and leave one number free. At fixed s and h the orientation angle θ of $(h_1, h_2) = h(\cos\theta, \sin\theta)$ does not enter the spectrum or the norm profile of K. It does enter the product of the roots:

$$e_3 = \sqrt{m_e m_\mu m_\tau} = \frac{s^3}{3\sqrt{3}} - \frac{s\,h^2}{2\sqrt{3}} + \frac{h^3}{3\sqrt{6}}\,\sin 3\theta \tag{89}$$

[DERIVED; COMPUTED], the same cubic record as C_3 in (58). So e_3, equivalently Brannen's δ, is what a selection principle would still have to fix.

A flow that keeps the cone. The stress descent $\dot{Z} = -2[C, Z]$ with $C = [Z, Z^\top]$ is the author's relaxation flow (13) [71]. It is isospectral, so it preserves $\det Z$ and with it $h^2 - s^2$. In root coordinates it reads $\dot{h}_j = -16s^2 h_j$ and $\dot{s} = -16h^2 s$. A Koide start stays Koide, $Z(t) = Z(0)/\sqrt{1 + 32s(0)^2 t}$, and a start off the cone keeps its defect for all time [DERIVED; COMPUTED]. The flow preserves the constraint; it does not select it.

Cooling does not select the wall. In the author's Grassmannian framework [48] the two-level slow-driving friction is

$$\zeta_{\rm fr} = \tau\beta\,\mathrm{sech}^2(\beta\Delta/2)\,\dot{r}_H^2 + 2c(\Delta)\,\Delta\tanh(\beta\Delta/2)\,g_P(\dot{P}, \dot{P}), \tag{90}$$

with $\Delta = 2r_H$ the gap and c fixed by the declared bath. The two terms are the two parts of a moving two-level generator $H = d \cdot \sigma$, which add in quadrature: $|\dot{d}|^2 = \dot{\rho}^2 + \Delta^2 g_P(\dot{P}, \dot{P})$ with $\rho = |d|$, $\Delta = 2\rho$ and $g_P = \frac{1}{2}\,\mathrm{Tr}\,\dot{P}^2$ [50] (§16.4) [CITED; DERIVED; COMPUTED] (Figure 18f). At fixed positive gap and finite relaxation time, cooling sends the scale coefficient $\tau\beta\,\mathrm{sech}^2(\beta\Delta/2)$ to zero; it does not give $\dot{r}_H = 0$. Along $\Delta = 1/\beta$ the same coefficient grows linearly in β [DERIVED; COMPUTED]. No identification of r_H with the root-mass radius has been derived. The reset bath

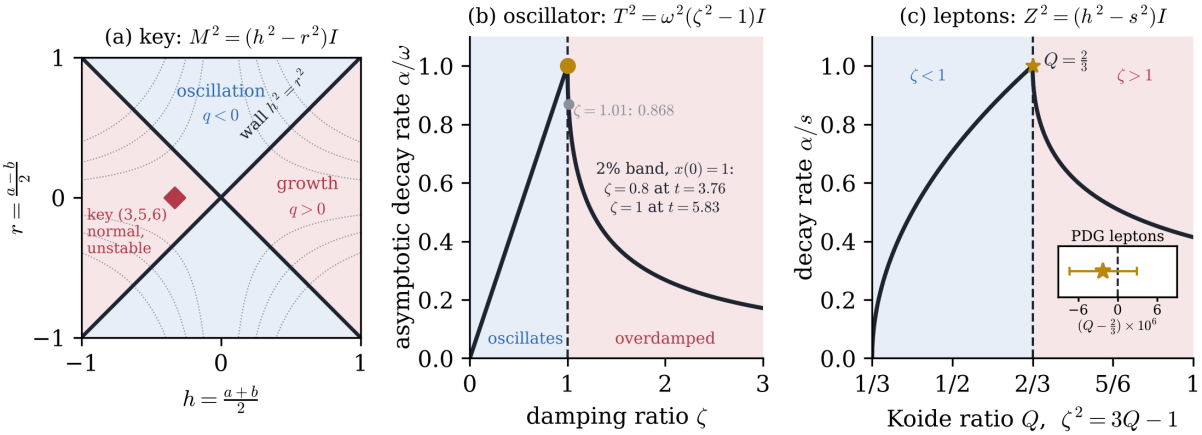


Figure 15: One wall in three places. (a) The key's linearisation $M = \left(\begin{smallmatrix} 0 & a \\ b & 0 \end{smallmatrix}\right)$: $q = h^2 - r^2$ decides growth against oscillation; dotted curves are levels of the non-normality $32h^2r^2$. The key $(3, 5, 6)$ is normal and unstable. (b) The damped oscillator: the asymptotic decay rate peaks only at critical damping, the wall $T^2 = 0$. At a 2% tolerance an underdamped response can finish first. (c) The charged leptons through $\zeta^2 = 3Q - 1$: the same rate curve against Koide's ratio, peaking at $Q = \frac{2}{3}$. Inset: the measured value with its τ-mass error bar.

$\dot{\varrho} = -i[H, \varrho] - (\varrho - \omega_\beta)/\tau$ at fixed gap has transverse generator $\left(\begin{smallmatrix} -1/\tau & -\Delta \\ \Delta & -1/\tau \end{smallmatrix}\right)$, normal at every temperature [DERIVED; COMPUTED]. Cooling moves the fixed point, not the defect of the generator. So cooling alone does not drive a system to the wall; the optimisation result above is untouched.

The measured masses sit on the wall. With $m_e = 0.51099895069\,\text{MeV}$, $m_\mu = 105.6583755\,\text{MeV}$ and $m_\tau = 1776.93 \pm 0.09\,\text{MeV}$ [38], $Q = 0.6666644634$ and $Q - \frac{2}{3} = -2.2 \times 10^{-6}$. The τ error alone gives $\sigma_Q = 5.08 \times 10^{-6}$, so that is 0.43 standard deviations: the inputs are consistent with $\frac{2}{3}$, which is not a proof of equality. Exact Koide would need $m_\tau = 1776.969\,\text{MeV}$ [CITED MEASUREMENT; COMPUTED]. In the oscillator reading, $\zeta = 0.9999967$ (Figure 15c).

So one wall, $q = 0$ with a nonzero nilpotent, appears in the key, the damped oscillator, the circular orbit, the four-body transport in its Gram chart, the lepton encoding and the companion of the prime-trace recurrence. Of the selectors tried, fastest asymptotic settling is the one that lands on it. It does so for the single oscillator, for many degrees of freedom as a local fold, and, under the stated assumptions, for the charged leptons [CONDITIONAL]. It fixes the cone. The cubic record C_3 stays free.

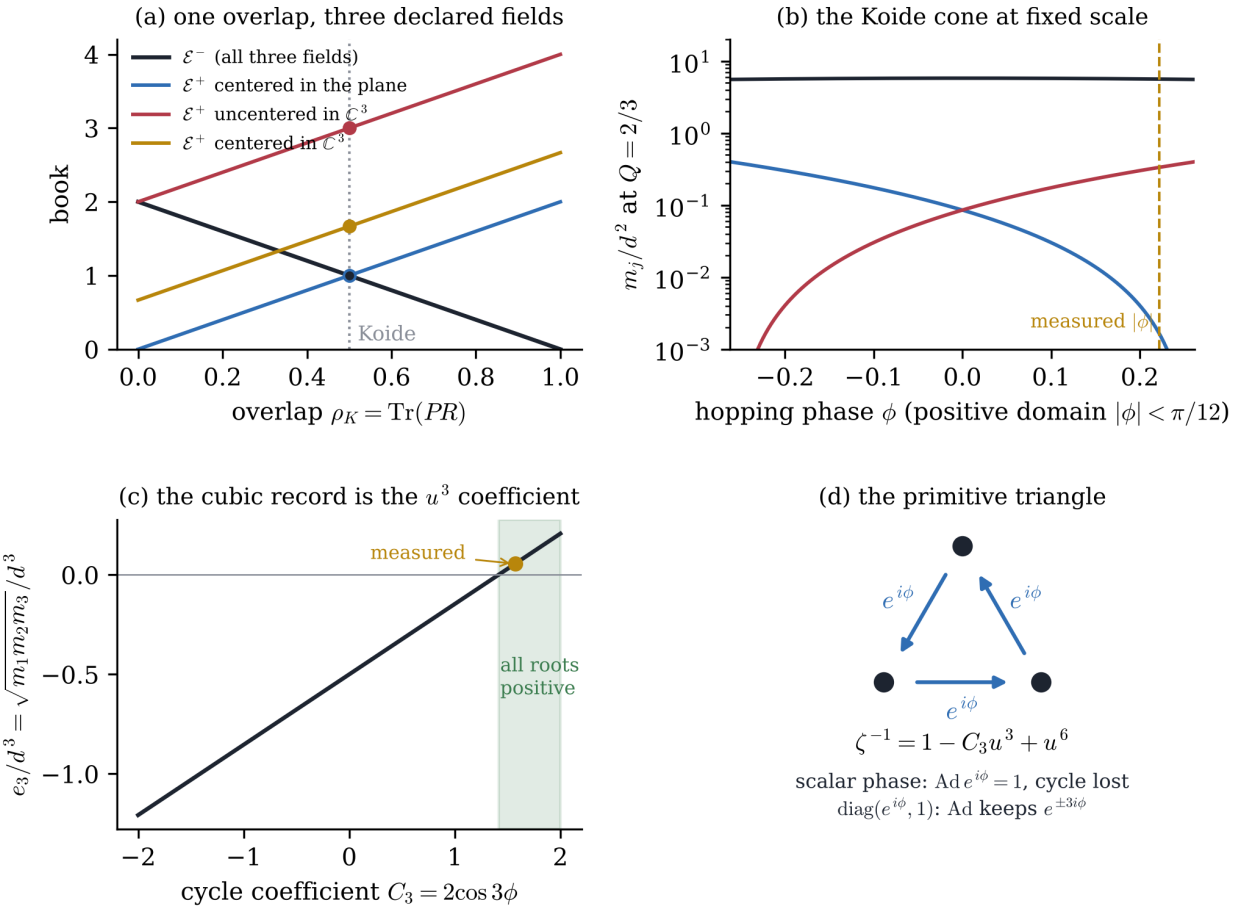


Figure 16: What Koide fixes and what it leaves. (a) One overlap ρ_K, three declared fields: the connection energy is $2(1-\rho_K)$ on all three; the opposite is $2\rho_K$ on the centered plane, which balances at Koide, $2(1+\rho_K)$ uncentered in $\mathbb{C}^3$, and $2(1+\rho_K) - \frac{4}{3}$ centered in $\mathbb{C}^3$. (b) Every spectrum shown has $Q = \frac{2}{3}$; moving the hopping phase changes the individual masses, and the roots stay positive on $|\phi| < \pi/12$. (c) The cubic invariant is linear in the cycle coefficient C_3, and positive roots need $C_3 > \sqrt{2}$; the measured masses sit just inside. (d) The triangle with connection $e^{i\phi}$, whose primitive cycles carry C_3; a scalar phase is lost to the induced transport, a noncentral one is kept.

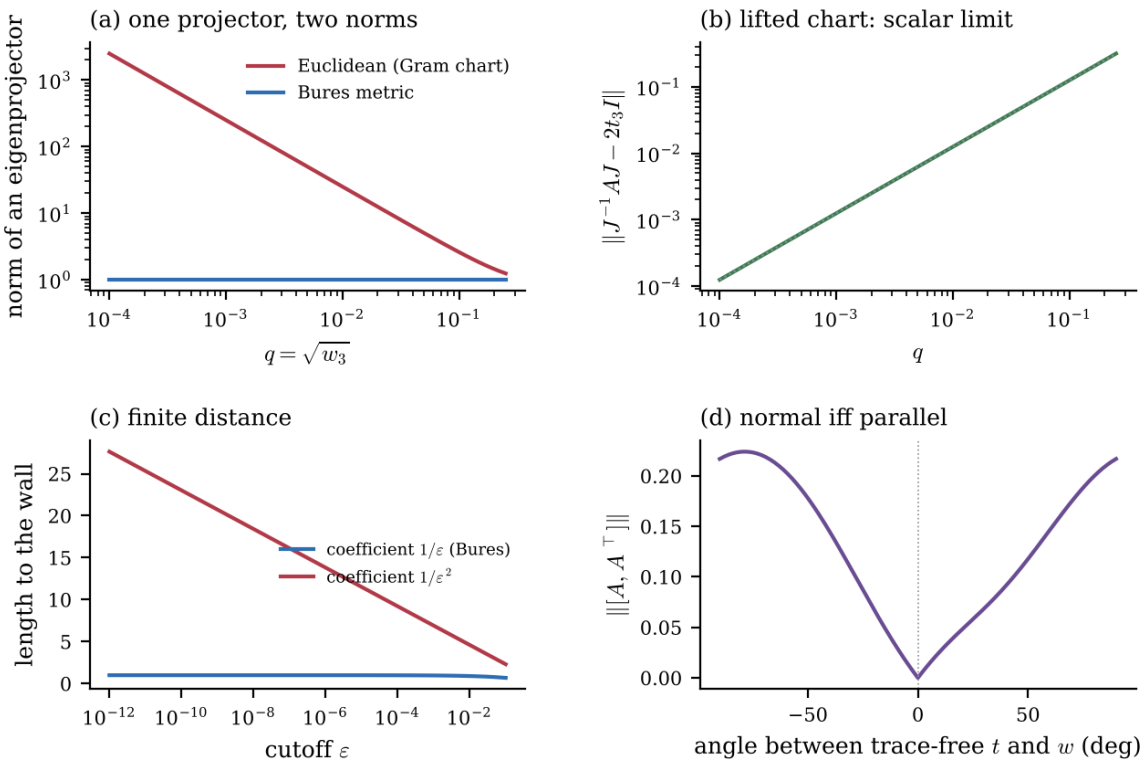


Figure 17: The four-body wall in two charts, $t = (2, 1, 1.25)$, $w_1 - w_2 = 0.5$, joint condition at $w_3 = 0$. (a) Approaching the wall, the Euclidean norm of an eigenprojector grows like $1/q$, $q = \sqrt{w_3}$, while its norm in the Bures metric stays 1. (b) In the lifted chart the block tends to the scalar $2t_3 I$, linearly in q. (c) The length to the wall with a metric coefficient $1/\varepsilon$ is finite, $\arcsin x_0$; a coefficient $1/\varepsilon^2$ would make it grow like $\log(1/\varepsilon)$. (d) Off the wall, at $w = (0.5, 0.3, 0.2)$, the Gram-chart block is normal exactly when the trace-free parts of t and w are parallel.

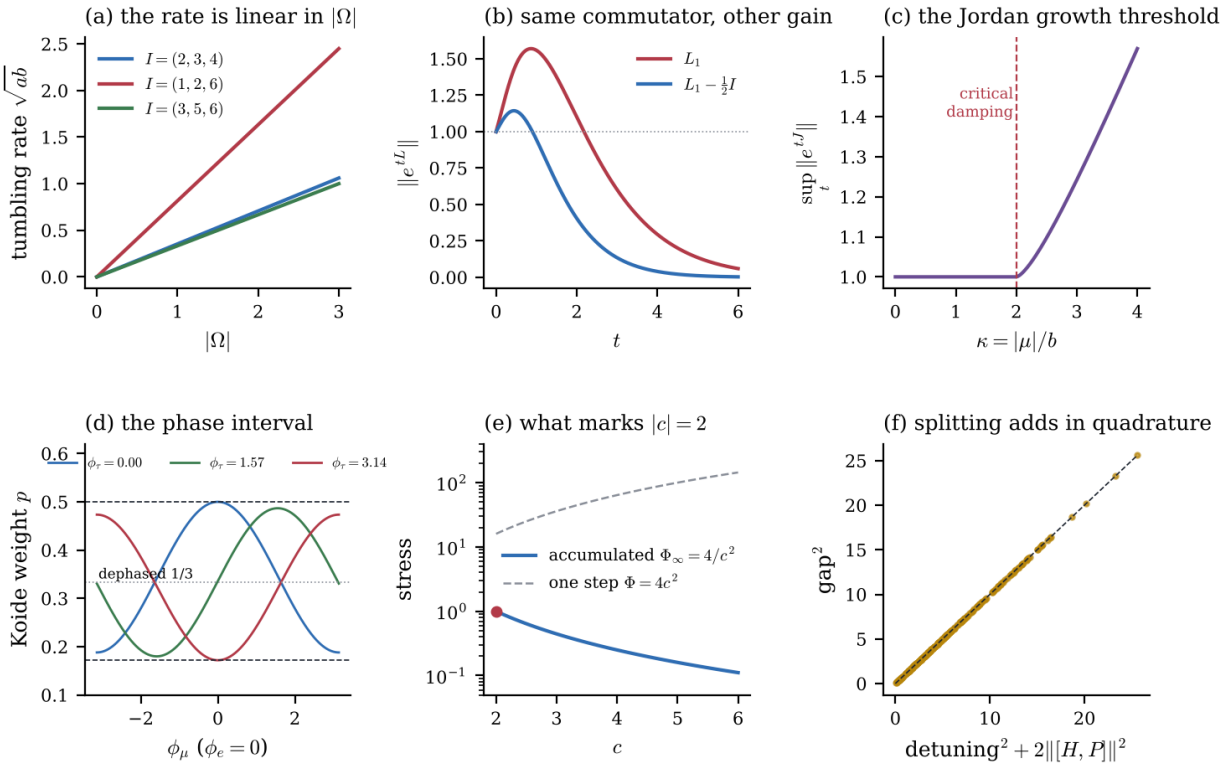


Figure 18: Gain and thresholds. (a) The tumbling rate of the key grows linearly in $|\Omega|$. (b) L_1 and $L_1 - \frac{1}{2}I$ have one self-commutator and different transient gains. (c) The Jordan block $\left(\begin{smallmatrix} -b & \mu \\ 0 & -b \end{smallmatrix}\right)$ grows before it decays exactly when $\kappa = |\mu|/b > 2$; critical damping sits at $\kappa = 2$. (d) The Koide weight of the measured masses over relative phases fills the interval (85) (dashed); full dephasing gives $\frac{1}{3}$. (e) The companion of the prime-trace recurrence: the accumulated stress $\Phi_\infty = 4/c^2$ reaches 1 at $|c| = 2$, the single-step stress does not mark it. (f) Two levels: the gap squared is the detuning squared plus $2\|[H, P]\|^2$.

11 Records the two books do not keep

The two books are even. They see squared jumps and squared sums, and every sign that changes under a swap or a reversal passes through them unseen. For a declared reversal $\mathcal{I}$, any reading F splits into $F_{\text{even}} = \frac{1}{2}(F + F \circ \mathcal{I})$ and $F_{\text{odd}} = \frac{1}{2}(F - F \circ \mathcal{I})$; the books are even parts. Sections 8 and 9 met two odd records, the cycle coefficient C_3 and the sign of a_p, and the key of Section 10 a third, its signed angular momentum against its unsigned axis. There are others, and each needs its own carrier.

The author asked whether a reflection is all there is: whether the mirror half is all that may be known, and whether it can be read correctly. The mathematics answers in two parts. The even half is read exactly; the books, the Gram data and the determinants below are fixed by it. What the even half cannot return is listed exactly: which end is larger, the sign of a_p, the cycle coefficient, the orientation of a loop, the endpoint of a route, the signed curvature, the future of a hidden channel. Each needs its own carrier, and with that carrier it is recovered.

Several even records are exact. Transposition changes neither book:

$$\left[H^\top, (H^\top)^*\right] = -[H, H^*]^\top, \qquad (H^\top)^2 - \left((H^\top)^*\right)^2 = \left(H^2 - H^{*2}\right)^\top \tag{91}$$

(`NonNormality.transpose_selfCommutator`, `NonNormality.transpose_opposite` [67]), so $\mathcal{E}^{\mp}(H^\top) = \mathcal{E}^{\mp}(H)$, while H and $H^\top$ carry signal in opposite directions. The books cannot tell which way an edge runs; the resolvent can. For the one-way $L = \left(\begin{smallmatrix} -1 & 0 \\ 0.3 & -2 \end{smallmatrix}\right)$ at $z = 0.5i$ the transfer $|R_{21}|$ is 0.130158 and the reverse 0, swapped for $L^\top$, while the books agree [DERIVED; LEAN; COMPUTED] (Figure 21g). Under a mirror R, $\det R = -1$, the Gram data $X^\top X$ of a frame are unchanged and $\det X$ changes sign [DERIVED; COMPUTED]. And the determinant is even in a skew coupling. For real symmetric S and real skew K, $\det(S + \varepsilon K) = \det(S - \varepsilon K)$; for Hermitian D and skew-Hermitian A, $\det(D - \varepsilon A) = \overline{\det(D + \varepsilon A)}$; under a grading that keeps D and reverses A, $\det(D + A) = \det(D - A)$ (`NonNormality.det_add_eq_det_sub_of_grading` [67]); and for positive definite M and real skew E,

$$\log\det(M + tE) - \log\det M = \sum_j \log\left(1 + t^2\omega_j^2\right) \geq 0, \tag{92}$$

with $\pm i\omega_j$ the eigenvalues of $M^{-1/2}EM^{-1/2}$ [52] (Theorem 5.5) [DERIVED; LEAN; COMPUTED]. A spectral ledger sees a skew transport only at second order. Across an interface the two kinds of coupling move it in opposite directions: for positive definite blocks A, B and a coupling E, a Hermitian coupling $\left(\begin{smallmatrix} A & E \\ E^* & B \end{smallmatrix}\right)$ changes $\log\det$ by $\log\det(I - K) \leq 0$, and the skew coupling $\left(\begin{smallmatrix} A & E \\ -E^* & B \end{smallmatrix}\right)$ by $\log\det(I + K) \geq 0$, with the same $K = A^{-1}EB^{-1}E^*$ [DERIVED; COMPUTED] (Figure 22b).

Which end is larger. On the scalar edge (20), exchanging the ends negates Γ_e and leaves both books unchanged, so $\mathcal{E}^- - \mathcal{E}^+ = -4d_id_j$ does not say which end is larger (`OperatorFirst.Offset.asymmetry_swap` [60]) [DERIVED; LEAN; COMPUTED]. The signed offset is the extra record $\Gamma_e = \tanh(\frac{1}{2}\ln d_i/d_j)$. For a fermionic occupation $0 < \nu < 1$ take $d_i = 1 - \nu$ and $d_j = \nu$:

$$\mathcal{E}^- = (1 - 2\nu)^2, \qquad \mathcal{E}^+ = 1, \qquad \tau_\nu = \log\frac{1-\nu}{\nu} = 2\,\operatorname{artanh}(1 - 2\nu). \tag{93}$$

Here the budget $1 + (1 - 2\nu)^2$ is not constant in ν, because the two ends are not transported copies of one field [DERIVED; COMPUTED]. The record is $1 - 2\nu = \tanh(\tau_\nu/2)$, zero exactly at $\nu = \frac{1}{2}$,

and the occupation flip $\nu \mapsto 1-\nu$ negates it (`EventHorizon.Edition10.fermion_smith`, `fermion_center`, `particle_hole` [59]) [DERIVED; LEAN]. The same flip acts on geometry. On a family of projectors P, the complement $1-P$ has the same metric and the opposite curvature,

$$g_{1-P} = g_P, \qquad \Omega_{1-P} = -\Omega_P, \qquad \operatorname{Tr}(P\,\partial_x P\,\partial_y P) = g_{xy} - \tfrac{i}{2}\Omega_{xy}, \qquad |\Omega| \le 2\sqrt{\det g}, \tag{94}$$

with $g_{\mu\nu} = \frac{1}{2}\operatorname{Tr}(\partial_\mu P\,\partial_\nu P)$ and $\Omega_{xy} = i\operatorname{Tr}(P[\partial_x P, \partial_y P])$, and equality in the bound for two bands (`PriceOfDirection.metric_curvature` [81], `EventHorizon.Edition10.sine_guard` [59], `DiracTime.ProjectorBlocks.hermitian_form_split` [56]) [DERIVED; LEAN; COMPUTED]. The metric is an even record of the flip and the curvature an odd one (Figure 22c). For a gauge-invariant, number-conserving Gaussian state with correlation matrix C, the probabilities that every mode is full or every mode is empty are $\det C$ and $\det(I-C)$, so

$$\tau = \log\frac{\det(I-C)}{\det C} = \sum_j \tau_{\nu_j} \tag{95}$$

over the eigenvalues ν_j of C [KNOWN; COMPUTED]. The check builds such states on three modes in Fock space and confirms (95) to 8×10^{-15}. Paired Gaussian states need more covariance data. An internal pairing $\nu \leftrightarrow 1-\nu$ needs a symmetry or purity structure and does not follow for an arbitrary C: if a unitary U gives $UC_AU^* = I - C_A$ or $(I-C_A)^\top$, the occupations are symmetric under $\nu \mapsto 1-\nu$ and $\tau_A = 0$ exactly [51] (Theorem 5), and the determinant form, $\det(1-C) = \det C$ whenever $SCT = (1-C)^\top$ with $ST = 1$, is `OperatorFirst.Offset.complement_det_eq_of_conjugacy` [60]. When the pairing holds, an odd number of modes forces at least one half-filled mode, and an even number allows them without forcing them [DERIVED; CITED; LEAN]. The finite product identity behind (95), $\sum_j \log\frac{1-\nu_j}{\nu_j} = \log\prod_j(1-\nu_j) - \log\prod_j \nu_j$, the flip $\tau_{1-\nu} = -\tau_\nu$, the vanishing of the offset for a spectrum paired by $\nu \leftrightarrow 1-\nu$, and $\frac{m-p}{m+p} = \tanh\left(\frac{1}{2}(\log m - \log p)\right)$ for the empty and full probabilities m and p are machine-checked in the author's offset library, the first as `OperatorFirst.Offset.finite_log_odds` (the others in Appendix B) [51, 60] [CITED; LEAN; COMPUTED]. The Gaussian-state reading of those products is separate from their algebra. When C is the compression to the region of a global projector $\left(\begin{smallmatrix} C & B \\ B^* & D \end{smallmatrix}\right)$, idempotence gives $C - C^2 = BB^*$. So each $\nu(1-\nu) = \frac{1}{4} - (\nu - \frac{1}{2})^2$ is a weight of the coupling across the cut, largest at the self-dual centre $\nu = \frac{1}{2}$, and counting modes in a window $\varepsilon \le \nu \le 1-\varepsilon$ is counting coupling weights at least $\varepsilon(1-\varepsilon)$ (`LightBridges.projector_block_coupling` and the census statements in Appendix B; the spectral-mapping step is in the written supplement there) [52, 61] [CITED; LEAN; COMPUTED]. This B is the coupling of the hidden channel (104) below. It also bounds the census: at most $\operatorname{rank} B \le \min(|A|, |\bar{A}|)$ modes can be open. When a region of six sites is coupled to its outside with growing strength, the census climbs to six and stays there, $\max \nu(1-\nu)$ tends to $\frac{1}{4}$, and the total weight $\sum \nu(1-\nu)$ keeps growing: past saturation, added coupling only redistributes weight among open channels. A coupling of rank three leaves exactly three channels open at strong coupling [DERIVED; COMPUTED] (Figure 22d).

The boundary sets the sign. The author's offset paper locates the sign of τ at the boundary [51] (Theorem 8). Add one site x to a block B and let $s_1 = C_{xx} - c^* C_B^{-1} c$ and $s_0 = 1 - C_{xx} - c^*(I - C_B)^{-1}c$ be its full-side and empty-side Schur residuals, c the coupling column. Then

$$e^{\tau_{B+x}} = e^{\tau_B}\,\frac{s_0}{s_1}, \tag{96}$$

and if the interior is protected, $\det C_B = \det(I - C_B)$, then $\tau_{B+x} = \log(s_0/s_1)$: the sign of the offset flips exactly when the two residuals trade places, the numerator becoming the denominator [CITED; DERIVED; COMPUTED] (Figure 22a). The sublattice sign $\Sigma = \mathrm{diag}((-1)^j)$ is the sector flip (17) acting on the offset: in the author's Rice–Mele model [90], a chain with alternating hoppings t_1, t_2 and staggering $\pm v$, $C_A(-v) = \Sigma\big(I - C_A(v)\big)\Sigma$, so $\tau_A(v) = F_A(-v) - F_A(v)$ with $F_A = \log\det C_A$: the offset is the odd part of one log-determinant [51] (Theorem 4; `OperatorFirst.OffsetEndpoint.sublattice_conjugation` [60]) [CITED; LEAN; COMPUTED].

The self-dual mode and its opposite. At $v = 0$ the Rice–Mele chain with $(t_1, t_2) = (0.6, 1)$ has one mode at $\nu = \frac{1}{2}$ in every odd block and none in even blocks: a self-dual mode of the occupation flip, with record 0. A small staggering tips it into one book. At $v = 0.05$ the tipped mode carries about 112% of τ in size and keeps one sign, while the rest of the spectrum changes sign with the block, so that $\tau = \pm 0.1246$ alternates as $(-1)^n$ for $L = 2n + 1$: the self-dual mode sets the size and the bulk sets the sign. A registered prediction that the tipped mode would carry the sign as well failed [COMPUTED]. As the region grows the offset moves between the books: it is zero in every even block, it alternates in odd blocks, and $(-1)^n\tau$ tends to $2\,\mathrm{artanh}\left(v/\sqrt{E_{\min}E_{\max}}\right)$ with $E_{\min} = \sqrt{v^2 + (t_1 - t_2)^2}$ and $E_{\max} = \sqrt{v^2 + (t_1 + t_2)^2}$ [51] [CITED; COMPUTED]. In the author's reading this is light as stored, moving energy: the fixed total sits in one book or the other according to the region, and the offset is the record of where. The opposite chain is Kitaev's [91], in which pairing replaces part of the hopping; the phase turn $c \mapsto ic$ reverses the sign of every pairing term, the sign-twisted transport of the opposite book. In its topological phase two Nambu modes of a block approach $\frac{1}{2}$ exponentially in the length, for odd and even lengths alike; in the trivial phase none do; and the Nambu spectrum is always paired, $\nu \leftrightarrow 1 - \nu$, so its offset vanishes by construction [KNOWN; COMPUTED]. Rice–Mele alternates with the parity of the block, and Kitaev does not (Figure 21d,e).

Synchronising. The author asked whether one rule synchronises all of these. As a test it reads: each system keeps two books with a fixed sum, exchanged by a swap of order two; parity decides whether the swap has a self-dual fixed point; where it has one, a small push tips it into one book and the signed difference carries the hidden constant; where it has none, the constant vanishes or the system is frustrated. Six predictions were registered. Four held: a ring with trivial transport carries an anti-parallel field exactly when it is even; odd blocks carry one half-mode and even blocks none; both books together lower the worst frustration on odd rings only; and cI is invisible to $[H, H^*]$. Two failed: the tipped mode does not carry the sign, and the rank-two murmuration profile does not side with rank zero (Section 9) [COMPUTED]. For phase oscillators the classical rule is sharper: two oscillators with frequency difference $\Delta\omega$ and coupling K lock exactly when $|\Delta\omega| \le 2K$, and at $|\Delta\omega| = 2K$ the stable and unstable locked states meet [92] [KNOWN; COMPUTED] (Figure 22e).

The local twist record Γ_p of (68) and the occupation record τ_ν use the same positive-ratio coordinate. Their self-dual centres are different events and stay separate: $a_p = 0$ for point counts, $\nu = \frac{1}{2}$ for occupations, $\rho_K = \frac{1}{2}$ for Koide's overlap, and $a_p^2 = 2p$ for the balance of the Frobenius books.

Route and endpoint. A chain of scalar edges keeps a record that one edge cannot show. Let $E_0, \dots, E_m > 0$ sit on a path and put $r_j = \frac{1}{2}\ln(E_{j+1}/E_j)$. The reflection coefficient (20) of the edge from E_j to E_{j+1} is $\Gamma_j = \tanh r_j = (E_{j+1} - E_j)/(E_{j+1} + E_j)$. This is the directed peel coordinate of

the author's VOTKP paper, where the edges compose by $u \oplus v = (u+v)/(1+uv)$ and telescope to the end-to-end coefficient $(E_m - E_0)/(E_m + E_0)$ [49] (Proposition 19.1; `VOTKP.Directed.directed_composite`, `directed_reverse`, `oplus_identity_inverse` [62]). On the real diameter of the disk with the Poincaré normalisation $ds = 2|d\rho|$, $\rho = \frac{1}{2}\ln E$, the record has a route length and an endpoint distance, and they differ by an exact amount:

$$L_{\mathrm{rec}} = 2\sum_j |r_j|, \qquad D_{\mathrm{end}} = 2\Big|\sum_j r_j\Big|, \qquad L_{\mathrm{rec}} - D_{\mathrm{end}} = 4\min(R_+, R_-), \tag{97}$$

with $R_+ = \sum_{r_j>0} r_j$ and $R_- = -\sum_{r_j<0} r_j$, and equality exactly when every nonzero increment has the same sign [49] (Proposition 19.2; `VOTKP.Directed.cancellation_defect`, `VOTKP.Directed.no_defect_iff` [62]) [CITED; LEAN; COMPUTED]. A route out by 0.4 and back by 0.4 has $L_{\mathrm{rec}} = 1.6$ and $D_{\mathrm{end}} = 0$ (`VOTKP.Directed.out_and_back`).

The two books see one side of this. On each edge they are $(E_{j+1} - E_j)^2$ and $(E_{j+1} + E_j)^2$, with ratio $\Gamma_j^2 = \tanh^2 r_j$. So the books fix every $|r_j|$, and with them the route (Figure 19),

$$L_{\mathrm{rec}} = 2\sum_j \operatorname{artanh}\sqrt{\mathcal{E}_j^- / \mathcal{E}_j^+}\,, \tag{98}$$

but not the endpoint: D_{end} needs the signs of the r_j, which the books erase, and (97) says exactly what those signs are worth [DERIVED; COMPUTED]. The duality (23) splits the same way, with $P_e = \tanh 2r_j$ odd and $V_e = \operatorname{sech} 2r_j$ even (`VOTKP.Smith.round_trip`, `VOTKP.Smith.euclid_form` [62]). The increments $(0.4, 0.4, -0.3)$ and $(0.4, -0.4, 0.3)$ have the same normalised books on every edge and endpoint distances 1.0 and 0.6 [COMPUTED]. The signed rapidity adds along the chain and changes sign under reversal, and every closed loop of scalar edges has total zero. By the path-ledger descent theorem of the author's Dirac Time paper, a ledger on a connected chain is exactly an endpoint potential, here $\rho = \frac{1}{2}\ln E$ [50] (Theorem P3; Atlas bridge B159 [68]; `DiracTime.PathLedger.descent_iff` [56]) [CITED; LEAN]. The route length is even under reversal and is not a ledger in that sense. The relation is exact on scalar edges: the books keep the route, the signs keep the endpoint. The circle gives the same lesson in one line: for $-i\,d/d\theta + a$ the endpoints a and $a+1$ have the same spectrum and the same η invariant, yet the spectral flow between them is 1, and in general $\mathrm{SF}(a_0 \to a_1) = \lfloor a_1 \rfloor - \lfloor a_0 \rfloor = (a_1 - a_0) + \frac{1}{2}(\eta_1 - \eta_0)$ [50] (§8.2) [CITED; DERIVED; COMPUTED]. The scalar record fixes nothing beyond the route and the endpoint. A positive ladder with its full directed record does not fix the path of a retained spectral projector: the lifts $R(b\rho)\,\mathrm{diag}(e^{2\rho}, e^{4\rho})R(b\rho)^\top$ have the same eigenvalues and record for every b, while their projector moves at speed $|b|$ [49] (Proposition 19.3; `VOTKP.Directed.nonunique_lift`, `lift_isospectral`, `lift_metric` [62]) [CITED; LEAN; COMPUTED] (Figure 22g,h). On matrix edges the books are Born-weighted sums (6), and no route length is defined from them here.

One coordinate, several realisations. For an impedance z with $\mathrm{Re}\, z > 0$ the Cayley map $w = (z-1)/(z+1)$ lands in the unit disk, the Smith chart; for the upper half-plane the corresponding map is $(z-i)/(z+i)$, and the two conventions must not be mixed [KNOWN; COMPUTED]. For $z = x + iy$ with $x \geq 0$, $1 - |w|^2 = 4x/|z+1|^2 \geq 0$ (`LightBridges.smith_power_identity` for the equality and `LightBridges.smith_passive` for the inequality [61]) [CITED; LEAN]. The matrix form survives elimination with no normality assumption. Let L be passive, $\mathrm{Herm}\, L \succeq 0$, with boundary and interior blocks b and i, and let $Z_b = L_{bb} - L_{bi}L_{ii}^{-1}L_{ib}$ be the Schur complement. With $W = \begin{pmatrix} I \\ -L_{ii}^{-1}L_{ib} \end{pmatrix}$, $V_b = (Z_b + I)^{-1}$ and $S_b = (Z_b - I)V_b$,

$$Z_b = W^* L W, \qquad \mathrm{Herm}\, Z_b = W^*(\mathrm{Herm}\, L)\, W, \qquad I - S_b^* S_b = 4\,(WV_b)^*(\mathrm{Herm}\, L)(WV_b), \tag{99}$$

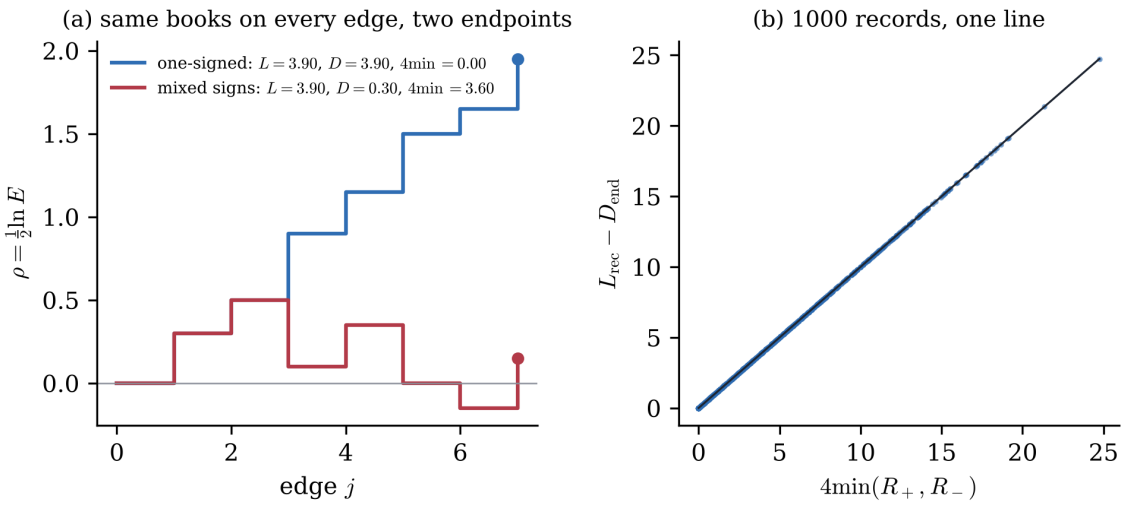


Figure 19: Route and endpoint. (a) Two chains of seven scalar edges with the same $|r_j|$, so the same normalised books on every edge and the same route length $L_{\mathrm{rec}} = 3.9$. One-signed steps end at $D_{\mathrm{end}} = 3.9$; mixed signs end at 0.3, and the gap is $4\min(R_+, R_-) = 3.6$. (b) 1000 random directed records lie on the line (97), to 1.1×10^{-14}.

so $\|S_b\| \le 1$, and the power not returned is the Hermitian half of L pulled back to the boundary [33] [CITED; LEAN; COMPUTED]. The chain is machine-checked with every inverse stated as an equation, ending in `LightBridges.passive_boundary_chain` [61]; its steps are listed in Appendix B. The Hermitian half is the one that governs the loss of norm in Section 10; when it is not positive, $\|S_b\| > 1$ can occur [COMPUTED]. A positive ratio z lies on the real diameter, at $w = \tanh(\tau/2)$ with $\tau = \log z$. So the two point counts of (67) fix an exact point of that diameter, $w = \Gamma_p$, and the occupation edge fixes another. A unit-modulus Frobenius eigenvalue is a point on the circle instead (Figure 20a). Algebraically the circle is the purely reactive loads: $|(y - i\kappa)/(y + i\kappa)| = 1$ for $y > 0$, and $\kappa/y = -\tan(\theta/2)$ gives $\Gamma = e^{i\theta}$ (`EventHorizon.Edition10.total_reflection` [59]) [DERIVED; LEAN; COMPUTED]. No physical impedance is supplied for the Frobenius eigenvalue. The question that led the author to the opposite book sits on this chart. The Sun's trapped acoustic modes are totally reflected, $|\Gamma| = 1$, on the circle; a horizon is a matched load that returns nothing, $\Gamma = 0$, at the centre (Atlas bridge B175 [68]; [33]) [STRUCTURAL COMPARISON] (Figure 21f). The metric $(dx^2 + dy^2)/y^2$ on $y > 0$ is the optical metric of the index $n(y) = 1/y$, and its geodesics obey Snell's first integral $n(y) \sin\vartheta = \text{const}$, with ϑ measured from the vertical [KNOWN; COMPUTED]. That relates one refractive profile to hyperbolic geometry. The factor $\sin^2\theta$ in the Sato–Tate law does not make that law a law of refraction. For a weight-two modular form one prime Hecke operator is

$$(T_p f)(z) = p\, f(pz) + \frac{1}{p} \sum_{b=0}^{p-1} f\Big(\frac{z+b}{p}\Big), \tag{100}$$

whose maps have determinant-p representatives and preserve the upper half-plane; after a Cayley change they act on the disk. For the newform of an elliptic curve $T_p f = a_p f$ at good primes [KNOWN]. This is a sum of correspondences, not a single ray or a transport path. Modularity links these coefficients to the L-function of the curve, and nothing here adds to modularity or to the conjecture of Birch and Swinnerton-Dyer. The signed lapse $\lambda = (\rho - a)/(\rho + a) = \tanh(\frac{1}{2}\log(\rho/a))$ of the author's black-hole work [33] uses the same identity, and $\rho \mapsto a^2/\rho$ negates it [DERIVED;

COMPUTED]; Section 12 shows where it comes from. A regular signed-lapse collar and this fold do not by themselves specify an exceptional-point operator, and reciprocal and signed-lapse reversals are different operations.

Overlaps beyond the first. For rank-k orthogonal projectors with squared principal cosines c_a, three different quantities measure the overlap:

$$\rho = \frac{1}{k}\sum_a c_a, \qquad F = \Big(\frac{1}{k}\sum_a \sqrt{c_a}\Big)^2, \qquad D = \prod_a c_a. \tag{101}$$

F is the squared Uhlmann fidelity of P/k and R/k [46], and D is the squared overlap of the two Slater determinants. Expanding and using the arithmetic–geometric mean,

$$\rho - F = \mathrm{Var}\,(\sqrt{c_a}), \qquad D^{1/k} \le F \le \rho \tag{102}$$

[DERIVED; COMPUTED]. More precisely, $\rho/k \le F \le \rho$ and $\max(0, k\rho - k + 1) \le D \le \rho^k$; the first k power sums $\mathrm{Tr}\,((PR)^j)$ fix every c_a, and with them F and D; and if the k-plane is read as a Slater determinant, the number N_R of particles found in R has generating function $\mathbb{E}\, z^{N_R} = \prod_a (1 - c_a + z c_a)$, whose top coefficient is D. Near coincidence $1-\rho$ and $1-F$ agree to leading order, $\rho - F = \mathrm{Var}(\sqrt{c_a})$ is of fourth order in the angles, and $1 - D \approx k(1-\rho)$ [DERIVED; COMPUTED] (Figure 22f). The books see only ρ (25). The rank-two lists $c = (1,0)$ and $c = (\frac{1}{2}, \frac{1}{2})$ have the same $\rho = \frac{1}{2}$ but $(F, D) = (\frac{1}{4}, 0)$ and $(\frac{1}{2}, \frac{1}{4})$ (Figure 20b). Even all pairwise overlaps do not fix the orientation of a loop. The rays $(1,0)$, $(1,1)/\sqrt{2}$ and $(1, \pm i)/\sqrt{2}$ have every pairwise overlap equal to $\frac{1}{2}$, yet

$$\mathrm{Tr}\,(P_0 P_1 P_2^{\pm}) = \frac{1 \pm i}{4} \tag{103}$$

[DERIVED; COMPUTED]. This triple product is Bargmann's invariant [47]. The cubic loop is exactly where a signed phase survives a pairwise summary, as C_3 survives the books on the triangle. Nor do the books fix a matrix field. On one edge they fix only $\|D_i\|^2 + \|D_j\|^2$ and the overlap $\langle D_i, \mathcal{U}_{ij}(D_j)\rangle$: with $D_i = \mathrm{diag}(1,0)$, seven fields D_j of different spectra all have the books $(1.4, 2.6)$. Scalar fields are another matter: both books together fix a path of three vertices up to an overall sign, and a single edge up to sign and the exchange of its ends [DERIVED; COMPUTED].

Same footprint, other future. In the author's hidden-channel framework [49] a retained block is coupled to a hidden one,

$$H = \begin{pmatrix} A & B \\ B^* & D \end{pmatrix}, \qquad dM(E) = B\, dE_D(E)\, B^*, \tag{104}$$

with self-energy $\Sigma(z) = B(zI - D)^{-1}B^*$, memory kernel $K(t) = Be^{-itD}B^*$ and moments BD^nB^*. The present footprint is itself a commutator energy. With P the retained projector and $C = [H, P]$,

$$\|C\|_F^2 = 2\,\mathrm{Tr}\,BB^* = 2\,\mathrm{Tr}\,K(0), \qquad q(C) = -\,\mathrm{Tr}\,BB^*, \qquad q(-iC) = +\,\mathrm{Tr}\,BB^*, \tag{105}$$

since C is skew-Hermitian and lies entirely in the skew half of the trace form (`UPGAlgebra.commutatorC_energy` [74]; `VOTKP.Channels.commutator_coupling` [62]; [75], Proposition 33); with $B = (0.7,\ 0.3i)$, $\frac{1}{2}\,\mathrm{Tr}\,C^2 = -0.58$ [CITED; LEAN; COMPUTED]. On two levels it is the splitting

law: the gap satisfies $(\text{gap})^2 = (H_{11} - H_{22})^2 + 2\|[H, P]\|_F^2$ [DERIVED; COMPUTED]. Compressing and then squaring loses exactly the exit and return through the hidden block,

$$PH^2P - (PHP)^2 = \big((1-P)HP\big)^*\big((1-P)HP\big) \succeq 0 \tag{106}$$

(`NonNormality.compression_defect` [67]) [DERIVED; LEAN; COMPUTED], and the compression is blind to the hidden block, $P(X + QYQ)P = PXP$ with $Q = 1 - P$. The author describes the two sides as a tower and a well. Below the hidden spectrum the self-energy lowers the retained energy, $\Sigma(E) \preceq 0$ for $E < \min \operatorname{spec} D$, and above it the sign reverses [DERIVED; COMPUTED] (Figure 21c).

The present footprint $K(0)$ need not fix the future kernel. With $B = (1,1)/\sqrt{2}$ and hidden spectra $(0,2)$ against $(1,1)$, the zeroth and first moments agree, but at $t = \pi$ the kernels are $+1$ and -1 [DERIVED; COMPUTED] (Figure 20c). How many moments fix it is answered by a finite horizon. For a hidden block of dimension q, $B(zI - D)^{-1}C$ vanishes identically exactly when $BD^jC = 0$ for every $j < q$, by Cayley–Hamilton, and the bound is sharp: the shift of size q with $B = e_1$ and $C = e_q$ is silent for $j < q - 1$ and speaks at $j = q - 1$ (`VOTKP.Memory.transfer_silence`, `VOTKP.Memory.moment_horizon` [62]; `DiracTime.Headline.future_decided_by_first_dim_steps` [56]; Atlas bridge B104 [68]) [CITED; LEAN; COMPUTED]. Applied to two channels side by side, with $\operatorname{diag}(D_1, D_2)$, $(B_1, -B_2)$ and $(B_1, B_2)^*$, it gives the answer: two hidden channels have the same kernel at every t exactly when their moments agree for $n < q_1 + q_2$ [DERIVED; COMPUTED]. In the example $q_1 + q_2 = 4$ and the moments first differ at $n = 2$ (Figure 21a). In finite dimension the moment-recovery question is closed. The same holds for states. The two states $(|01\rangle + e^{i\phi}|10\rangle)/\sqrt{2}$ with $\phi = \pm\pi/2$ have the same local states $I/2$, yet under the exchange coupling $g = 0.7$ their readouts at $t = 0.4$ are $\pm \sin 0.56 = \pm 0.531186$ [49] (§20.5.2; `VOTKP.Witnesses.same_present`, `VOTKP.Witnesses.opposite_futures` [62]), a witness the author first gave in the Dirac Time paper [50] (§11.4) [CITED; LEAN; COMPUTED]; the correlation phase is the missing record (Figure 21b).

A contour can keep a whole isolated spectral cluster while its eigenvectors exchange labels or become ill-conditioned, which is the climb-or-swap behaviour of Section 8; at a Jordan point the single eigenprojector diverges as in (82) while the cluster's trace-log stays finite. The author's black-hole paper states what crosses a wall in the same terms [64] (§4.7 and §5): the Riesz projector of a retained cluster keeps its trace and ledger, and forgets the splitting into vectors and the hidden block. Across the wall a confining stiffness $\kappa = 2\lambda$ acts on the transverse motion; at fixed energy E its displacement amplitude is $\sqrt{2E/\kappa}$, its velocity amplitude $\sqrt{2E}$, and its phase $\int \sqrt{\kappa}\, dt$. As the stiffness grows the displacement, an even record, dies like $\kappa^{-1/2}$, while the phase, a signed record, keeps counting [CITED; DERIVED; COMPUTED] (Figure 21h). That paper gives this in conditional form, since its kinetic metric alone supplies no such stiffness. Eliminating the hidden block is the Schur complement of (99); where the coupling back across a boundary vanishes, the operator is block-triangular there and the boundary is one-way [33] [CITED].

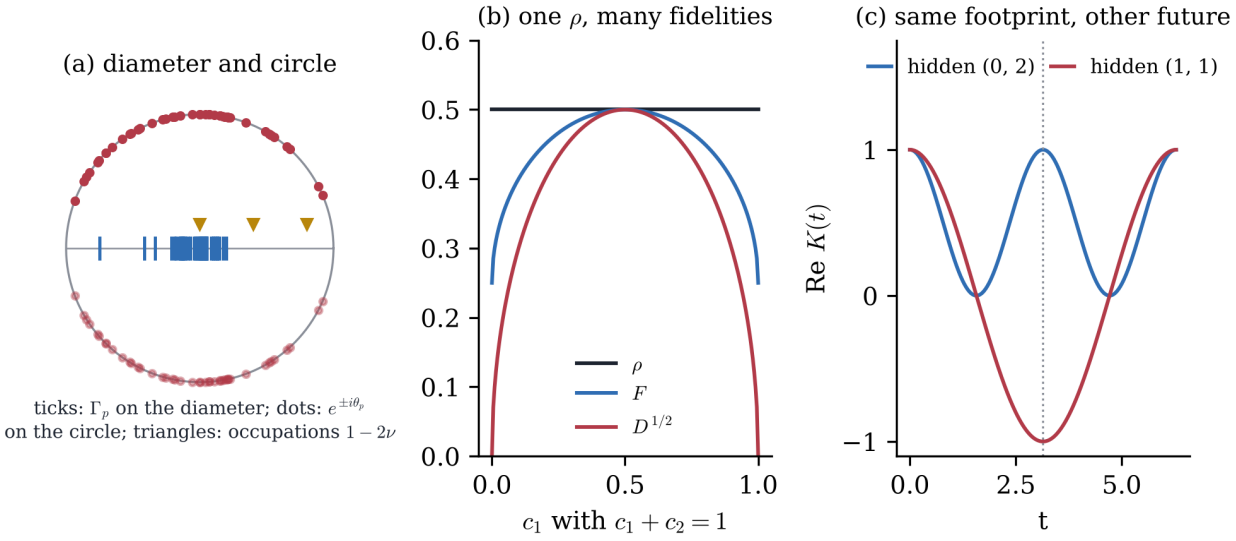


Figure 20: Records outside the books. (a) The Cayley disk: the local twist records Γ_p of 37a1 for $p < 200$ sit on the real diameter (ticks), the normalised Frobenius eigenvalues $e^{\pm i\theta_p}$ on the circle (dots), and occupation records $1 - 2\nu$ on the same diameter (triangles, shown above it). (b) Rank two with $\rho = \frac{1}{2}$ fixed: the fidelity F and the Slater overlap D still vary. (c) Two hidden channels with the same zeroth and first moments: the memory kernels agree at $t = 0$ and are opposite at $t = \pi$.

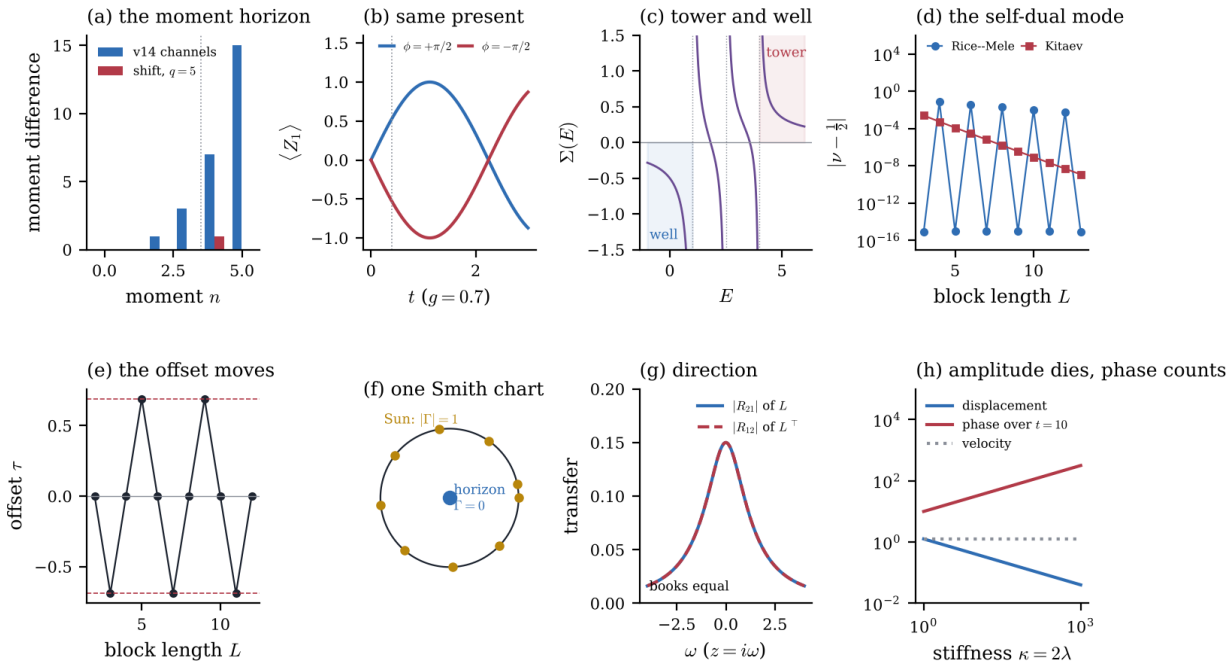


Figure 21: More records outside the books. (a) The moment horizon: two hidden channels with the same zeroth and first moments first differ at $n = 2 < q_1 + q_2 = 4$; the shift of size five speaks only at $n = 4$. (b) The same local state, opposite futures: readouts $\pm \sin 2gt$ from states with marginals $I/2$. (c) The self-energy below the hidden spectrum is negative and above it positive (the tower and the well). (d) Rice–Mele: the mode nearest $\frac{1}{2}$ is pinned in odd blocks only; Kitaev: two modes approach $\frac{1}{2}$ for every length. (e) The offset of a Rice–Mele block: zero in even blocks, alternating in odd blocks towards $\pm 2 \operatorname{artanh}(v/\sqrt{E_{\min} E_{\max}})$. (f) One Smith chart: a horizon is the matched load at the centre, the Sun's trapped modes lie on the circle, and purely reactive loads trace it. (g) Direction: the transfer of a one-way block in each direction, for L and $L^\top$; the books are the same. (h) A stiffening wall at fixed energy: the displacement amplitude falls like $\kappa^{-1/2}$ while the accumulated phase grows.

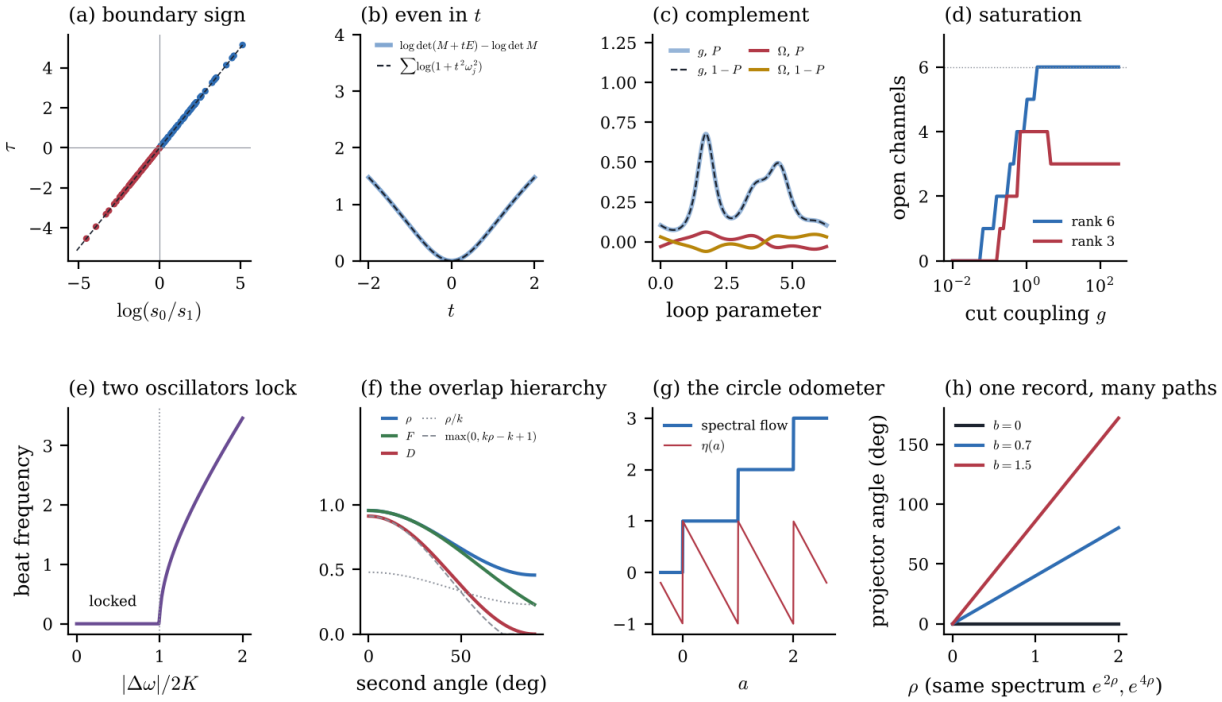


Figure 22: Signs, evenness and saturation. (a) The boundary sets the sign: τ against $\log(s_0/s_1)$ for protected interiors, on the diagonal. (b) The determinant is even in a skew coupling: $\log\det(M+tE)-\log\det M$ against t, with $\sum\log(1+t^2\omega_j^2)$. (c) Along a loop of projectors, P and $1-P$ have the same metric and opposite curvature. (d) Open channels against the coupling across a cut: a full-rank coupling saturates at the six sites of the region, a rank-three coupling ends at three. (e) Two phase oscillators: the beat frequency is zero for $|\Delta\omega| \le 2K$. (f) The overlap hierarchy for two planes, $k=2$, one angle fixed and one turning: $D \le F \le \rho$, with ρ/k and $\max(0, k\rho-k+1)$ below. (g) The circle odometer: spectral flow is a staircase, while the spectrum and η return after one unit. (h) Lifts with one spectrum: the projector angle stays fixed for $b=0$ and turns at rate b otherwise.

12 Penrose and the two books

This section sets the two books beside the Penrose inequality, item by item, in the way the opposite book was set beside the first. The comparison is made against the OpenAI manuscript *Spacetime Penrose inequalities: enclosing area, charge, and rigidity* [93], which proves sharp spacetime Penrose inequalities between the invariant ADM mass and the minimum enclosing area, with rigidity in the equality case, a charged inequality and a local anti-de Sitter inequality. Nothing in this paper is such a bound. There is no area here, and no inequality between two global invariants. What is shared is smaller, and each item below is graded. An exact identity is an identity, checked symbolically or numerically. A structural analogy has the same shape on different objects, and nothing transfers as a theorem.

Exact identities. The product of the books is a difference of squares, $\|DA\|_F^4 - (\mathrm{Re}\,\mathrm{Tr}(DA)^2)^2$, and edge by edge $s^2 - 4\langle a, b\rangle^2$ (9), in the shape of a mass shell $m^2 = E^2 - |P|^2$; the identity is exact and the product is not a mass. On a scalar edge the pair $(d_i + d_j,\ d_i - d_j)$ is a Lorentz vector with invariant $4d_id_j$, and a boost is the composition (21). Eliminating a block is a Schur complement on both sides, and a compression is blind to the block it eliminates, $P(X + QYQ)P = PXP$ (99), (106).

The closest point is the lapse. On the Schwarzschild slice in isotropic coordinates, $\psi = 1 + a/\rho$ and $\lambda = (1 - a/\rho)/(1 + a/\rho)$. To prove rigidity the manuscript doubles the static slice by the method of Bunting and Masood-ul-Alam [94], with the two metrics $h_\pm = \big((1 \pm \lambda)/2\big)^4 h$. On this slice

$$\frac{(1+\lambda)\psi}{2} = 1, \qquad \frac{(1-\lambda)\psi}{2} = \frac{a}{\rho}, \tag{107}$$

so one sheet is flat space and the other, $(a/\rho)^4\delta$, is its image under the inversion $\rho \mapsto a^2/\rho$, which turns λ into $-\lambda$. Read $(1, \lambda)$ as a scalar edge. Then $(1 \pm \lambda)/2$ are the half-amplitudes of its two books, their ratio is the reflection coefficient $\Gamma = (1 - \lambda)/(1 + \lambda) = a/\rho$, the weights $p_\pm = (1 \pm \lambda)/2$ have $\log(p_+/p_-) = \log(\rho/a)$, and $\lambda = \tanh\big(\frac{1}{2}\log(\rho/a)\big)$, as in (20). The inversion that swaps the sheets is the sign flip that swaps the books (17) [DERIVED; COMPUTED]. The identity is exact. The objects are not the same: a doubled metric is not a field on a graph [STRUCTURAL COMPARISON] (Figure 23a,b).

Structural analogies. Near the wall of Section 10 and near a non-degenerate horizon the same fold appears,

$$ds^2 = \frac{dX^2}{4c^2X} = \frac{d\lambda^2}{c^2}, \qquad X = \lambda^2, \tag{108}$$

with $\lambda \mapsto -\lambda$ an isometry; $c = 1$ at the Bures wall and $c = \kappa$, the surface gravity, at a Schwarzschild horizon. The author graded this himself as structural: the constants differ, the base is a quotient by a flow that becomes null, and the normal form is generic [64] (§§9.3–9.9). The charged bound uses the coordinate of the scalar edge. With $r = Qe^\tau$, $\frac{1}{2}(r + Q^2/r) = Q\cosh\tau$; the Reissner–Nordström horizons satisfy $r_+r_- = Q^2$, so $\tau_+ = -\tau_-$, and the extremal hole sits at $\tau = 0$, $\Gamma = 0$ [DERIVED; COMPUTED] (Figure 23c). In the anti-de Sitter part the map from a transverse-traceless seed to its quadratic correction is a projector self-adjoint in the manuscript's inner product, so the area correction and the deficit add as orthogonal halves, as the two halves of Section 2 do; a finite projector self-adjoint in a metric N splits $\|q\|_N^2 = \|Pq\|_N^2 + \|(1-P)q\|_N^2$ [DERIVED; COMPUTED]. There too a quadratic deficit that vanishes does not give equality, and the decision falls at fourth order; here the same lesson is "same footprint, other future" (104). The operator of a marginally

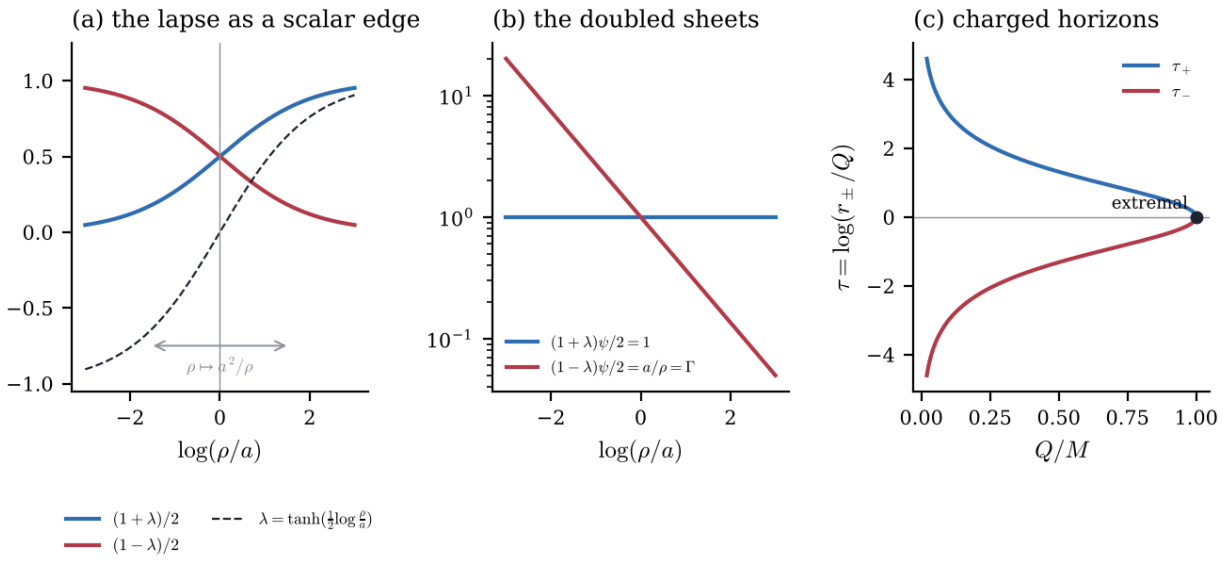


Figure 23: The lapse as a scalar edge. (a) On the isotropic Schwarzschild slice, the half-amplitudes $(1 \pm \lambda)/2$ of the two books against $\log(\rho/a)$; $\lambda = \tanh(\frac{1}{2}\log(\rho/a))$ and the inversion $\rho \mapsto a^2/\rho$ is the reflection of the axis. (b) The doubled sheets: $(1+\lambda)\psi/2 = 1$ is flat space, and $(1-\lambda)\psi/2 = a/\rho$ is the reflection coefficient of the edge. (c) Reissner–Nordström horizons in the coordinate $\tau = \log(r/Q)$: $\tau_+ = -\tau_-$, meeting at $\tau = 0$ for the extremal hole.

outer trapped surface loses its drift under conjugation by e^{ψ}, as the four-body block becomes self-adjoint in a weighted metric (Section 10). A Killing horizon has its kernel along the stratum, while the coplanar wall has it across. Minimizers that tie carry a multiplier measure, as the ring floors of (37) tie at $d = \pi$ with a corner (Section 7). A quadratic form that matches a projector Hessian identifies nothing, since any positive form can be one [95]. Of Penrose's cosmology one structural point reaches the books: the author's Dirac Time asks which records survive a conformal transition [50] (§24.1), and here that is the scale blindness of (34): ratios of books and the Born matrices survive $D \mapsto sD$, absolute rates do not [STRUCTURAL COMPARISON].

No link. The mass–area inequality itself; the twist identity, already excluded since a static spacetime with zero twist need not give a normal operator (Section 10); the adjoint of the constraint map, the Hawking mass on constant-mean-curvature leaves, inverse mean curvature flow and the conformal deformation of the manuscript; conformal cyclic cosmology and Hawking points; objective reduction; the Penrose process; and Penrose tilings, diagrams and twistors have no counterpart in this paper.

13 What is classical and what is observed here

The underlying self-commutator identity and graph-connection framework are classical; the scalar specialization reduces to the weighted Dirichlet identity [6]. Its opposite at the scalar level is the signless Laplacian, whose least eigenvalue detects bipartiteness [7, 8]; the sign that odd cycles carry is the balance of signed and gain graphs [9, 10, 11]; the splitting of a spectrum over a double

cover is that of 2-lifts [12]; and connection and sheaf Laplacians on graphs are [2, 4, 5]. The Born rule on subspaces and its uniqueness are Gleason's and Hossenfelder's setting [14, 15], and the duality on an edge is the complementarity relation of Jakob and Bergou [87, 88]; the orthogonal representations of odd cycles and their contextuality bound are those of Klyachko–Can–Binicioğlu–Shumovsky, Lovász and Cabello–Severini–Winter [16, 17, 18]; the overlap expansion is the author's earlier Gravity Ledger result [13]. The twisted zeta, the Bass factorisation and the graph Riemann hypothesis are classical [19, 21, 24, 25]. Koide's relation and its 45° form are Koide's and Foot's [34, 35, 36], and the circulant parametrisation of the roots and its phase observations are Brannen's [37]; neither is a mass-selection law. Hasse's bound, the Sato–Tate law, the point counts of the LMFDB curves, the partial Euler products and the murmurations of elliptic curves are established [40, 41, 42, 43, 44, 45]. Fidelity and the Bargmann invariant are standard [46, 47], Pincherle's theorem on minimal solutions is classical [53, 54], transient growth is read from pseudospectra [89], the Rice–Mele and Kitaev chains and the locking of two oscillators are known [90, 91, 92], and the Penrose inequalities and their rigidity are the manuscript's and Bunting and Masood-ul-Alam's [93, 94]. The route-and-endpoint defect, the common clock, the moving frame, the path ledger, the offset algebra and its boundary ratio, the Schur–Cayley boundary, the four-body wall in its Bures metric, the relaxation flow, the defect and guard of a relator, the moment horizon and the Jordan growth threshold are the author's earlier results [49, 50, 51, 52, 33, 64, 71, 73, 76], cited with their Lean declarations; many are stated earlier as bridges of the author's Atlas [68]. No priority is claimed for elementary constructions. The present observations are the exact identification of the self-commutator energy of this block transport operator with the induced endomorphism-connection energy, and of $\frac{1}{8}\|H^2 - H^{*2}\|_F^2$ with its sign-twisted partner, the two being the Hermitian and skew halves of DA, sharing a fixed budget and split by the double cover; the reading of both as Born-weighted sums; the sector flip as a quarter turn with its exact defect; the appearance of the contextuality configurations as the fields that balance both books on an odd loop; the two ends of the Bass pencil as the two book operators; the triangle's primitive cycle as the cubic record both books leave free, kept by a noncentral transport and lost by a scalar one; the minimal solution of an eigenvalue's prime-trace recurrence as the condition for its zeta zeros to leave the circle, with the companion's trace form as the wall on the bound; the good-prime Frobenius edge with its sign-blind books and its signed twist record; the books of a scalar chain as its route length, with the signs as its endpoint; Koide's relation as the balance of the centered books on one declared plane; the two books as differences of three numbers, with the relaxation flow spending the connection energy as the departure from normality; the blindness of both books to direction; and the doubled Schwarzschild slice read as the two books of one scalar edge. It arose from the author's block transport construction of 18–21 June 2026, $H_N = D + A$ with the skew transport $A_{n,n+1} = J$, whose self-commutator $[D + A, (D + A)^\top] = 2[A, D]$ contains the edge term $JB_{n+1} - B_nJ$; on a ring, $\frac{1}{8}\|[H, H^\top]\|_F^2 = \sum_n \|JB_{n+1} - B_nJ\|_F^2$, the connection energy of (1) with the unitary J [DERIVED; COMPUTED]. Those drafts are formalised in `SpectralStability.Recovered` (`skew_transport_commutator`, `skew_transport_normal_iff`, `commutator_gradient`, `commutes_forces_uniform` [79]), whose centred difference repairs the drafts' own. The paper the author published on 24 June uses the symmetric transport $\propto J \otimes \Delta_1$ [78], for which $D_0 + A$ is normal; the opposite book entered with the skew form. In the author's reading, A is time-like transport and D space-like obstruction, and the connection energy is a budget for transient growth, made exact by the relaxation flow (13). These names describe roles; no spacetime signature or causal field equation is inferred from the decomposition.

Scope. The budget is an identity of a fixed field, not a conservation law. The product of the books has a Lorentzian shape and is not a mass. The wall result concerns the asymptotic exponent, not settling at a finite tolerance. The weight reading of Koide assumes coherent positive amplitudes; dephasing gives $\frac{1}{3}$. The relation is one among pole masses. The Frobenius representative U_p is not a physical inner product, Hasse's inequality is strict, the Pincherle reading restates the graph Riemann hypothesis without proving any case of it, and nothing here proves the Birch–Swinnerton-Dyer conjecture, a Riemann hypothesis, a universal law of exceptional-point selection, a rank predictor, or a prime origin of lepton masses. No galactic or cosmological law is claimed, and no Penrose-type inequality: Section 12 grades every point of contact.

Open. The selection question is now concrete. A physical generator equivalent to $Z - hI$ has to be derived, with its norm and resource, and with dynamics for its parameters. It must select both the cone and the cubic C_3, and it must address the overall scale, the number of generations and the difference between pole and running masses. Preserving a cone that was imposed at the start is not enough. On the arithmetic side the signed traces and quadratic characters have to be kept, local twists separated from global ones, and tests run on conductor-controlled families with held-out data, against the established murmuration and rank heuristics; squared books cannot recover an odd statistic (Theorem 6). On the graph side the question is which holonomy probes can be measured, rather than inferring a full connection from one field's energies; why exceptional points of the twisted Hashimoto spectrum on non-bipartite graphs so often carry two transpositions at once, off $|w| = 1$; and whether the rate of the opposite book along the relaxation flow is never positive, as it was in every run. The author reads the admissibility result (10) physically: matter whose coupling runs across sectors, as in closed-shell atoms, and matter with strong same-sector coupling, as in ordinary bonding, should sit at different values of the defect $2\,\mathrm{Tr}\,B^2$; the noble gases are the proposed test, and it has not been run. A further question is when the skew book must vanish, the analogue for H of the twist identity of a static spacetime. And the quantitative form of the statement that frustration needs loops with no common invariant subspace, a lower bound on the Born shortfall by the distance from a common fixed subspace, holds numerically in a curator's test but has no stated constant yet.

Acknowledgements. The Koide relation reached the author from Caleigh Fisher (@Kali_fissure), who wrote the lepton generations as stress expressions; the wavelength form in Section 10 is that form.

A Proofs

The two identities. With $H^* = D - A$: $HH^* - H^*H = (D + A)(D - A) - (D - A)(D + A) = -2(DA - AD)$, and $H^2 - H^{*2} = 2(DA + AD)$. The diagonal blocks of $DA \pm AD$ are $D_iA_{ii} \pm A_{ii}D_i = 0$. For an edge, $(DA \mp AD)_{ij} = D_iA_{ij} \mp A_{ij}D_j = (D_i \mp \mathcal{U}_{ij}(D_j))A_{ij}$, of Frobenius norm $\|D_i \mp \mathcal{U}_{ij}(D_j)\|$ since A_{ij} is unitary. Off edges the blocks vanish. The (j, i) block has the same norm, so $\|DA \mp AD\|^2 = 2\sum_E \|D_i \mp \mathcal{U}_{ij}(D_j)\|^2$ and the factor 4 from $\|2(\cdot)\|^2$ gives 8.

The zero sets. Normality is $[H, H^*] = 0$ and the Hermitian square is $H^2 = (H^2)^* = H^{*2}$; each is a sum of non-negative edge terms, zero exactly when every edge term vanishes. On a connected graph, an anti-parallel field satisfies $D_{i_0} = (-1)^\ell W_p D_v W_p^*$ along any walk p of length ℓ from i_0 to

v, so on a closed walk $D_{i_0} = (-1)^\ell W_p D_{i_0} W_p^*$. Conversely, an X fixed by every signed holonomy defines $D_v = (-1)^\ell W_p^* X W_p$ independently of the walk, because two walks differ by a closed one, and this field is anti-parallel. Evaluation at i_0 is real-linear and injective on anti-parallel fields, which gives (16).

The double cover. With $a_\pm = S_i \pm T_i$ and $b_\pm = \mathcal{U}(S_j \pm T_j)$, the two lifted edges give $\|a_+ - b_-\|^2 + \|a_- - b_+\|^2$. Writing $s = S_i - \mathcal{U}S_j$ and $t = T_i + \mathcal{U}T_j$, $a_+ - b_- = s + t$ and $a_- - b_+ = s - t$, so the sum is $2\|s\|^2 + 2\|t\|^2$ by the parallelogram law.

The scalar shore. For $r = 1$ and arbitrary nonzero edge entries, $[D, A]_{ij} = (d_i - d_j)A_{ij}$ and $\{D, A\}_{ij} = (d_i + d_j)A_{ij}$, which gives (35). If $Q_w d = 0$ then $\sum w_{ij}(d_i + d_j)^2 = 0$, so $d_j = -d_i$ along every edge; on a component this is consistent exactly when the component has no odd cycle, and then the solution is unique up to scale.

The ring. With $D_k = \cos\vartheta_k \sigma_z + \sin\vartheta_k \sigma_x$ and the edge transport a rotation by φ in the z–x plane, $\|D_k \mp \mathcal{U}(D_{k+1})\|^2 = 2|e^{i\vartheta_k} \mp e^{i(\vartheta_{k+1}+\varphi)}|^2 = 4(1 \mp \cos x_k)$. At a critical point of $\sum_k (1 - \cos x_k)$ under a fixed sum every $\sin x_k$ is equal, so each x_k is α or $\pi - \alpha$; that the equal share is the lowest of these is verified numerically, by comparing (37) with direct minimisation from many random starts.

The Born reading. With $D_i = \sum_a \lambda_a P_a$ and $\mathcal{U}_{ij}(D_j) = \sum_b \mu_b \mathcal{U}_{ij}(Q_b)$, $\|D_i \mp \mathcal{U}_{ij}(D_j)\|^2 = \sum_a \lambda_a^2 + \sum_b \mu_b^2 \mp 2\sum_{a,b} \lambda_a \mu_b W_{ab}$. Since $\sum_b W_{ab} = \operatorname{Tr} P_a = 1$ and $\sum_a W_{ab} = \operatorname{Tr} Q_b = 1$, the first two sums are $\sum_{a,b} W_{ab}\lambda_a^2$ and $\sum_{a,b} W_{ab}\mu_b^2$, which gives (6).

The sector flip. $\operatorname{Tr}(AB) = \operatorname{Tr}(\Gamma A \Gamma\, \Gamma B \Gamma) = -\operatorname{Tr}(AB)$, so $\operatorname{Tr}(AB) = 0$. Next $(\Gamma X)^2 = \Gamma X \Gamma X = (B - A)(A + B)$, whose trace is $\operatorname{Tr} B^2 - \operatorname{Tr} A^2$, while $\operatorname{Tr} X^2 = \operatorname{Tr} A^2 + \operatorname{Tr} B^2$; adding gives (10). From $\Gamma A \Gamma = -A$ and $\Gamma^* = \Gamma$, $A^*\Gamma = -\Gamma A^*$, so $\Gamma A + (\Gamma A)^* = \Gamma(A - A^*)$ and $\Gamma A - (\Gamma A)^* = \Gamma(A + A^*)$. For (11), $U = e^{-i\pi\Gamma/4}$ acts as $e^{\mp i\pi/4}$ on the two sectors, so on the crossing blocks UAU^* is A times $e^{-i\pi/2}$ on one block and $e^{i\pi/2}$ on the other, which is $-i\Gamma A$.

The overlap. $\operatorname{Tr}((P - R)^2) = \operatorname{Tr} P + \operatorname{Tr} R - 2\operatorname{Tr}(PR) = 2k - 2\operatorname{Tr}(PR)$ for idempotents of trace k. Along the curve, $\operatorname{Tr}((P(t) - P_0)^2) = t^2 \operatorname{Tr} V^2 + o(t^2)$.

The odd floor in $\mathbb{C}^2$. With Bloch vectors, $p_e = \frac{1}{2}(1 + \cos\alpha_e)$. Put $m_k = (-1)^k n_k$; consecutive m's are separated by $\beta_k = \pi - \alpha_k$, and for odd N the path $m_1, \dots, m_{N+1}$ runs from $-n_1$ to n_1, so $\sum \beta_k \geq \pi$. Maximising $\sum \cos\beta_k$ under $\sum \beta_k = \pi$, the stationary points have all $\sin\beta_k$ equal, so each β_k is β or $\pi - \beta$; one value $\pi - \beta$ forces $\beta = 0$ and the value $N - 2$, while none gives $N\cos(\pi/N)$, which is larger for $N \geq 3$. Hence $\sum p_e \geq \frac{N}{2}(1 - \cos\frac{\pi}{N})$, attained by planar vectors turning by $\pi - \pi/N$ at each step.

The bow tie. For one triangle with closing holonomy a Pauli matrix, the field at the shared vertex n_0 must reach its image under the half turn about the Pauli axis in three steps. If θ is the angle from n_0 to that axis, the image is 2θ away, and sharing it equally gives the most, $\frac{3}{2}(1 + \cos\frac{2\theta}{3})$. The two axes are orthogonal, so $\theta_x + \theta_z \geq \frac{\pi}{2}$, and the optimum is $\theta_x = \theta_z = \frac{\pi}{4}$: $\sum p = 3 + \frac{3\sqrt{3}}{2}$ over six edges

and $\mathcal{E}^- = 2(6 - \sum p) = 6 - 3\sqrt{3}$. The shared-edge value is computed by direct optimisation from many random starts.

The odd floor by the adjacency spectrum. The same floor follows in one line. The least adjacency eigenvalue of an odd cycle of length N is $-2\cos(\pi/N)$. Applied to each Bloch component, $\sum_i n_i \cdot n_{i+1} = \frac{1}{2}\sum_{ij} A_{ij}\, n_i \cdot n_j \geq -\cos(\pi/N)\sum_i |n_i|^2 = -N\cos(\pi/N)$, so $\sum_i \mathrm{Tr}(P_i P_{i+1}) = \frac{N}{2} + \frac{1}{2}\sum_i n_i \cdot n_{i+1} \geq \frac{N}{2}(1 - \cos\frac{\pi}{N})$, attained by a coplanar winding.

Centered projectors. In the difference the scalar parts cancel, so $\|D - UEU^*\|^2 = \|P - UQU^*\|^2 = 2k - 2k\rho$. For the sum, $\|P + UQU^* - \frac{2k}{r}I\|^2 = \|P + UQU^*\|^2 - \frac{4k}{r}\,\mathrm{Tr}(P + UQU^*) + \frac{4k^2}{r^2}\,r = 2k(1 + \rho) - \frac{8k^2}{r} + \frac{4k^2}{r}$, which is (33).

The Bass factorisation. Let O map vertex fibres to arc fibres by $(Ox)_e = x_{o(e)}$, with $o(e)$ the origin of e, and let J be the weighted reversal $(Jy)_e = \rho_e\, y_{\bar{e}}$. Since $\rho_{\bar{e}} = \rho_e^{-1}$, $J^2 = I$; also $O^*O = \mathrm{Deg} \otimes I$, $O^*JO = A_\rho$, and $J(OO^* - I)$ is the non-backtracking matrix in the convention $(B)_{ef} = \rho_e$ when the head of e is the tail of f and $f \neq \bar{e}$, which has the same characteristic polynomial as B_ρ. For $u \neq \pm 1$, $(I + uJ)^{-1}J = (J - uI)/(1 - u^2)$ and each unoriented edge gives $\det(I + uJ) = (1 - u^2)^d$ on its two arcs. Then $I - uB = (I + uJ) - uJOO^*$, and Sylvester's identity gives

$$\det(I - uB) = \det(I + uJ)\,\det\big(I - uO^*(I + uJ)^{-1}JO\big) = (1 - u^2)^{md}\,\det\tfrac{I - uA_\rho + u^2(\mathrm{Deg} - I)\otimes I}{1 - u^2},$$

which is (41); the exceptional values follow from the polynomial identity. Each of these matrix facts is checked separately. At $u = \pm 1$ the pencil is $\mathrm{Deg} \otimes I \mp A_\rho$, which is (42), and on a $(q+1)$-regular graph $K(1/(qu)) = I - A_\rho/(qu) + I/(qu^2) = (qu^2)^{-1}K(u)$, which is (47).

The triangle. A non-backtracking walk on a triangle must continue around it in one sense, so every closed one is a power of one of the two oriented primitive cycles, of length 3 and holonomy $e^{\pm 3i\phi}$; the product (40) gives (57), and $\log \zeta_\phi = \sum_n (e^{3in\phi} + e^{-3in\phi})u^{3n}/n$ has C_3 as its u^3 coefficient. The eigenvalues of Φ are $d + y$ with $y = 2t\cos\alpha$, $\alpha = \phi + 2\pi j/3$, and $4\cos^3\alpha - 3\cos\alpha = \cos 3\alpha = \cos 3\phi$ gives $y^3 - 3t^2 y - t^3 C_3 = 0$, which is (58); the elementary symmetric functions then fix the unordered roots. For Proposition 3, in the basis $E_{11}, E_{22}, E_{12}, E_{21}$ conjugation by U fixes the first two and multiplies the others by $e^{\pm i\phi}$, so B splits into four scalar triangles with phases $0, 0, \phi, -\phi$, and (59) is the product of their factors. The field σ_z commutes with every edge transport, so each edge contributes 0 and $\|2\sigma_z\|_F^2 = 8$.

The positive phase domain. At $t = d/\sqrt{2}$ the trace $3d$ and $e_2 = 3d^2/2$ are positive. For three real roots these and a positive determinant force all three positive: two negative roots $-a, -b$ and a positive $c > a + b$ would give $e_2 = ab - c(a + b) < 0$. By (56), $e_3 = d^3(\cos 3\phi/\sqrt{2} - \frac{1}{2})$, positive exactly when $\cos 3\phi > 1/\sqrt{2}$; necessity follows from the same formula.

The Frobenius edge. Conjugation by U_p rotates σ_x by the angle $2\theta_p$ in the plane of σ_x, σ_y, so $\mathrm{Tr}(\sigma_x U_p \sigma_x U_p^*) = 2\cos 2\theta_p$ and, with $\|\sigma_x\|_F^2 = 2$, $\|D_p \mp U_p D_p U_p^*\|^2 = \frac{p}{2}(4 \mp 4\cos 2\theta_p)$, that is $4p\sin^2\theta_p$ and $4p\cos^2\theta_p$. The overlap is $|\langle +|U_p|+\rangle|^2 = \cos^2\theta_p$ with $|+\rangle = (1,1)/\sqrt{2}$, and $D_p = \sqrt{2p}\,(P_x - \frac{1}{2}I)$ gives the factor $2p$. Theorem 6 is $\mathrm{Ad}(-U)X = (-U)X(-U)^* = UXU^*$.

The twists. The model $dy^2 = f(x)$ of $E^{(d)}$ has

$$N = p + 1 + \sum_x \chi_p\big(d\, f(x)\big) = p + 1 + \chi_d(p) \sum_x \chi_p\big(f(x)\big),$$

which gives $a_p(E^{(d)}) = \chi_d(p) a_p(E)$. If $\chi_d(p) = 1$ the counts coincide and the logarithm is 0; if $\chi_d(p) = -1$ it is $\log \frac{p+1+a_p}{p+1-a_p} = 2\operatorname{artanh} \frac{a_p}{p+1}$. A local nonsquare twist is the case $\chi = -1$ at one prime, which gives (67) and (68).

The finite-time norms. For $\zeta = 0.8$ the eigenvalues are $-0.8 \pm 0.6i$ and $e^{tG} = e^{-0.8t}\big(\cos(0.6t) I + \frac{\sin 0.6t}{0.6}(G + 0.8I)\big)$, which is $-e^{-0.8t_*} I$ at $0.6t_* = \pi$. At $\zeta = 1$, $I + tT = \left(\begin{smallmatrix} 1+t & t \\ -t & 1-t \end{smallmatrix}\right)$ has determinant 1 and Frobenius norm squared $2 + 4t^2$, so its larger singular value is $t + \sqrt{1+t^2}$.

The stress flow. For $Z = h_1\sigma_z + h_2\sigma_x + sJ$, $C = [Z, Z^\top] = 4s(h_2\sigma_z - h_1\sigma_x)$, and $-2[C, Z]$ has coordinates $\dot h_j = -16 s^2 h_j$, $\dot s = -16 h^2 s$. Then $\frac{d}{dt}(h^2 - s^2) = -32 s^2 h^2 + 32 h^2 s^2 = 0$, and on $h = s$, $\dot s = -16 s^3$ integrates to $s(t) = s(0)/\sqrt{1 + 32 s(0)^2 t}$.

The reset bath. With $H = \frac{\Delta}{2}\sigma_z$ and $\varrho = \frac{1}{2}(I + x\sigma_x + y\sigma_y + z\sigma_z)$, $-i[H, \sigma_x] = \Delta\sigma_y$ and $-i[H, \sigma_y] = -\Delta\sigma_x$, so $(\dot x, \dot y)$ has generator $\left(\begin{smallmatrix} -1/\tau & -\Delta \\ \Delta & -1/\tau \end{smallmatrix}\right)$, a scalar plus a skew matrix, hence normal.

Overlaps and the hidden channel. With $\sqrt{P/k} = P/\sqrt{k}$, the eigenvalues of $\sqrt{P/k}\,(R/k)\sqrt{P/k}$ are c_a/k^2, so $\sqrt{F} = \frac{1}{k}\sum_a \sqrt{c_a}$. Then $\rho - F$ is the mean of c_a minus the squared mean of $\sqrt{c_a}$, a variance; $F \le \rho$ is the same statement, and $D^{1/k} = (\prod_a \sqrt{c_a})^{2/k} \le F$ is the arithmetic–geometric mean. For (103), $\operatorname{Tr}(P_0 P_1 P_2^{\pm}) = \langle v_0|v_1\rangle\langle v_1|v_2^{\pm}\rangle\langle v_2^{\pm}|v_0\rangle = \frac{1}{\sqrt2} \cdot \frac{1 \pm i}{2} \cdot \frac{1}{\sqrt2}$. For the hidden channel, $BB^* = 1$ and $BDB^* = 1$ for both spectra, while $K(\pi) = \frac{1}{2}(1 + e^{-2\pi i}) = 1$ and $e^{-i\pi} = -1$. For a gauge-invariant Gaussian state, a unitary change of modes makes it a product over the eigenmodes of C with occupations ν_j, so the full and empty probabilities are $\prod \nu_j = \det C$ and $\prod(1 - \nu_j) = \det(I - C)$.

Additions: identities. For (2), $(S + K)^* = S - K$ and $[S + K, S - K] = -[S, K] + [K, S] = 2[K, S]$. For (9), $\|a \mp b\|^2 = s \mp 2\langle a, b\rangle$, and $s^2 = (\|a\|^2 - \|b\|^2)^2 + 4\|a\|^2\|b\|^2$. For (14), $\|KK^* - K^*K\|^2 = 2\|K^*K\|^2 - 2\operatorname{Tr}(KK^*K^*K) = 2\|K^*K\|^2 - 2\|K^2\|^2$ and $\|K^2 - K^{*2}\|^2 = 2\|K^2\|^2 - 2\operatorname{Re}\operatorname{Tr} K^4$; for normal K these give 0 and $\frac{1}{4}\sum(|\lambda|^4 - \operatorname{Re}\lambda^4) = 2\sum(\operatorname{Re}\lambda \operatorname{Im}\lambda)^2$. Along (13), $\frac{d}{dt}\|K\|^2 = 2\operatorname{Re}\operatorname{Tr}(K^*\dot K) = -4\operatorname{Tr}(K^*[C, K]) = -4\operatorname{Tr} C^2$, since $\operatorname{Tr}(K^*CK - K^*KC) = \operatorname{Tr}(C(KK^* - K^*K))$. For (32), write $M = mI + M_0$; M_0 is symmetric and trace-free, so $M_0 J = -JM_0$, and $\|[M, J]\|^2 + \|\{M, J\}\|^2 = 2\|MJ\|^2 + 2\|JM\|^2 = 4\|M\|^2$. For (46), $\|v \mp \lambda v\|^2 = |1 \mp \lambda|^2$ and $|1 - \lambda|^2 + |1 + \lambda|^2 = 2 + 2|\lambda|^2$.

Additions: graphs. If the unsigned incidence matrix kills x, then $x_j = -x_i$ along every edge, which is consistent on a connected graph exactly when it is bipartite; so the edge budgets determine the vertex norms exactly on connected non-bipartite graphs. For (36), expand D in eigenvectors of L_U: $\mathcal{E}^-(D) = \sum \lambda \|D_\lambda\|^2 \ge \lambda_+ \sum_{\lambda > 0} \|D_\lambda\|^2$. For the ring corner, the two branches $w = 0$ and $w = 1$ of (37) meet at $d = \pi$ with derivatives $\pm 4\sin(\pi/N)$. For a loop with $W^*\eta W = \eta$ and $W = \left(\begin{smallmatrix} 1 & 1 \\ 0 & 1 \end{smallmatrix}\right)$, the $(2,2)$ entry gives $\eta_{11} + \eta_{12} + \eta_{21} = 0$ and the $(1,2)$ entry $\eta_{11} = 0$. For $P = \frac{1}{2}(I + n \cdot \sigma)$, $[P, \sigma_x] = \frac{1}{2}(n_y[\sigma_y, \sigma_x] + n_z[\sigma_z, \sigma_x])$, of norm squared $2(n_y^2 + n_z^2)$, and likewise $2(n_x^2 + n_y^2)$ for σ_z.

Additions: overlaps. For (27), $V = P_0VQ_0 + Q_0VP_0$ with $Q_0 = 1 - P_0$, so $\Gamma V = P_0VQ_0 - Q_0VP_0$ and $P_0\Gamma V + \Gamma VP_0 = \Gamma V$; ΓV crosses the sectors, so (10) gives $q(\Gamma V) = -q(V)$, and $X = [\Gamma V, P_0]$ has $[X, P_0] = \Gamma V$, so the curve has tangent ΓV and (26) gives the expansion. For the Fisher information, P/k has eigenvalues $1/k$ and 0, the tangent couples only the range to the kernel, and the symmetric-logarithmic-derivative formula gives $F_Q = 2\sum|\dot\varrho_{ij}|^2/(p_i + p_j) = \frac{4}{k}\|Q_0VP_0\|^2 = 4g(V, V)/k$. For the hierarchy, $(\sum\sqrt{c_a})^2 \geq \sum c_a$ gives $F \geq \rho/k$; $\prod c_a \geq 1 - \sum(1 - c_a)$ gives the lower bound on D, and the arithmetic–geometric mean the upper. The generating function is $\det\big(I_k + (z-1)U_P^*RU_P\big)$. Near coincidence $\sqrt{c} = 1 - \frac{1}{2}(1-c) + O((1-c)^2)$, so $\mathrm{Var}(\sqrt{c_a}) = \frac{1}{4}\mathrm{Var}(c_a) + \ldots$, of fourth order in the angles.

Additions: the wall. For (76), $ab = \Omega^2(I_2 - I_3)(I_1 - I_2)/(I_1I_3)$. For (53), the right and left eigenvectors of $\left(\begin{smallmatrix} c & -1 \\ 1 & 0 \end{smallmatrix}\right)$ for λ_d are $(\lambda_d, 1)$ and $(\lambda_d, -1)$; with $\lambda_d + \lambda_d^{-1} = c$, $(u \cdot v)^2 = (\lambda_d^2 - 1)^2/(\lambda_d^2 + 1)^2 = (c^2 - 4)/c^2$, and for a rank-one $B = uv^\top$ with unit u, v, $\frac{1}{2}\|uu^\top - vv^\top\|^2 = 1 - (u \cdot v)^2$. For (81), expand the entries of A; the commutator of a real 2×2 matrix is $(A_{12} - A_{21})$ times a matrix with entries $A_{12} + A_{21}$ and $A_{22} - A_{11}$. For (85), $|\sum_k x_k e^{i\phi_k}| \leq S$, with equality at equal phases, and $|\sum_k x_k e^{i\phi_k}| \geq x_{\max} - (S - x_{\max})$, attained by opposing the largest root to the other two. For the Jordan threshold, $\|I + tN\|_2 = (\sqrt{4 + \mu^2t^2} + |\mu|t)/2$ for $N = \left(\begin{smallmatrix} 0 & \mu \\ 0 & 0 \end{smallmatrix}\right)$.

Additions: records. For (92), $M + tE = M^{1/2}(I + tJ)M^{1/2}$ with $J = M^{-1/2}EM^{-1/2}$ real and skew, whose eigenvalues come in pairs $\pm i\omega_j$, so $\det(I + tJ) = \prod(1 + t^2\omega_j^2)$. For the interface, $\det\left(\begin{smallmatrix} A & E \\ \pm E^* & B \end{smallmatrix}\right) = \det A \det B \det(I \mp K)$ with $K = A^{-1}EB^{-1}E^*$, whose eigenvalues are those of $A^{-1/2}EB^{-1}E^*A^{-1/2} \succeq 0$, below 1 when the Hermitian block is positive. For (94), $\partial(1 - P) = -\partial P$, so g is unchanged and $\Omega_{1-P} = i\,\mathrm{Tr}((1 - P)[\partial_x P, \partial_y P]) = -\Omega_P$, the trace of a commutator being zero. For (96), the Schur complements give $\det C_{B+x} = \det C_B\, s_1$ and $\det(I - C_{B+x}) = \det(I - C_B)\, s_0$. For (106), $PH^2P = PH(P + Q)HP$. For the moment horizon, Cayley–Hamilton writes D^q through lower powers, and $B(zI - D)^{-1}C = \sum_j BD^jC\, z^{-j-1}$; the two channels side by side give $B_1D_1^nB_1^* - B_2D_2^nB_2^* = (B_1, -B_2)\,\mathrm{diag}(D_1, D_2)^n(B_1, B_2)^*$. For the opposite futures, in the span of $|01\rangle, |10\rangle$ the exchange is $g\sigma_x$ and $\langle Z_1\rangle(t) = \sin 2gt\, \sin\phi$.

Additions: Penrose. With $\psi = 1 + a/\rho$, $(1 \pm \lambda)\psi/2 = \big((1 + a/\rho) \pm (1 - a/\rho)\big)/2$, which is 1 and a/ρ. The pullback of δ under $\rho \mapsto a^2/\rho$ is $(a/\rho)^4\delta$ in isotropic coordinates, and $\lambda(a^2/\rho) = -\lambda(\rho)$. For the charged bound, $r_\pm = M \pm \sqrt{M^2 - Q^2}$ gives $r_+r_- = Q^2$. For (108), $dX = 2\lambda\, d\lambda$.

Oblique pairs. From $T^*\eta_0T = \eta$, $Q^*\eta_0 = T^{-*}P^*\eta T^{-1} = T^{-*}\eta PT^{-1} = \eta_0Q$. With $S = \eta_0^{1/2}$, SP_0S^{-1} and SQS^{-1} are orthogonal projectors of rank k, and (26) applied to them is (28). Differentiating $Q = TPT^{-1}$ at 0 gives $\dot TP_0 + \dot P - P_0\dot T$. For the oblique idempotent, the metric $G_1 = \left(\begin{smallmatrix} 3 & 0 & 0 \\ 0 & 10 & -7 \\ 0 & -7 & 5 \end{smallmatrix}\right)$ is positive definite, $G_1P = 4ww^\top$ with $w = (\frac{3}{4}, \frac{3}{4}, -\frac{1}{2})$ and $G_1E_{11} = 3E_{11}$ are symmetric, so P and E_{11} are G_1-orthogonal projectors with $\mathrm{Tr}(PE_{11}) = \frac{3}{4}$; exchanging the first two coordinates gives E_{22}.

B The formal companion

The core identity of the one-page note [65], (1) and (3) with the holonomy direction of (4), is formalised in Lean 4 with Mathlib in the repository https://github.com/dicipler-pixel

/-connection-energy-lean [66], which also proves the two transport facts behind Theorem 6: the induced transport ignores the central sign, `ConnectionEnergy.transport_neg`, and reverses along the reversed edge, `ConnectionEnergy.transport_inverse`. The extended statements are in the repository https://github.com/dicipler-pixel/nonnormality-connection-energy-lean [67], which formalises (1)–(4) in full, adds the module for the opposite, the sector flip, the overlap identities and the Koide forms in `NonNormality/Admissible`, and the census identities in `NonNormality/Census`. The table lists the main declarations.

eq.	statement	Lean declaration
(1)	connection-energy identity	`norm_sq_selfCommutator_div_eight`
(3)	normal iff parallel	`isStarNormal_iff_isParallel`
(4)	kernel = holonomy-fixed	`parallelSectionsEquivHolonomyFixed`
(5)	opposite identity	`norm_sq_mul_self_sub_conjTranspose_mul_self_div_eight`
(7)	budget, degree form and $2\|DA\|^2$	`connectionEnergy_add_oppositeEnergy_eq_degree`, `norm_sq_selfCommutator_add_norm_sq_mul_self_sub_div_eight`
(8)	difference $2\,\mathrm{Re}\,\mathrm{Tr}(DA)^2$	`norm_sq_selfCommutator_sub_norm_sq_mul_self_sub_div_eight`
Cor. 1	normal and H^2 Hermitian force $D = 0$	`eq_zero_of_isStarNormal_of_mul_self_eq`
product	$\mathcal{E}^-\mathcal{E}^+ = \|DA\|^4 - (\mathrm{Re}\,\mathrm{Tr}(DA)^2)^2$	`connectionEnergy_mul_oppositeEnergy`
(15)	H^2 Hermitian iff anti-parallel	`mul_self_eq_conjTranspose_mul_self_iff_isAntiParallel`
(16)	kernel = parity-twisted holonomy-fixed	`antiParallelSectionsEquivTwistedHolonomyFixed`
	untwisted odd loop kills the field	`IsAntiParallel.eq_zero_of_odd_loop_of_connected`
(17)	bipartite sign flip	`connectionEnergy_eq_oppositeEnergy_of_bipartite`, `antiParallelSectionsEquivParallelSections`
(18)	double cover	`connectionEnergy_doubleCover`
(20)	scalar edge; tanh form	`scalar_edge_reflection`, `scalar_edge_flux`, `tanh_half_log_odds`
(22)	passive fields	`norm_sub_conj_sq_le_norm_add_conj_sq_of_posSemidef`
(23)	$P^2 + V^2 + L^2 = 1$	`duality_sum_sq`, `frobeniusInner_sq_le`, `duality_le_one`
(1)	any edge blocks: $\|[H, H^*]\|^2 = 4\sum \|D_i A_{ij} - A_{ij} D_j\|^2$	`norm_sq_selfCommutator_eq`
(24)	projector budget $4k$	`norm_sub_conj_sq_add_norm_add_conj_sq_of_projector`
(30)	trace split	`connectionEnergy_trace_split`, `oppositeEnergy_trace_split`

eq.	statement	Lean declaration
(31)	constant shift	`selfCommutator_add_smul_one`, `mul_self_sub_conjTranspose_mul_self_diagonal_add_smul_one`
(35)	weighted Dirichlet form	`norm_sq_selfCommutator_scalar`
(10)	sector flip: $\mathrm{Tr}(AB) = 0$ and defect $2\,\mathrm{Tr}\,B^2$	`trace_mul_eq_zero_of_odd_of_even`, `trace_swap_defect`, `trace_swap_of_odd`
(10)	half swap of the Hermitian and skew parts	`add_conjTranspose_mul_of_odd`, `sub_conjTranspose_mul_of_odd`
(26)	tangent: $PVP = 0$, $\mathrm{Tr}(PV) = 0$	`mul_mul_eq_zero_of_tangent`, `trace_mul_eq_zero_of_tangent`
(26)	second order: $\mathrm{Tr}(PW) = -\,\mathrm{Tr}\,V^2$	`trace_mul_eq_neg_of_second_order`
(83)	Koide = Born weight $\frac{1}{2}$ = null vector	`koide_iff_born_half`, `koide_iff_null`

The core identity, (1)–(3) and the holonomy direction of (4), was first formalised for the one-page note in the repository `dicipler-pixel/-connection-energy-lean` (20 theorems, among them `energy_identity`, `self_commutator`, `orientation_symm`, `normal_iff_parallel`, `transport_neg`, `transport_inverse`, `parallel_loop_commutes` and `scalar_dirichlet`, with three false controls) [66]. The table above is from `dicipler-pixel/nonnormality-connection-energy-lean` [67], which now has 163 declarations and 17 false controls, each rejected for a mathematical reason; every declaration uses only the standard axioms, and the continuous-integration runs of the heads of the pull requests `claude-admissible` and `claude-v15` pass. The Lean statement behind the odd-loop row is stronger than the table: it needs only that the holonomy commutes with the field at i_0. Proved in the text but not formalised: the equality case of (22), the quarter turn (11), the projector forms (25), the odd floor (19), the ring maximum (38), the bow tie (39), the signless half of (35) for non-unitary weights and the count of zero eigenvalues of Q_w. The tanh form of Γ in (20) is `tanh_half_log_odds` together with `four_mul_mul_one_sub`, and a binary rule with $F(s) + F(1-s) = 1$ gives $F(\frac{1}{2}) = \frac{1}{2}$ (`apply_half_of_complement`); the energy vanishes exactly on parallel fields (`connectionEnergy_eq_zero_iff`), normality survives flattening the blocks (`isStarNormal_comp_iff_isParallel`), an anti-parallel field is conjugated by the signed holonomy (`IsAntiParallel.eq_conj_holonomy`), and on bipartite graphs parallel and anti-parallel fields correspond (`isParallel_iff_isAntiParallel_of_bipartite`); the principal-angle forms in (24) are formalised for rank one and in matrix form in the author's other libraries, and the doubly stochastic part of the Born reading (6) as well (table below); the expansion of the squares in (6) is not. All of these are in the numerical checks.

Version 15 additions. The module `NonNormality/Census.lean` (pull request `claude-v15`) adds the following, on the standard axioms, with two more false controls rejected (163 declarations, 17 false controls in all).

statement	Lean declaration
both books are blind to direction: $[H^\top, \bar{H}] = -[H, H^*]^\top$ and $H^{\top 2} - \bar{H}^2 = (H^2 - H^{*2})^\top$	`transpose_selfCommutator`, `transpose_opposite`
the Hermitian part of $D + A$ is D (instantaneous gain ignores the transport)	`add_conjTranspose_of_skew`
compression defect $PH^2P - (PHP)^2 = ((1-P)HP)^*((1-P)HP)$	`compression_defect`
a grading makes the determinant even in the coupling, $\det(D + A) = \det(D - A)$	`det_add_eq_det_sub_of_grading`
$(2P - 1)^2 = 1$ for an idempotent P	`reflection_of_idempotent`
two books of a unit eigenvalue: $\lvert 1 - z\rvert^2 + \lvert 1 + z\rvert^2 = 2 + 2\lvert z\rvert^2$, $\lvert 1 + z\rvert^2 - \lvert 1 - z\rvert^2 = 4\,\mathrm{Re}\, z$	`normSq_one_sub_add_normSq_one_add`, `normSq_one_add_sub_normSq_one_sub`

Of the statements in Sections 8–12, the algebraic core of Theorem 6 is `ConnectionEnergy.transport_neg`, and the census identities listed above are formalised; the Bass pencil, the triangle, the arithmetic edges, the Koide fields and the remaining records are proved in the text and in this appendix, and each is in the numerical checks.

Several statements are cited from the author's other Lean libraries, all built with Mathlib, replayed by Lean's independent kernel checker and audited to the standard axioms in their continuous integration. Each was read at source before it was cited here; the table gives the declaration and where it is used. Lean proves exactly the statement written, under its hypotheses; the scope of each library is in its `LIMITATIONS.md`.

used at	Lean declaration	library
(26)	`GravityOverlap.overlap_exact`, `overlap_quadratic_limit`, `negative_direction_exceeds_cap`	`dicipler-pixel/gravity-ledger-lean`
(29)	`DiracTime.MovingFrame.moving_frame_identity`	`dicipler-pixel/dirac-time-lean`
(34)	`DiracTime.MovingFrame.common_clock`, `DiracTime.CommonClock.common_gap_scaling`, `rate_shift_unique`, `rescale_same_eigenvectors`	`dicipler-pixel/dirac-time-lean`
(51)	`RamanujanChallenge.pincherle`, `pincherle_of_ratio`, `technion_pincherle_fails`	`dicipler-pixel/ramanujan-challenge-lean`
(68)	`OperatorFirst.Offset.offset_of_assumed_connection_factors`	`dicipler-pixel/offset-lean`
(82)	`EventHorizon.disc_form`, `disc_det`, `spectrum_real`, `wall_triangular`, `wall_jordan`, `normal_if_T_isotropic`, `normal_if_W_isotropic`, `projector_norm_gap`, `snapped_law`, `ledger_at_jordan`	`dicipler-pixel/event-horizon-lean`

used at	Lean declaration	library
(95)	`OperatorFirst.Offset.finite_log_odds`, `energy_flip`, `protected_zero_of_pairing`, `OffsetLean.Headline.asymmetry_eq_tanh_half_offset`	`dicipler-pixel/offset-lean`
(95)	`LightBridges.projector_block_coupling`, `boundary_mixing_peak`, `census_equals_coupling_count`	`dicipler-pixel/light-ledger-lean`
(97)	`VOTKP.Directed.cancellation_defect`, `no_defect_iff`, `directed_composite`, `directed_reverse`, `oplus_identity_inverse`, `out_and_back`, `nonunique_lift`, `lift_isospectral`, `lift_metric`	`dicipler-pixel/votkp-lean`, branch `claude-finish-lean` (commit bd4d15a)
(98)	`DiracTime.PathLedger.descent_iff`	`dicipler-pixel/dirac-time-lean`
(99)	`LightBridges.smith_power_identity`, `smith_passive`, `boundary_hermitian_identity`, `boundary_accretive`, `cayley_defect_identity`, `boundary_loss_pullback`, `passive_boundary_chain`	`dicipler-pixel/light-ledger-lean`
(1)	`ConnectionEnergy.energy_identity`, `normal_iff_parallel`, `parallel_loop_commutes`, `transport_neg`, `transport_inverse`	`dicipler-pixel/-connection-energy-lean`
(2)	`LightBridges.symmetric_skew_commutator`; `RelationalAtlas.normal_iff_commute`	`light-ledger-lean`; `relational-atlas-lean`
(6)	`SqrtOpEnt.entryNormSq_mem_doublyStochastic`	`dicipler-pixel/sqrt-lower-bound-lean`
(11)	`FOFT.odd_moment_zero_X`; `AtlasFormal.chiral_eigenvalue_pair`	`foft-lean`; `relational-atlas-lean`
(12)	`LightBridges.redistribute_double_commutator`; `UPGAlgebra.redistribution_eq_commutator_form`; `DiracTime.SectorReduction.redistribution_zero_iff_commute`	`light-ledger-lean`; `upg-lean`; `dirac-time-lean`
(13)	`FOFT.henrici_rate`, `dual_flow_conserves`, `flow_smul`	`dicipler-pixel/foft-lean`
(20)	`EventHorizon.Edition10.step_matching`, `flux_balance`, `tanh_half_log`; `OffsetLean.Headline.asymmetry_eq_tanh_half_offset`	`event-horizon-lean`; `offset-lean`
(21)	`VOTKP.Smith.tanh_add'`, `round_trip`, `euclid_form`	`dicipler-pixel/votkp-lean`

used at	Lean declaration	library
(24)	`OperatorFirst.HypersurfaceSquareLineage.rank_one_projector_hs_distance_sq`; `LightBridges.frame_angle_kernel`	`square-case-lean`; `light-ledger-lean`
(26)	`GravityOverlap.local_cap_requires_nonnegative`	`dicipler-pixel/gravity-ledger-lean`
(32)	`SpectralStability.Coupling.anticomm_eq_trace`, `anticomm_traceless`	`dicipler-pixel/spectral-stability-lean`
origin	`SpectralStability.Recovered.skew_transport_commutator`, `skew_transport_normal_iff`, `commutator_gradient`, `commutes_forces_uniform`	`dicipler-pixel/spectral-stability-lean`
(34)	`MatterAtAScale.stress_scales`, `departure_span_free`	`dicipler-pixel/matter-at-a-scale-lean`
(46)	`UPGTorusAnchor.unit_defect_add_guard`, `clock_refused_at_two`; `LightBridges.graph_parallelogram`	`upg-lean`; `light-ledger-lean`
climb or swap	`Suns.exchange_one_loop`, `restore_two_loops`	`dicipler-pixel/suns-lean`
(79)	`FilamentFracture.growth_iff`, `gain_eq`	`dicipler-pixel/filament-fracture-lean`
four-body	`SquareCase.Transport.weighted_symmetric`	`dicipler-pixel/square-case-lean`
(93)	`EventHorizon.Edition10.fermion_smith`, `fermion_center`, `particle_hole`; `OperatorFirst.Offset.asymmetry_swap`, `complement_det_eq_of_conjugacy`; `OperatorFirst.OffsetEndpoint.sublattice_conjugation`	`event-horizon-lean`; `offset-lean`
(94)	`PriceOfDirection.metric_curvature`; `EventHorizon.Edition10.sine_guard`; `DiracTime.ProjectorBlocks.hermitian_form_split`	`price-of-a-direction-lean`; `event-horizon-lean`; `dirac-time-lean`
one coordinate	`EventHorizon.Edition10.total_reflection`	`dicipler-pixel/event-horizon-lean`
(74)	`PriceOfDirection.wall_charpoly`, `wall_real_iff`, `wall_complex_iff`; `PriceOfDirection.nonzero_eigen_swap`, `specProj_sum` (the pair projector of (82))	`dicipler-pixel/price-of-a-direction-lean`
the orbit	`RussellOrbits.isco_from_potential`	`dicipler-pixel/what-russell-saw-lean`
(25), (26)	`EmergentTransport.persistence_frobenius`, `half_commutator_norm`; `IqgtGrassmannian.trace_sq_offdiag`; `DiracTime.ProjectorBlocks.metric_block` (for $q(V) = g(V,V)$)	`emergent-transport-lean`; `iqgt-grassmannian-lean`; `dirac-time-lean`
(28)	`LightBridges.oblique_trace_two` (an oblique pair with $\mathrm{Tr}(P_0P_1) = 2$)	`dicipler-pixel/light-ledger-lean`

used at	Lean declaration	library
(105)	`UPGAlgebra.commutatorC_energy`; `VOTKP.Channels.commutator_coupling`	`upg-lean`; `votkp-lean`, branch `claude-finish-lean`
(104)	`VOTKP.Memory.transfer_silence`, `moment_horizon`; `VOTKP.Witnesses.same_present`, `opposite_futures`; `DiracTime.Headline.future_decided_by_first_dim_steps`	`votkp-lean`, branch `claude-finish-lean`; `dirac-time-lean`

The libraries are at https://github.com/dicipler-pixel/, followed by the name in the last column. The VOTKP modules `Directed`, `Channels`, `Memory` and `Witnesses` are on the branch `claude-finish-lean` of `votkp-lean` (head commit bd4d15a, the release accompanying VOTKP v2.9); the default branch has only `Smith`, `Film`, `Peel`, `Knot` and `Ordinal`.

C Checks

Six scripts recompute every numbered statement from the full matrices, on random graphs with random Hermitian blocks and random unitary edges, and compare both sides independently. `ce12_checks.py` (SCRIPT: CE12-CHECKS-01) covers Sections 1–7 of the first edition; `ce12_new_checks.py` (SCRIPT: CE12-NEW-CHECKS-01) covers the Born reading, the sector flip, the overlap, the odd loops, the ring maximum and the two-loop values; `check_helper_v12.py` (SCRIPT: CE12-HELPER-CHECKS) covers the graph primes and the wall; `check_ce13_merge.py` (SCRIPT: CE13-MERGE-CHECKS) covers the centered fields, the circulant and the triangle, the Bass pencil, the arithmetic edges with their point counts, and the records of Section 11; `check_ce14_github.py` (SCRIPT: CE14-GITHUB-CHECKS) covers the statements cited from the author's other repositories, the prime-trace recurrence and its continued fraction, the companion matrix, the route and the endpoint, the common clock and the moving frame, the four-body wall, the Schur–Cayley boundary and the occupation algebra; `check_ce15_census.py` (SCRIPT: CE15-CENSUS-CHECKS) covers every statement added in this edition, gates G16–G75. The two arithmetic runs of Section 9 are `primes_boost_twist_02.py` (SCRIPT: PRIMES-BOOST-TWIST-02) and `murmuration_two_books_02.py` (SCRIPT: MURMURATION-TWO-BOOKS-02), on Cremona's tables with PARI; their outputs are read by gates G41 and G42. Each runs its opposite where one exists: a non-unitary transport, the slowest settling, a Hermitian-only family, $a_p \to -a_p$, a scalar against a noncentral phase, uncentered against centered fields, a fixed global twist against a local one, $|c| < 2$ against $|c| > 2$, a dropped frame connection, a scalar reference generator, a wall block off its joint condition, an indefinite Hermitian part, a dual flow, an anti-parallel start, a Jordan loop, a three-level band, a rank-three cut, a trivial Kitaev chain, a time-reversed flow. Point counts are made from the Weierstrass equations; no table is imported. Their outputs, in full, are in the archive; the largest errors are listed here.

First edition (Sections 1–7) and its sightings.

check	statement	largest error
(1)	1/8 ‖[H,H*]‖^2 = sum ‖D_i − U D_j‖^2	5.9e-16
(4)	1/8 ‖H^2 − H*^2‖^2 = sum ‖D_i + U D_j‖^2	6.6e-16
	H^2 − H*^2 = 2D,A	9.5e-15
(5)	E− + E+ = 2 sum deg(i) ‖D_i‖^2	7.0e-16
(5)	E− + E+ = 2 ‖DA‖^2	6.0e-16
(6)	E− − E+ = 2 Re Tr (DA)^2	3.3e-16
(2)	parallel field gives a normal H	1.4e-14
(7)	anti-parallel field gives H^2 = H*^2	1.3e-14
(3),(8)	kernels = holonomy-fixed / parity-twisted fixed	0.0e+00
(9)	bipartite sign flip swaps E− and E+	0.0e+00
(10)	double cover energy = 2 E−(S) + 2 E+(T)	5.0e-16
(11)	scalar edge: ratio Gamma^2, tanh form, 4 d_i d_j	2.1e-13
(13)	P^2 + V^2 + L^2 = 1 per edge	8.9e-16
	scalar edges: L = 0	4.1e-16
(14)	projectors: E− + E+ = 4k per edge; principal angles	3.2e-14
(16)	cI leaves [H,H*] unchanged	6.4e-15
(16)	cI moves H^2 − H*^2 by exactly 4cA	9.9e-15
(15)	trace / trace-free split of both energies, no cross term	5.2e-14
(17)	scalar: E− = d^T L d, E+ = d^T Q d (signless)	8.5e-14
(18)	ring floors (formula vs direct minimisation)	2.0e-14
(S1)	end reversal: P odd; V, L, E−, E+ even	5.9e-14
(S1)	opposite run, sign flip: V odd; P, L even; books swap	0.0e+00
(S2)	E− E+ = s^2 (P^2 + L^2); scalar root = s P	5.7e-14
(S3)	scalar circle: doubled angle; tanh, sech, tanh(tau/2)	1.0e-15
(S4)	boost: E+ − E− invariant, tau + 2f, Gamma (+) tanh f	3.2e-12
(S5)	occupation edge: Gamma = 1−2nu, tau = 2 artanh Gamma, PH odd	6.2e-12
(S6)	offset = Tr K = sum 2 artanh(1−2nu); PH odd; entropy even	3.7e-14
(S7)	boundary: tau_A = tau_B + log(s0/s1), any interior	1.5e-14
(S7)	protected interior: tau_B = 0 and tau_A = log(s0/s1)	1.9e-14
(S8a)	unitary: |l−1|^2 + |l+1|^2 = 4	1.0e-14
(S8b)	interface ledger: log det(I − K) and log det(I + K)	3.6e-15
(S8c)	one site: MJ+JM = (Tr M)J; budget 4‖M‖^2	5.7e-14
(S9)	two-band: |Omega| = 2 sqrt(det g)	4.6e-14
(S9)	conjugation: g even, Omega odd	0.0e+00
(S10)	Gram G = X^T X even under a mirror; det X odd	1.5e-14

Born reading, sector flip, overlap, odd loops, ring, two loops.

check	statement	largest error
(N1)	both books are Born averages; W doubly stochastic	1.3e-13
(N2)	quarter turn, half swap, defect 2Tr(B^2), Tr(AB)=0	1.1e-14
(N3)	k − Tr(P0 P) = 1/2 Tr((P−P0)^2) for equal-rank idempotents	2.8e-12
(N3b)	q = 0 tangent with overlap 1/(1−t^4) > 1	2.2e-19
(N4)	projector edge: E−/+ = 2k(1−/+p), V = p, L^2 = 1 − p^2	5.3e-15
(N5)	odd N−cycle in C^2: min sum p = N(1−cos(pi/N))/2	1.8e-12
(N6)	R^3 mirror fields: triangle total 1, pentagon total sqrt5	2.2e-16
(N6b)	on the pentagon mirror field E− = E+ = 2|E|	0.0e+00
(N7)	twisted ring: max sum p = (N/2)(1+cos(delta/N)), proof route	1.5e-13
(N7b)	complex projector (I+sigma_y)/2 fixed by every in−plane turn	7.2e-17
(N8)	bowtie with sigma_x, sigma_z loops: min E− = 6 − 3 sqrt3	1.2e-10
(N8b)	triangles sharing an edge: min E− = 4 − 2 sqrt2	6.8e-13
(N8c)	opposite run, compatible loops (both sigma_z): min E− = 0	1.2e-10

check	statement	result

Graph primes.

check	statement	result
A1	twisted Ihara-Bass, unitary gains and Ad U on Herm(r), 100 graphs	4.50e-15
A1b	Bass also holds for non-unitary gains with U_ji = U_ij^-1, 50 graphs	1.35e-15
A2	Bass factor P(+-1) from spec(B) = det(Deg -/+ A), rho = Ad A (error / prod(1+|lam|))	1.07e-16
A2b	same for the gain transport rho = U (generically nonzero ends)	1.61e-14
A2c	Ad transport: lambda_min(Deg - A_Ad) = 0 always (the constant field is parallel)	4.36e-15
A3	x.(Deg - A_Ad)x = 1/8||[H,H*]||^2 and x.(Deg + A_Ad)x = 1/8||H^2-H*^2||^2	1.09e-15
A4	Tr B_{-rho}^k = (-1)^k Tr B_rho^k, k<=8 (prime cycles carry (-1)^length)	0.00e+00
A4b	double cover: det(I-uB~) = det(I-uB_rho) det(I+uB_rho)	9.95e-16
A5	spec(A_G) contained in spec(A_Ad): Ad-zeta has the plain zeta as a factor	2.55e-15
A6	mirror P(u) = (q u^2)^N P(1/(qu)), unitary twists, 1000 regular graphs	2.64e-14
A7	off-circle poles = 2 #{|lambda| > 2 sqrt q}, unitary twists	1000/1000
A8-OPP	non-unitary U_ji=U_ij^-1: mirror holds	1.36e-15
A8-OPP	non-unitary U_ji=U_ij^-1: poles leave the circle (mean fraction off)	1.000
A8-OPP	non-regular graphs: no q gives a mirror (min over q of mirror error)	min 3.39e-01
A10	around one exceptional point: always a swap (only 2-cycles), K4 random+trivial	40 loops
A10b	K4 random gains: swaps chain into one orbit; a two-point loop climbs	orbits [8] climb [4]
A10c	K4 trivial gains: symmetry splits the orbits (no full chain)	orbits [4, 2, 1, 1]

The wall.

check	statement	result
B1b	M^2=(h^2−r^2)I, ||[M,MT]||^2=32h^2r^2, q(M)=h^2−r^2=(||Herm||^2−||Skew||^2)/2	5.68e−14
B1c	wall h^2=r^2 (b=0, a!=0): nonzero nilpotent, one eigenvector (Jordan)	exact
B2	T=G+zeta*w*I: T^2=w^2(zeta^2−1)I, ||Herm T||^2=2w^2zeta^2, ||Skew T||^2=2w^2	2.84e−14
B5	fastest settling, n=2,3, 40 random systems: a coalesced (defective) pair	40/40 (1 restarted)
B5b	fastest settling: median fraction of modes sharing the decay rate	median 1.00 mean 0.86
B5-OPP	slowest settling (maximise abscissa): no fold	0/40 folds; median frac 0.33
B5-OPP	time reversal M -> −M leaves q unchanged	1.42e−15
B5-OPP	Hermitian-only family: optimum always diagonalisable (eigvec cond)	1.000000000000
B6	4x4 counterexample: q=0, X^2 != 0, normal, eigenvalues +−1, +−i simple	exact
B7	Z^2=(h^2−s^2)I, h^2/s^2=3Q−1, Born weight p=1/(3Q) (1000 positive triples)	3.55e−15
B8	K=Z−hI: max eig Herm K = 0 (minimally passive), spec K = spec of oscillator w=s, zeta=h/s	2.10e−15
B8b	at h=s: Q=2/3, Z^2=0 with Z!=0, 45 deg to (1,1,1), p=1/2	Q=0.666666666666667 ang=45.000000000000
B9	max asymptotic rate at h=s: fixed s, and on a h^2+b s^2 = 1 (4 choices)	6.5e−05
B10b	Brannen form: mu = s/sqrt3, coefficient sqrt2*h/s (Koide <=> sqrt2)	1.85e−12
B12	equal positive phases p=1/(3Q)~1/2; dephased average p=1/3	coh 0.5000017 deph 0.3335
B13	ISCO-type generator [[0,1],[−k^2,0]]: A^2=−k^2 I; at k=0 nonzero nilpotent	0.00e+00

check	statement	result

Arithmetic primes, Koide records, cycle completion (1): one edge, Koide fields, circulant.

check	statement	result
M1	Born sum with degenerate eigenspaces: rows = rank P_a, cols = rank Q_b, W/r a joint law	1.78e-14
M2-OPP	books balance (zero cross-moment) yet the covariance is nonzero: balance is not independence	E-=E+=10.000 cov=-0.750
M3	centered projector books (2k(1-rho), 2k(1+rho)-4k^2/r); balance at rho = k/r	7.77e-15
M3-OPP	orthogonal pair (rho=0): uncentered books balance, centered books do not	2.000=2.000; 2.000!=0.667
M4	Koide triples: centered 2D books (1,1); uncentered C^3 (1,3); centered C^3 (1,5/3)	1.78e-15
M4b	measured masses: rho_K and the centered 2D books 2(1-rho), 2rho	rho=0.5000016525 (0.999997,1.000003)
M5	full dephasing gives Tr(diag(m)R)/M = 1/3 exactly; relative phases move Tr(PR) at fixed Q	1.7e-16; spread 0.97
M6	circulant Phi = F diag(x) F*: form (d,z), spectrum, Tr Phi^2, Q, e2, e3, Tr Phi^3; 3d^2=s^2, 6t^2=h^2	4.26e-14
M7	Koide: t = d/sqrt2, e2 = S^2/6, roots solve v^3 - S v^2 + (S^2/6) v - e3 = 0	5.33e-15
M8	Koide circulant: all roots > 0 exactly when cos 3phi > 1/sqrt2 (4001 phases; both sides)	min root 1.0e-06 / -1.0e-06
M9	measured masses: reduced hopping phase |phi| in [-pi/3,pi/3]; sigma_Q from the tau error	|phi|=0.22222476 sQ=5.081e-06

Arithmetic primes, Koide records, cycle completion (2): the wall.

check	statement	result
M10	AM-GM: ||[Z,Z^T]||^2 = 32 s^2 h^2 <= 2||Z||^4, equality at h = s	1.71e-13
M11	fixed extra scalar loss shifts the rate curve, argmax stays h = s	argmax 0.999 0.999
M11-OPP	total scalar loss fixed independently of h: undercritical plateau, no unique maximiser	spread on h<s 1.3e-15
M12	stress flow dZ/dt = -2[C,Z]: dh_j = -16 s^2 h_j, ds = -16 h^2 s; det Z, h^2 - s^2 conserved (RK4)	4.68e-09
M12-OPP	Koide start stays Koide as Z0/sqrt(1+32 s0^2 t); an off-cone start keeps its cone defect	1.7e-12; defect 0.1600

check	statement	result
M13	finite time: e^{t*K_0.8} = -e^{-0.8t*} I, norms 0.0151646 vs e^{-t}(sqrt(1+t^2)+t)=0.0562309	0.0151646 0.0562309
M13b	both generators are contractions (Herm K <= 0); zeta=0.8 stays under 2% after t*	max Herm 0.0e+00; sup 0.0152
M14	centered single edge: X = DA is normal with XX* = X*X = I/4 at every overlap, also rho = 1/2	8.33e-17
M15	complex traceless 2x2: Re Tr X^2 = 0 while X^2 = iI != 0 (no wall without the real family)	ReTrX2=3.6e-16

Arithmetic primes, Koide records, cycle completion (3): the arithmetic edges.

check	statement	result
M16	37a1: brute-force point counts equal the character-sum formula (66) at every good p <= 1000	0.00e+00
M17	Frobenius edge on 37a1, p <= 1000: books (4p - a_p^2, a_p^2), budget 4p, rho_p = a_p^2/(4p)	1.82e-12
M17b	the same books are 2p times the centered rank-one active-plane books (2(1-rho), 2rho)	1.36e-12
M18	no odd prime <= 20000 has a^2 = 2p in the Hasse range; no prime has a^2 = 4p; p=2 allows a = +-2	0 hits; p=2 a^2=4p: 0
M18b	formal Koide preimage Q_p = 4p/(3a_p^2): a positive triple exists iff rho_p > 1/3 (37a1, p<=1000)	6.7e-16 (162 primes)
M19	sign-blindness: Ad(-U) = Ad(U); books at a_p and -a_p coincide on every 37a1 prime	1.82e-12
M19-OPP	the odd records flip under a_p -> -a_p: Tr U_p = a_p/sqrt p and Gamma_p change sign	True True
M20	Sato-Tate: P(a_p^2 > 2p) = (4/pi) int_0^{pi/4} sin^2 = 1/2 - 1/pi	0.1816901138
M21	local nonsquare twist counted directly: N-/+ = p+1 -/+ a_p, sum 2(p+1) (37a1, odd p <= 1000)	0.00e+00
M21b	Gamma_p = a_p/(p+1) = tanh(tau_p/2), |Gamma_p|<1; scalar edge (N+,N-) books (4a_p^2, 4(p+1)^2)	2.22e-16
M22	global twist d = 5, -1, -3 of 37a1: a_p(E^d) = chi_d(p) a_p(E) and the log-ratio formula (41)	2.22e-16
M22-OPP	no universal complement: y^2=x^3-x vs x^3-4x: p=17 (16,16) sum 32; p=13 (8,20) sum 28	(16, 16) (8, 20)
M23	finite peel T_{E,5}(1000) from both curves equals sum (1-chi) artanh(a_p/(p+1)) from E alone	8.88e-16

check	statement	result
M24	local factor 1 - a_p u + p u^2: roots on |u| = p^{-1/2} (Hasse = graph circle); normalised form (48)	1.78e-15
M25	three curves, good p <= 5000: count, mean rho_p, fraction E+ > E-, number of a_p = 0	3 curves as in table
M25b	Sato-Tate share with cos(theta_p) > 1/sqrt2 is 1/4 - 1/(2pi); 37a1 empirical share (descriptive)	0.090845 vs 0.079341

Arithmetic primes, Koide records, cycle completion (4): the triangle and the Bass pencil.

check	statement	result
M26	triangle with U(1) connection e^{i phi}: det(I - uB) = 1 - C3 u^3 + u^6, C3 = 2cos 3phi	4.48e-15
M26b	log zeta = sum Tr B^n u^n/n: no terms of order 1, 2; the u^3 coefficient is C3	2.00e-15
M27	(d, t, C3) recover the unordered spectrum: det(vI - Phi) = (v-d)^3 - 3t^2(v-d) - t^3 C3	1.73e-12
M28	noncentral U = diag(e^{i phi},1): Ad(U^3) eigs 1,1,e^{+-3i phi}; zeta^-1 = (1-u^3)^4 (1-C3u^3+u^6)^2	7.11e-14
M28-OPP	scalar phase: Ad(e^{i phi} I) = identity for every phi; the cycle phase is invisible	3.33e-16
M28b	field sigma_z on the noncentral triangle: books (0, 24) for every phi, though C3 varies	see M28
M29	Sylvester proof objects: J^2 = I, O*O = Deg, O*JO = A_R, B_R = J(OO* - I), (I+uJ)^-1 J = (J-uI)/(1-u^2)	6.94e-14
M29b	Bass factorisation with GL(d) gains (inverse reversal) and det(I+uJ) = (1-u^2)^{md}, 30 graphs	7.07e-15
M30	Bass pencil at u = +-1: K(1) = L-, K(-1) = L+, quadratic forms = (1/8)||[H,H*]||^2, (1/8)||H^2-H*^2||^2	1.07e-14
M30-OPP	the zeta itself is singular at u = 1 when m > n: det(I - B) = 0; the pencil carries the value	det(I-B)=0 on all 20; ratio 6.0e-12
M31	matrix mirror K(1/(qu)) = K(u)/(qu^2) on cubic graphs, unitary and GL gains	2.22e-15
M31-OPP	non-regular graph: no q in [0.5, 4] gives the matrix mirror	min err 1.79e+00

Arithmetic primes, Koide records, cycle completion (5): records the books do not keep.

check	statement	result
M32	scalar edge: swapping ends negates Gamma, leaves both books and E- - E+ = -4ab unchanged	2.22e-16
M33	occupation edge a=1-nu, b=nu: books ((1-2nu)^2, 1), tau = log((1-nu)/nu) = 2 artanh(1-2nu)	1.78e-15
M33b	Gaussian fermion state (3 modes, Fock space): P(full) = det C, P(empty) = det(I-C), tau = sum tau_nu	8.22e-15
M33-OPP	the occupation budget is not fixed: E- + E+ = 1 + (1-2nu)^2 varies with nu	1.64 vs 1.00
M34	Cayley maps: right half-plane and upper half-plane to the disk; z = N+/N- lands at w = Gamma_p	2.22e-16
M35	hyperbolic geodesics obey n(y) sin(v) = const with n = 1/y; signed-lapse fold rho -> a^2/rho negates	4.44e-16
M36	normal generator: ||e^{tG}|| = e^{t max Re spec G} exactly	3.55e-14
M36-OPP	[[-2,1],[0,-2]] non-normal yet contractive (Herm < 0); [[-1,10],[0,-2]] grows transiently	Herm max -1.50; sup 1.000; 2.56
M37	middle-axis key: ab > 0 for every sampled body (generic flips sit away from the wall ab = 0)	min ab 1.71e-06
M38	reset bath: transverse generator [[-1/tau,-Delta],[Delta,-1/tau]], normal at every temperature	0.00e+00
M38b	friction scale coefficient tau beta sech^2(beta Delta/2): -> 0 at fixed gap, linear along Delta = 1/beta	2.1e-24; slope 0.7864
M39	overlap hierarchy: F = Uhlmann fidelity of P/k, R/k; rho - F = Var(sqrt c); D^{1/k} <= F <= rho	1.83e-08
M39b	rank two, rho = 1/2: c = (1,0) gives (F,D) = (1/4,0); c = (1/2,1/2) gives (1/2,1/4)	(0.25,0.00) (0.50,0.25)
M40	all pairwise overlaps 1/2, yet Tr(P0 P1 P2+-) = (1 +- i)/4: the triple product keeps orientation	0.250+0.250j 0.250-0.250j
M41	hidden channel B=(1,1)/sqrt2, spectra (0,2) vs (1,1): moments 0,1 agree, K(pi) = +1 vs -1	K=+1,-1; m2 2/1

Arithmetic primes, Koide records, cycle completion (6): reversals and the Born scope.

check	statement	result
M42	odd coupling: (Gamma X)^2 = -X^2 and the self-commutator norm is unchanged	0.00e+00
M42-OPP	a sign anticommutes with each two-parameter slice of Z, none with all of sz, sx, J	null dims [1, 1, 1, 0]
M43	oblique transport: k - Tr(P0 Q) = 1/2||eta0^1/2 (P0-Q) eta0^-1/2||^2 >= 0, tangent P. + [T.(0),P0], gauge term	1.68e-13
M44	binary partitions admit f(s) = s + eps sin(2 pi s): consistent, bounded, certain (|eps| <= 0.15)	2.22e-16
M45	oblique idempotent (1,1,1)(3/4,3/4,-1/2): each (P, E_ii), i=1,2, is an orthogonal pair of overlap 3/4	P^2=P 0e+00; weights [0.75 0.75 -0.5]
M46	odd cycle: least adjacency eigenvalue -2cos(pi/N), which gives the C^2 floor (71) in one line	1.33e-15
M46b	an orthonormal triangle admits the equal-root state, whose Koide ratio is 1/3	Q = 0.333333

Items from the author's repositories (1): route, endpoint, frames and clocks.

check	statement	result
G1	route minus endpoint: L_rec - D_end = 4 min(R+,R-), 1000 random directed records	1.07e-14
G1-OPP	out and back (0.4,-0.4): L=1.6, D=0; one-signed records: defect 0; mixed records: defect > 0	1.6,0.0,0e+00,0.04
G2	scalar chain: G_j = Gamma_e = tanh r_j, sum artanh sqrt(E-/E+) = L_rec/2, P_e = tanh 2r, V_e = sech 2r	1.78e-15
G2-OPP	same |r_j|, other signs: same normalised books on every edge, D_end 1.0 vs 0.6, signs of P_e differ	0e+00; 1.00 vs 0.60
G3	closed loop of scalar edges: signed rapidities sum to 0 (silent loop), route length stays > 0	5.0e-16; min L 0.57
G4	moving frame: i chi' = (R*HR - i R*R') chi for psi = R chi, 100 random frames	1.56e-14
G4-OPP	dropping the frame connection: R*HR alone misses chi' (smallest miss over 100 frames)	1.14
G5	common clock G = t'H0 + aI: [G,G*] = t'^2[H0,H0*], G^2 - G*^2 = t'^2(...) + 4t'aA, gaps scale by t'	4.26e-14

check	statement	result
G5b	rescaling D -> sD: Born matrix W unchanged, books times s^2, every ratio of books unchanged	1.51e-14
G5-OPP	non-scalar H0: (t', a) recovered from G; scalar H0 = I: rates 1 and 0 give the same generator	5e-16; 0e+00

Items from the author's repositories (2): the prime-trace recurrence and its continued fraction.

check	statement	result
G6	|c| > 2: convergents of c - 1/(c - 1/(c - ...)) -> a0 - Z1/Z0 = lambda_d, Z = lambda_s^n minimal	8.88e-16
G6b	|c| > 2: t_l = 2T_l(c/2) = lambda_d^l + lambda_s^l solves the recurrence; minimal/t_l = rho^l/(1+rho^l)	6.4e-15; 8.0e-15
G6-OPP	|c| < 2: convergents keep oscillating (spread of arctan over n in [1000,3000]), Z/D does not -> 0	2.92; 25.05
G6c	boundary c = 2: Z = 1 is minimal against D = n; P_n/Q_n = (n+1)/n -> 1, error n^-1 (not geometric)	1.000000
G6d	twisted cubic graphs, d = 2: Tr B^l = sum_lambda q^(l/2) t_l(lambda/sqrt q) + (m-n)d(1+(-1)^l), l <= 8	1.07e-13
G7	cubic graphs, plain and U(1)-twisted: continued fraction converges exactly for |lambda| > 2 sqrt q	2400/2400 eig; 200/200 graphs
G8	37a1, every odd good p < 1000: |c_p| = |a_p|/sqrt p < 2, convergents do not settle	max 1.9760; 166/166

Items from the author's repositories (3): walls, boundaries and occupations.

check	statement	result
G9	companion [[c,-1],[1,0]]: T^2 = (c^2/4 - 1)I, halves c^2/2 and 2, Phi = 4c^2; c = 2 is a nonzero nilpotent	2.84e-14
G9-OPP	c = 0 is normal and inside the bound; Phi = 4c^2 is smooth through c = 2: non-normality is not the signal	0e+00
G10	single eigenprojector: ||P||_F gap = ||M - lambda_s I||_F -> ||N||_F = 2; pair projector I and det M = 1 stay	3.22e-13
G10b	approach to the wall: ||P_d|| gap at c = 2 + 1e-1 ... 2 + 1e-8 tends to 2	2.1000 -> 2.000000

check	statement	result
G11	period-2 counterexample: Z = 2^-n solves it, Q_n = 0 at every even n, odd convergents -> 8, no limit	0e+00; 0e+00; 0e+00
G11-OPP	constant |c| > 2: Q_n != 0 for every n >= 1, so the corrected definition holds as well	min |Q_n| 1.00
G12	four-body block: disc = 4 q(T) on 2000 simplex points, and q(T) >= 0 throughout	5.68e-14
G12b	coplanar wall w3 = 0 with the joint condition: (A - 2t3)^2 = 0, A21 = 0, A12 != 0 (a nonzero nilpotent)	0.00e+00
G12-OPP	wall without the joint condition: two distinct real eigenvalues, no Jordan block	gap 2.840
G13	Schur-Cayley: Z_b = W*LW, Herm Z_b = W*(Herm L)W, I - S*S = 4(WV)*Herm L(WV); scalar 1-|w|^2 = 4x/|z+1|^2	1.62e-14
G13-OPP	passive samples keep ||S|| <= 1 (largest seen); an indefinite Hermitian part can give ||S|| > 1	0.980; 3.167
G14	compressed projector: C - C^2 = BB*, spec BB* = nu(1-nu) = 1/4 - (nu-1/2)^2; window count = weight count	1.00e-12
G14b	finite log-odds: sum tau_nu = log prod(1-nu) - log prod nu; flip negates; asymmetry = tanh(offset/2); pairing gives 0	1.78e-15
G14-OPP	an unpaired spectrum (0.2, 0.3, 0.6) has nonzero offset	1.8281
G15	overlap_exact (real part, oblique equal-trace idempotents); (overlap - k)/t^2 -> -q(P'(0)), rel. at t=1e-3	2.3e-14; 5.2e-06
G15-OPP	unequal traces (1 and 2): the finite identity fails, so constant trace is a real hypothesis	0.50

check	statement	result

Census additions (1): the identity, its hypotheses, the halves and the relaxation flow.

check	statement	result
G16	S Hermitian, K skew: [S+K,(S+K)*] = 2[K,S]; real: [H,H^T] = −2[S,K]; (1) is S = D, K = A	2.6e−14
G16-OPP	commuting halves give a normal matrix; random non−commuting halves never do (least norm)	5.4e−15; 7.635
G17	weights: 1/8||[H,H*]||^2 = sum w||Di − U Dj U*||^2; any edges: ||[H,H*]||^2 = 4 sum_ordered ||Di Aij − Aij Dj||^2	1.8e−12; non−unitary normal example 0e+00
G18	D0 = i, D1 = −i, A01 = 1: H normal while the edge term is 4; swap transport: D0 = diag(0,1), D1 = diag(1,0) normal, D0 != D1	0e+00 vs 4; 0e+00
G19	kernel of the connection energy on Herm(2): tree / one loop (holonomy with distinct eigenvalues) / two loops (sigma_x, sigma_z)	4 / 2 / 1
G19-OPP	two loops with commuting holonomies (sigma_z, diag(1,i)) keep the diagonal fields	2
G20	per edge: E−_e E+_e = s^2 − 4<a,b>^2 = s^2 (P_e^2 + L_e^2), s = ||a||^2 + ||b||^2	7.8e−16
G21	crossing X: [GX,(GX)*] = [X,X*] as matrices (not only in norm)	0.0e+00
G21-OPP	with a part B inside the sectors the matrices differ (largest difference seen)	69.21
G22	G = 2P − 1: (X − GXG)/2 = PX(1−P) + (1−P)XP = P[P,X] − [P,X]P; (2P−1)^2 = 1 also for oblique P	7.6e−15
G23	relaxation flow on D + A: Phi = (1/2)||[K,K*]||^2 = 4 E−, d||K||^2/dt = −8 Phi	0.0e+00; 1.1e−15
G23b	total drained 8 int Phi dt equals the Henrici departure ||K0||^2 − sum|lambda|^2; spectrum kept	8 int Phi 1.25073682, norm lost 1.25073682, departure 1.25073682; drift 3.5e−15
G23c	two vertices K = [[d1,1],[−1,d2]]: K′ = [[−8 delta,−4 delta^2],[4 delta^2, 8 delta]], delta = d1 − d2: the edge leaves modulus one	symbolic match: −8*delta, −4*delta**2, 4*delta**2, 8*delta
G23d	the opposite book along the flow ends at 2 sum (Re lambda Im lambda)^2, fixed by the spectrum; generic triangles: falls in	9.2e−14; 30 of 30

check	statement	result
G23e	any K: E− = (||K⋆K||^2 − ||K^2||^2)/4 and E+ = (||K^2||^2 − Re Tr K^4)/4 (20000 random matrices)	2.3e−12
G23e-OPP	rate of E+ under the relaxation flow on 20000 random matrices: never positive; under the time-reversed flow never negative	0 positive
G23-OPP	dual flow K′ = −2[[K,K⋆],K⋆]: ||K||^2 kept, stress moved into the spectrum (Phi and the Henrici gap at t = 40)	2.0e−14; 1.657 -> 2.5e−12; 1.251 -> 2.9e−11

check	statement	result

Census additions (2): odd loops, the scope of the Born form, one edge.

check	statement	result
G24	unsigned incidence has full rank exactly on non-bipartite connected graphs; there the edge budgets return every ||D_i||^2	0 exceptions needed, 0 found (93 bipartite, 107 not)
G24-OPP	even cycle C4: the invisible direction of the vertex norms alternates in sign	+1, −1, +1, −1
G25	dimension two: p = 1 if R = P, 0 if R = 1 − P, 1/2 otherwise is similarity invariant, consistent and certain	500 resolutions
G26	rank k: P (x) I_k with E11 (x) I_k and E22 (x) I_k are pairs of metric-orthogonal projectors of overlap 3/4 (k = 1, 2, 3)	0.0e+00; overlaps all 0.7500; sum of two 3/2 > 1
G27	Born matrix rows and columns sum to 1 in [0,1] (her (1)–(3)); symmetric state 1/N (H3); Fourier block K/N (H4)	1.1e−15; 5.6e−17; 2.2e−16
G27-OPP	binary rule s + sin(2 pi s)/(2 pi) is consistent on two outcomes, not on three (1/4, 1/4, 1/2)	1.1e−16; 1.3183
G28	a diagonalisable loop with unit-modulus spectrum keeps a positive metric; a Jordan loop forces eta_11 = 0	2.4e−15; 0.0e+00
G28-OPP	sigma_x and sigma_z pass the metric test and share no line: ||[P,X]||^2 + ||[P,Z]||^2 = 2(1 + n_y^2) >= 2	2.000000; direct 2.000000
G29	boost d_i e^f, d_j e^−f: E+ − E− = 4 d_i d_j kept, tau + 2f, Gamma (+) tanh f, (E,P) = (d_i+d_j, d_i−d_j) boosted by f	2.9e−13
G30	path state |0>a + |1>b in Hilbert-Schmidt space: predictability |P_e|, visibility |V_e|, concurrence L_e, sum of squares 1	1.4e−08
G31	G = 2P0 − 1: GV is an idempotent tangent with q(GV) = −q(V); its curve stays idempotent and its overlap rises as 1 + q(V)t^2/k	2.2e−10; q(V) in [1.06,32.20]; (overlap − 1)/t^2 against +q(V)/k, relative 8.3e−06
G31b	witnesses: rotation cos^2 t, hyperbolic e^(t sigma_x) cosh^2 t; transported by S^−1 back to 1; by R_th S^−1 cos^2 th	0.584984=0.584984; 1.575449=1.575449; 1.000000; 0.848353=0.848353
G32	F_Q of P/k = 4 g(V,V)/k (SLD formula; finite-difference Uhlmann fidelity from principal angles, h = 1e−3)	7.9e−08

check	statement	result
G33	q = (1/2)Re Tr D^2 on rank-k idempotent tangents at (n,k) = (3,1),(4,2),(5,2): signature (2k(n-k), 2k(n-k))	(4, 4) vs 4; (8, 8) vs 8; (12, 12) vs 12
G34	eigenspaces transported exactly, eigenvalues unequal: projector energy 0, full connection energy positive	0.0e+00; 12.000000
G35	unequal ranks: ||P_s - P_t||^2 = rk P_s + rk P_t - 2 Tr(P_s P_t); the v2 calibration 20(q-p)^2/(N(q)N(p)) and the 20/7 bridge	3.6e-15
G35-OPP	constant field cI: zero connection energy on any graph (the caveat of that application)	8.4e-32

Census additions (3): the constant, the shore, the ring, graph primes.

check	statement	result
G36	symmetric 2x2 M, J = [[0,1],[-1,0]]: MJ + JM = (Tr M)J; [M,J] sees only the trace-free part; budget 4||M||^2	5.7e-14
G36-OPP	a non-symmetric M breaks MJ + JM = (Tr M)J	3.250
G37	matrix fields: dist(D, ker L_U)^2 <= E-(D)/lambda_+ (largest ratio over 200 fields); equality on the lambda_+ mode	0.870; 1.000000
G38	twisted ring, N = 3..8: two windings tie at d = pi and the floor has one-sided slopes -+4 sin(pi/N)	3.5e-07
G38-OPP	at d = 0 the floor is smooth (one winding, slopes agree)	0.0e+00
G39	unit eigenvalue: ||v -+ Wv||^2 = |1 -+ lambda|^2, sum 4, difference 4 Re lambda; relators: delta + g^2 <= 4 (least slack)	9.8e-15; -3.55e-15
G39b	clock and shift, d = 2, 3, 5: (defect, guard^2) = (4 sin^2(pi/d), 4 cos^2(pi/d)); the guard closes at d = 2	(4.0000, 0.0000); (3.0000, 1.0000); (1.3820, 2.6180)
G40	companion [[c,-1],[1,0]], |c| > 2: Phi_inf = (1/2)||[B,B^T]||^2 of B = lim M^N/||M^N|| equals 4/c^2 (c = 2.5, 3, 5, -3)	1.7e-16; 0.640000, 0.444444, 0.160000, 0.444444
G40-OPP	at the bound c = 2 the cumulative stress reaches 1 (1e5 steps); the single-step stress at c = 3 is 36, not a sin^2	1.000000; 36.0

Census additions (4): the arithmetic runs and the wall.

check	statement	result
G41	120 curve-twist pairs reproduce: mean slopes ordered by rank difference; sign agreement; correlation below the registered 0.7	120 pairs; means −1.76, −0.93, +0.22, +0.95; 0.80 of 59; 0.468 < 0.7: fails as registered
G42	10293 isogeny classes: signed profiles of even and odd rank mirror; bins apart by more than 3 standard errors; shuffled control	corr −0.985; 24 of 25 bins, median 21.01 s.e.; control +0.732
G42b	the book balance cos 2 theta_p: both means at −1/2; bins apart by more than 3 s.e.; largest gap (first bin, p/N < 0.04)	corr −0.300; means −0.4997, −0.5004; 2 of 25 bins, median 0.59 s.e.; largest 0.0132 = 10.92 s.e.
G42c	rank 2 does not side with rank 0: profile correlations r0-r1, r2-r0, r2-r1 (registered prediction killed)	−0.966, −0.048, −0.151
G43	key: growth rate sqrt(ab) = |Omega| sqrt((I3-I2)(I2-I1)/(I1 I3)), linear in |Omega|	1.8e-15
G43b	I = (2,3,4): M has +-0.35355, sigma_z M has +-0.35355 i; q = +1/8 and −1/8; ||[.,.^T]||^2 = 9/128 for both	+0.35355, +0.35355i; 0.1250, −0.1250; 0.070312, 0.070312
G44	four-body block: A = TH + HT − 2Tr(TH)W on diagonal traceless tangents; g_W A = A^T g_W for g_W the Bures metric of W (symbolic)	True, True
G44b	g_W is the Bures (Hubner) metric: d_Bures^2 / Hubner form − 1 at eps = 1e-5, 20 random W	8.1e-05
G44c	approach to the wall, q = 1e-1, 1e-2, 1e-3 (w3 = q^2): Euclidean ||P|| ~ 1/q, Bures norm of P = 1, lifted block − 2t3 I ~ q	2.599 / 1.0000000000 / 1.25e-01; 25.01 / 1.0000000000 / 1.25e-02; 250 / 1.0000000000 / 1.25e-03
G44-OPP	in the Gram chart the wall block is still a nonzero nilpotent: ||N^2||, ||N|| (the matrix statement stands)	0.0e+00, 0.433013
G44d	Bures length from W(x0) to the wall along W(x) = diag(a(1-x^2),(1-a)(1-x^2),x^2) is arcsin x0 (x0 = 0.3, 0.6, 0.9)	1.0e-12

check	statement	result
G44d-OPP	a volume-type coefficient 1/eps^2 would give a length growing like log(1/cutoff)	9.21, 18.42, 27.63
G45	sqrt3(A12 − A21) = cross product of trace-free t and w; ||[A,A^T]||^2 = 2(A12−A21)^2((A12+A21)^2+(A11−A22)^2); t = alpha w + beta normal	0, 0, True
G45-OPP	both anisotropic: t = 2w + 1/2 is normal; generic t = (2,1,1.3) is not	0.0e+00; 0.2314
G46	Herm(D + A) = D, so d/dt ||e^(tH)x||^2 at 0 is 2<x,Dx> for every transport	4.0e−10
G46-OPP	for i y′ = H y the Hermitian part of −iH is −iA: there the transport sets the gain	0.0e+00
G47	L1 = [[−1,4],[0,−1]] and L1 − I/2: the same self-commutator, peak gains 1.5698 and 1.1433; gain scales by e^(−dt)	0e+00; 1.5698, 1.1433; 2.2e−14
G48	critical generator in Schur form [[−1, mu],[0,−1]] with |mu| = 2; some t has ||e^(tJ)|| > 1 iff |mu| > 2b (grid of 18)	|mu| = 2.000000; grid True
G48-OPP	at the threshold the gain never exceeds 1; at mu = 2.2 it does	1.000000; 1.027335
G49	Koide ratio from Compton wavelengths, sum lambda^−1 / (sum lambda^−1/2)^2, equals the mass form	0.6666644634 vs 0.6666644634
G50	Koide weight over relative phases: [max(0, 2 max x − S)^2/(3M), S^2/(3M)], both ends attained; mixture 1/3 + lambda(1/(3Q) − 1/3)	[0.171868, 0.500002] vs sampled [0.171868, 0.500000]; ends 0.171868, 0.500002; 6e−17
G51	H = d.sigma: |d′|^2 = rho′^2 + Delta^2 g, rho = |d|, Delta = 2 rho, g = (1/2)Tr P′^2 (finite differences)	3.4e−09
G52	two levels: gap^2 = detuning^2 + 2||[H,P]||^2 for P the projector of one level	1.6e−14

check	statement	result

Census additions (5): records the books do not keep.

check	statement	result
G53	E-(H^T) = E-(H), E+(H^T) = E+(H): [H^T, conj H] = -[H,H*]^T and H^T^2 - conj(H)^2 = (H^2 - H*^2)^T	0.0e+00
G53-OPP	one-way L = [[-1,0],[0.3,-2]] at z = 0.5i: |R21|, |R12| swap under transposition while the books agree	0.130158,0e+00; 0e+00,0.130158; books 0.024525 = 0.024525
G54	a mirror R (det R = -1): (RX)^T(RX) = X^T X, det(RX) = -det X	1.1e-14
G55	det(S + eK) = det(S - eK); det(D - eA) = conj det(D + eA); graded det(D + A) = det(D - A); log det(M + tE) - log det M = sum log(1 + t^2 w^2)	5.5e-08
G55-OPP	interface: a Hermitian coupling lowers the log-determinant, log det(I - K) <= 0; the skew coupling raises it, log det(I + K) >= 0	2.6e-15; signs True
G56	P and 1 - P: g equal, Omega opposite; two bands |Omega| = 2 sqrt(det g); Tr(P dxP dyP) = g_xy - (i/2)Omega	1.2e-11; 7.1e-14; 1.0e-14
G56-OPP	three levels (rank one in C^3): |Omega| <= 2 sqrt(det g) is only an inequality (largest excess)	0.0e+00
G57	boundary: e^tau_A = e^tau_B s0/s1 for any interior; protected interior: tau_A = log(s0/s1), its sign set by which residual is larger	2.0e-15; 1.5e-14; sign mismatches 0
G57b	Rice-Mele chain: C_A(-v) = Sigma (I - C_A(v)) Sigma, so tau_A is the odd part of log det C_A	2.3e-15
G58	Rice-Mele (t1, t2) = (0.6, 1), v = 0: modes at nu = 1/2 for L = 6, 7, 8, 9	0, 1, 0, 1
G58b	v = 0.05, L = 5, 7, 9: (tau, half-mode share, rest): the half-mode keeps one sign and sets the size, the rest sets the sign	L=5: +0.1246, +0.1381, -0.0135; L=7: -0.1246, +0.1393, -0.2640; L=9: +0.1246, +0.1397, -0.0150
G58c	Kitaev chain (opposite of Rice-Mele), topological mu = 0.5: two Nambu modes approach 1/2 for every length, odd and even (L = 4..9)	5.4e-04, 1.2e-04, 2.8e-05, 6.5e-06, 1.5e-06, 3.6e-07
G58c-OPP	trivial mu = 3: no mode near 1/2 at any length; Nambu spectrum paired nu <-> 1 - nu throughout	0.456; 1e-15

check	statement	result
G59	Rice–Mele v = 0.3: tau = 0 in even blocks (4, 8); odd blocks (−1)^n tau -> 2 artanh(v/sqrt(Emin Emax)) (L = 13 against the limit)	1e−53; signs alternate True; 4.0e−09
G60	||[H,P]||^2 = 2 Tr BB*; C = [H,P] skew; q(C) = −Tr BB*, q(−iC) = +Tr BB*; PH^2P − (PHP)^2 = (QHP)*(QHP) >= 0	7.1e−15; least eigenvalue −9.7e−16; example (1/2)Tr C^2 = −0.580000
G60-OPP	self-energy Sigma(E) = B(E − D)^−1 B*: below the hidden spectrum every eigenvalue <= 0; above it every eigenvalue >= 0	largest below 8.9e−16; least above 3.2e−02
G61	v14 channels B = (1,1)/sqrt2, spectra (0,2) and (1,1): moment differences n = 0..3; channels equal in all moments have equal kernels	0, 0, 1, 3; 1.9e−14
G61-OPP	sharpness: the shift of size 5 with B = e1, C = e5 is silent for n < 4 and speaks at n = 4 = q − 1	0, 0, 0, 0, 1
G62	(|01> + e^(i phi)|10>)/sqrt2, phi = +−pi/2: marginals I/2 for both; after g t = 0.28 the readouts are +−sin(0.56)	2e−16; +0.531186, −0.531186
G63	lifts R(b rho) diag(e^2rho, e^4rho) R^T: the same eigenvalues for every b, projector speed (1/2)Tr P'^2 = b^2 (b = 0, 0.7, 1.5)	2.2e−16; 0.0000, 0.4900, 2.2500
G64	circle odometer: spectral flow floor(a1) − floor(a0) = (a1 − a0) + (1/2)(eta1 − eta0); a and a + 1 share spectrum and eta	8.9e−16
G65	stiffness kappa = 2 lambda at fixed energy: displacement sqrt(2E/kappa), velocity sqrt(2E), phase rate sqrt(kappa); P(X + QYQ)P = PXP	1.8e−10; 4.8e−16
G66	reactive load: |(y − i kappa)/(y + i kappa)| = 1, kappa/y = −tan(theta/2) gives Gamma = e^(i theta); matched load z = 1 gives Gamma = 0	2.3e−16; 0
G67	region of 6 sites, full-rank cut coupling g = 0..256: open channels nu(1 − nu) > 0.0196 climb to 6 = |A| and stay	0, 1, 5, 6, 6, 6, 6
G67-OPP	a rank-3 cut coupling: very strong coupling leaves exactly 3 channels open (bonding pairs at nu = 1/2)	0, 1, 3, 4, 3, 3, 3
G68	phase difference phi' = dw − 2K sin phi: locked for |dw| <= 2K, drifting beyond; at |dw| = 2K the two locked states meet (K = 1)	True

Census additions (6): Penrose, the origin construction, overlaps, what the books fix.

check	statement	result
G69	Schwarzschild isotropic: (1+lam)psi/2 = 1, (1−lam)psi/2 = a/rho; rho −> a^2/rho negates lam; Gamma = a/rho; lam = tanh(log(rho/a)/2); log(p+/p−) = log(rho/a)	0, 0, 0, 0, 0, 0, 0
G70	Reissner–Nordstrom: r+ r− = Q^2, so tau+ = −tau− for tau = log(r/Q); (r + Q^2/r)/2 = Q cosh tau; extremal r+ = r− has tau = 0	0, 0, 0
G71	fold normal form: X = lambda^2 turns dX^2/(4c^2 X) into dlambda^2/c^2, even in lambda	0
G72	finite analogue of the AdS TT square: an N−self−adjoint projector splits ||q||_N^2 = ||Pq||_N^2 + ||(1−P)q||_N^2	3.2e−11
G73	skew−transport ring, A(n,n+1) = J (drafts of 18–21 June 2026): 1/8||[H,H^T]||^2 = sum ||J B(n+1) − B(n) J||^2, N = 3, 4, 5, 7	1.4e−14
G73-OPP	published 24 June form, transport alpha J (x) Delta_1 symmetric: ||A − A^T||, ||[H,H^T]|| at eps = 0	0e+00, 0e+00
G74	rho/k <= F <= rho; max(0, k rho − k + 1) <= D <= rho^k; the power sums Tr((PR)^j), j <= k, return the angles	8.3e−11
G74b	rho − F is fourth order near coincidence (log−log slope); Slater count E[z^N_R] = prod(1 − c_a + z c_a) in Fock space (n = 4, k = 2)	3.994; 5.6e−17
G75	one edge, D1 = diag(1,0): seven fields D2 with the same books, different spectra (books; first and last spectrum)	(1.4000, 2.6000), spread 9e−16; spectra (−0.841, 0.541) to (−0.095, 0.995)
G75-OPP	scalar fields: both books fix a path of three up to sign (solutions), a single edge up to sign and swap	2; 4

References

[1] R. A. Horn and C. R. Johnson, *Matrix Analysis*, 2nd ed., Cambridge, 2013.

[2] A. Singer and H.-T. Wu, Vector diffusion maps and the connection Laplacian, *Comm. Pure Appl. Math.* **65** (2012) 1067–1144.

[3] S. Kobayashi and K. Nomizu, *Foundations of Differential Geometry*, Vol. I, Wiley, 1963.

[4] A. S. Bandeira, A. Singer and D. A. Spielman, A Cheeger inequality for the graph connection Laplacian, *SIAM J. Matrix Anal. Appl.* **34** (2013) 1611–1630.

[5] J. Hansen and R. Ghrist, Toward a spectral theory of cellular sheaves, *J. Appl. Comput. Topol.* **3** (2019) 315–358.

[6] O. Ahmad, Special affine graph transforms and commutator defects of position-decorated graph Laplacians, *Ann. Univ. Ferrara* **72** (2026) 122.

[7] M. Desai and V. Rao, A characterization of the smallest eigenvalue of a graph, *J. Graph Theory* **18** (1994) 181–194.

[8] D. Cvetković, P. Rowlinson and S. K. Simić, Signless Laplacians of finite graphs, *Linear Algebra Appl.* **423** (2007) 155–171.

[9] T. Zaslavsky, Signed graphs, *Discrete Appl. Math.* **4** (1982) 47–74.

[10] N. Reff, Spectral properties of complex unit gain graphs, *Linear Algebra Appl.* **436** (2012) 3165–3176.

[11] C. Lange, S. Liu, N. Peyerimhoff and O. Post, Frustration index and Cheeger inequalities for discrete and continuous magnetic Laplacians, *Calc. Var. Partial Differential Equations* **54** (2015) 4165–4196.

[12] Y. Bilu and N. Linial, Lifts, discrepancy and nearly optimal spectral gap, *Combinatorica* **26** (2006) 495–519.

[13] J. Beasley, *The Ledger Outlives the Metric*, Gravity Ledger, full research edition 6, 24 September 2026, doi:10.5281/zenodo.22023237.

[14] A. M. Gleason, Measures on the closed subspaces of a Hilbert space, *J. Math. Mech.* **6** (1957) 885–893.

[15] S. Hossenfelder, Born's rule from almost nothing, arXiv:2006.14175 (2020).

[16] A. A. Klyachko, M. A. Can, S. Binicioğlu and A. S. Shumovsky, Simple test for hidden variables in spin-1 systems, *Phys. Rev. Lett.* **101** (2008) 020403.

[17] L. Lovász, On the Shannon capacity of a graph, *IEEE Trans. Inform. Theory* **25** (1979) 1–7.

[18] A. Cabello, S. Severini and A. Winter, Graph-theoretic approach to quantum correlations, *Phys. Rev. Lett.* **112** (2014) 040401.

[19] Y. Ihara, On discrete subgroups of the two by two projective linear group over $\mathfrak{p}$-adic fields, *J. Math. Soc. Japan* **18** (1966) 219–235.

[20] K. Hashimoto, Zeta functions of finite graphs and representations of p-adic groups, *Adv. Stud. Pure Math.* **15** (1989) 211–280.

[21] H. Bass, The Ihara–Selberg zeta function of a tree lattice, *Internat. J. Math.* **3** (1992) 717–797.

[22] T. Sunada, L-functions in geometry and some applications, in *Curvature and Topology of Riemannian Manifolds*, Lecture Notes in Math. **1201**, Springer, 1986, 266–284.

[23] H. M. Stark and A. A. Terras, Zeta functions of finite graphs and coverings, *Adv. Math.* **121** (1996) 124–165.

[24] M. Kotani and T. Sunada, Zeta functions of finite graphs, *J. Math. Sci. Univ. Tokyo* **7** (2000) 7–25.

[25] A. Terras, *Zeta Functions of Graphs: A Stroll through the Garden*, Cambridge, 2011.

[26] Y. Watanabe and K. Fukumizu, Graph zeta function in the Bethe free energy and loopy belief propagation, *Advances in Neural Information Processing Systems* **22** (2009) 2017–2025.

[27] K. Hammer, T. W. Mattman, J. W. Sands and D. Vallières, The special value $u = 1$ of Artin–Ihara L-functions, arXiv:1907.04910 (2019).

[28] R. Kenyon, Spanning forests and the vector bundle Laplacian, *Ann. Probab.* **39** (2011) 1983–2017.

[29] A. Lubotzky, R. Phillips and P. Sarnak, Ramanujan graphs, *Combinatorica* **8** (1988) 261–277.

[30] A. W. Marcus, D. A. Spielman and N. Srivastava, Interlacing families I: Bipartite Ramanujan graphs of all degrees, *Ann. of Math.* **182** (2015) 307–325.

[31] L. D. Landau and E. M. Lifshitz, *Mechanics*, 3rd ed., Pergamon, 1976, §37.

[32] J. V. Burke, A. S. Lewis and M. L. Overton, Optimal stability and eigenvalue multiplicity, *Found. Comput. Math.* **1** (2001) 205–225.

[33] J. Beasley, *Beyond the Event Horizon: What Survives at a Rigidity Wall*, research edition 10, 2026, doi:10.5281/zenodo.21147366.

[34] Y. Koide, Fermion–boson two-body model of quarks and leptons and Cabibbo mixing, *Lett. Nuovo Cimento* **34** (1982) 201–205.

[35] Y. Koide, A fermion–boson composite model of quarks and leptons, *Phys. Lett. B* **120** (1983) 161–165.

[36] R. Foot, A note on Koide's lepton mass relation, arXiv:hep-ph/9402242 (1994).

[37] C. A. Brannen, The lepton masses, preprint, 2 May 2006, https://brannenworks.com/MASSES2.pdf.

[38] S. Navas *et al.* (Particle Data Group), Review of Particle Physics, *Phys. Rev. D* **110** (2024) 030001.

[39] Y. Koide and T. Yamashita, Charged lepton mass relations in a SUSY scenario, arXiv:1805.09533 (2018).

[40] A. V. Sutherland, *18.783 Elliptic Curves*, Lecture 7: Hasse's theorem and point counting, MIT, 2021.

[41] A. V. Sutherland, Sato–Tate distributions, arXiv:1604.01256 (2016).

[42] The LMFDB Collaboration, *The L-functions and Modular Forms Database*, elliptic curves 32.a3 (32a2), 37.a1 and 389.a1, https://www.lmfdb.org.

[43] K. Conrad, Partial Euler products on the critical line, *Canad. J. Math.* **57** (2005) 267–297.

[44] Y.-H. He, K.-H. Lee, T. Oliver and A. Pozdnyakov, Murmurations of elliptic curves, *Experiment. Math.* (2024), arXiv:2204.10140.

[45] W. Sawin and A. V. Sutherland, Murmurations for elliptic curves ordered by height, arXiv:2504.12295 (2025).

[46] J. Watrous, *Theory of Quantum Information*, Lecture 4: Purifications and fidelity, University of Waterloo, 2011.

[47] V. Bargmann, Note on Wigner's theorem on symmetry operations, *J. Math. Phys.* **5** (1964) 862–868.

[48] J. Beasley, *Intrinsic Quantum Geometric Tensor on the Grassmannian*, v7.3.1, 2026.

[49] J. Beasley, *VOTKP: The Vector of Traits Kept under Peeling. Elemental Peeling of Atoms and Knots*, v2.9, 13 October 2026, §§19–20, doi:10.5281/zenodo.23011140.

[50] J. Beasley, *The Dirac Time of the Gigantefermion*, full longform v3.0.1, 2026, doi:10.5281/zenodo.22978630.

[51] J. Beasley, *The Offset Belongs to the Boundary*, complete edition v31, September 2026, doi:10.5281/zenodo.22181748.

[52] J. Beasley, *Light Keeps the Ledger*, Edition 7.2, 2026, doi:10.5281/zenodo.22123115.

[53] S. Pincherle, Delle funzioni ipergeometriche e di varie questioni ad esse attinenti, *Giorn. Mat. Battaglini* **32** (1894) 209–291.

[54] W. Gautschi, Computational aspects of three-term recurrence relations, *SIAM Rev.* **9** (1967) 24–82.

[55] J. Beasley, *gravity-ledger-lean*, Lean 4 library, module `GravityOverlap`, https://github.com/dicipler-pixel/gravity-ledger-lean.

[56] J. Beasley, *dirac-time-lean*, Lean 4 library, modules `MovingFrame`, `CommonClock`, `PathLedger`, https://github.com/dicipler-pixel/dirac-time-lean.

[57] J. Beasley, *ramanujan-challenge-lean*, Lean 4 library, module `RamanujanChallenge/Pincherle`, https://github.com/dicipler-pixel/ramanujan-challenge-lean.

[58] J. Beasley, *Companion-matrix normality diagnostic for candidate recurrences*, Python tool, https://github.com/dicipler-pixel/ramanujan-normality-diagnostic.

[59] J. Beasley, *event-horizon-lean*, Lean 4 library for *Beyond the Event Horizon*, research edition 10, https://github.com/dicipler-pixel/event-horizon-lean.

[60] J. Beasley, *offset-lean*, Lean 4 library, modules `OperatorFirst/Offset` and `OffsetLean/Headline`, https://github.com/dicipler-pixel/offset-lean.

[61] J. Beasley, *light-ledger-lean*, Lean 4 library, modules `LightBridges/Boundary`, `Census`, `ScalarOptics`, https://github.com/dicipler-pixel/light-ledger-lean.

[62] J. Beasley, *votkp-lean*, Lean 4 library, modules `VOTKP/Smith` (default branch) and `VOTKP/Directed`, `Channels`, `Memory`, `Witnesses` on the branch `claude-finish-lean`, head commit bd4d15a, the release accompanying VOTKP v2.9, https://github.com/dicipler-pixel/votkp-lean.

[63] J. Beasley, Born's rule on equal-rank partitions, working note, October 2026.

[64] J. Beasley, *Beyond the Event Horizon: What Survives at a Rigidity Wall*, research edition 8.5.1, October 2026, doi:10.5281/zenodo.21147366.

[65] J. Beasley, *Non-Normality Is Connection Energy*, one-page note, 17 September 2026, doi:10.5281/zenodo.22803572.

[66] J. Beasley, *-connection-energy-lean*, Lean 4 library for the one-page note, modules `ConnectionEnergy/Basic` and `ConnectionEnergy/Holonomy`, 20 theorems, https://github.com/dicipler-pixel/-connection-energy-lean.

[67] J. Beasley, *nonnormality-connection-energy-lean*, Lean 4 library for this paper, modules `NonNormality/*` including `Admissible` and `Census`, pull requests `claude-admissible` and `claude-v15`, https://github.com/dicipler-pixel/nonnormality-connection-energy-lean.

[68] J. Beasley, *The Operator-First Atlas*, continuous edition 3, 182 bridges, October 2026 (author's corpus).

[69] J. Beasley, *relational-atlas-lean*, Lean 4 library, https://github.com/dicipler-pixel/relational-atlas-lean.

[70] J. Beasley, *sqrt-lower-bound-lean*, Lean 4 library, module `RequestProject/EntropyMeasurement`, https://github.com/dicipler-pixel/sqrt-lower-bound-lean.

[71] J. Beasley, *Foundational Operator Field Theory on Stratified Manifolds*, version 2, 8 August 2026, doi:10.5281/zenodo.21254648.

[72] J. Beasley, *foft-lean*, Lean 4 library, module `FOFT/Basic`, https://github.com/dicipler-pixel/foft-lean.

[73] J. Beasley, *Universal Projector Geometry from Electrical Measurements*, v3.2, September 2026, doi:10.5281/zenodo.21305024.

[74] J. Beasley, *upg-lean*, Lean 4 library, modules `UPGAlgebra` and `UPGTorusAnchor`, https://github.com/dicipler-pixel/upg-lean.

[75] J. Beasley, *The Ledger Outlives the Metric*, research edition 7, 4 October 2026, doi:10.5281/zenodo.22023237.

[76] J. Beasley, *A Five-Dimensional Non-Normal Stability Operator with Gradient-Driven Interface Coupling for Zero-Precursor Filamentary Fractures*, 2026, doi:10.5281/zenodo.21184980.

[77] J. Beasley, *filament-fracture-lean*, Lean 4 library, https://github.com/dicipler-pixel/filament-fracture-lean.

[78] J. Beasley, *Spectral Stability Across Obstruction Interfaces in Geometric Transport Systems*, 24 June 2026, doi:10.5281/zenodo.20818899.

[79] J. Beasley, *spectral-stability-lean*, Lean 4 library, modules `SpectralStability/Coupling` and `SpectralStability/Recovered`, https://github.com/dicipler-pixel/spectral-stability-lean.

[80] J. Beasley, *matter-at-a-scale-lean*, Lean 4 library, https://github.com/dicipler-pixel/matter-at-a-scale-lean.

[81] J. Beasley, *price-of-a-direction-lean*, Lean 4 library for *The Price of a Direction*, doi:10.5281/zenodo.21918463, https://github.com/dicipler-pixel/price-of-a-direction-lean.

[82] J. Beasley, *square-case-lean*, Lean 4 library, https://github.com/dicipler-pixel/square-case-lean.

[83] J. Beasley, *suns-lean*, Lean 4 library for the author's study of the Sun, doi:10.5281/zenodo.21895551, https://github.com/dicipler-pixel/suns-lean.

[84] *Direction, Spin, and Throughput: Dual Measurements and Shared-Environment Coupling in a Three-Dimensional Rotor Network*, version 0.1, 19 October 2026, a working study in Jeromie Beasley's research programme.

[85] J. Beasley, *Certified Obstructions and Exact Forcing*, version 2, 17 September 2026, doi:10.5281/zenodo.22812167.

[86] J. Beasley, a trace identity for differences of idempotents, Mathlib pull request #43951, https://github.com/leanprover-community/mathlib4/pull/43951.

[87] M. Jakob and J. A. Bergou, Quantitative complementarity relations in bipartite systems: entanglement as a physical reality, *Opt. Commun.* **283** (2010) 827.

[88] X.-F. Qian *et al.*, Entanglement limits duality and vice versa, *Optica* **5** (2018) 942.

[89] L. N. Trefethen and M. Embree, *Spectra and Pseudospectra: The Behavior of Nonnormal Matrices and Operators*, Princeton, 2005.

[90] M. J. Rice and E. J. Mele, Elementary excitations of a linearly conjugated diatomic polymer, *Phys. Rev. Lett.* **49** (1982) 1455–1459.

[91] A. Yu. Kitaev, Unpaired Majorana fermions in quantum wires, *Phys.-Usp.* **44** (2001) 131–136.

[92] R. Adler, A study of locking phenomena in oscillators, *Proc. IRE* **34** (1946) 351–357.

[93] OpenAI, *Spacetime Penrose inequalities: enclosing area, charge, and rigidity*, research manuscript, 262 pp., dated 5 October 2026.

[94] G. L. Bunting and A. K. M. Masood-ul-Alam, Nonexistence of multiple black holes in asymptotically Euclidean static vacuum space-time, *Gen. Relativ. Gravit.* **19** (1987) 147–154, doi:10.1007/BF00770326.

[95] *Penrose and twenty Beasley papers*, complete comparison prepared for J. N. Beasley, 12 October 2026 (author's corpus).

[96] J. Beasley, *what-russell-saw-lean*, Lean 4 library for *What Russell Saw*, doi:10.5281/zenodo.22986656, https://github.com/dicipler-pixel/what-russell-saw-lean.

[97] J. Beasley, *emergent-transport-lean*, Lean 4 library for *Intrinsic Emergent Transport Geometry*, doi:10.5281/zenodo.21089303, https://github.com/dicipler-pixel/emergent-transport-lean.

[98] J. Beasley, *iqgt-grassmannian-lean*, Lean 4 library, https://github.com/dicipler-pixel/iqgt-grassmannian-lean.